Nanoporous Carbon Capture Materials from Sustainable Sources

Gregor Sneddon, MChem

SUBMITTED FOR THE DEGREE OF DOCTOR OF PHILOSOPHY

HERIOT-WATT UNIVERSITY

SCHOOL OF ENGINEERING AND PHYSICAL SCIENCES

July 2017

ABSTRACT

Rising CO_2 levels in the atmosphere from anthropogenic sources can be seen as one of the greatest problems faced by mankind in modern history. CO_2 capture and subsequent storage or utilisation is one possible solution to increasing CO_2 levels in the short-term, until humanity is less reliant on fossil fuels. This thesis will investigate currently available state of the art CO_2 capture technologies and provide a critical evaluation on their suitability. Furthermore, current research into the storage and utilisation of captured CO_2 will also be studied and the long-term suitability of these approaches to increasing CO_2 levels determined.

New solid-state CO_2 adsorption materials have been developed using waste polymeric materials as the primary agent for selective adsorption of CO_2. The approach of using waste materials for CO_2 adsorption is advantageous in that the waste material is being used to deal with another waste material, namely CO_2. The waste materials utilised in this research were chitosan, a waste material derived from chitin, a large waste from the seafood industry, and polyvinylchloride (PVC), a polymer mainly used in the fabrication of household products. It is demonstrated in this thesis that with minimal modification, these waste materials can be utilised for the capture of CO_2 at levels comparable to that of the currently available state-of-the-art materials.

ACKNOWLEDGEMNTS

I would firstly like to thank my family, friends and colleagues who have supported me throughout my studies. A special thanks goes to my supervisor Dr Humphrey Yiu, whose knowledge and support have been invaluable. Most of all I would like to thank my fiancée Jennifer, without you, this would not have been possible.

SUMMARY OF CONTENTS

Much literature is available in the area of carbon capture, storage and utilisation as climate change is one of the most pressing issues in today's society. In order to aid in the understanding of the present literature and the current state of carbon capture, storage and utilisation, Chapter 1 of this thesis will review the current literature and serves as an introduction to the thesis. This chapter will cover the currently available methods of CO_2 adsorption as well as their limitations to the application of carbon capture. The option of storage of captured CO_2 will also be briefly discussed and the effects this approach to dealing with CO_2 could have on the environment. Utilisation of CO_2 will also be discussed, with the currently available and newly discovered pathways for conversion of CO_2 into useful feedstocks.

Chapter 2 will cover the use of chitosan as a solid-state adsorbent for CO_2 capture. With the aid of high surface are silica supports to improve the availability of surface amine groups, chitosan can be used to adsorb CO_2 at levels comparable to other solid-state adsorbents specifically designed for CO_2 adsorption. These chitosan/silica composite materials will be shown not only to be efficient for CO_2 adsorption, but also regenerable at low temperatures.

Chapter 3 will explore the use of amine modified PVC as a solid-state adsorbent for CO_2 capture. Following the methodology demonstrated in Chapter 2, the aminated-PVC material was supported on mesoporous silica supports to improve the availability of amine groups for CO_2 adsorption. The aminated-PVC/silica composite materials will be shown to achieve CO_2 adsorption values comparable to adsorbent materials from the literature.

Chapter 4 will cover unpublished work utilising aminated-PVC on hydrophobic carbon supports for the application of CO_2 adsorption. Water within the gas stream can compete for active adsorption sites for CO_2. The use of hydrophobic supports should

discourage water from reaching the surface, thus lessen the role of water in the CO_2 adsorption process, leading to less competition for adsorption sites.

A conclusion of the main outcomes of the research undertaken will be included in Chapter 5. Initial research using aminated-PVC/silica composite materials in the form of a membrane for CO_2 adsorption will also be briefly discussed. The use of a membrane type material rather than a powdered solid-state adsorbent can be advantageous, as rather than using a packed column, membranes of adsorbent can bisect the flue gas stream. Recommendations will also be made for future research that could be conducted in the area of carbon capture using sustainable sources.

TABLE OF CONTENTS

CHAPTER 1

The Potential Applications of Nanoporous Materials for the Adsorption, Separation, and Catalytic Conversion of Carbon Dioxide

1.1 Background

Current research on adsorbents for CO_2 capture and sequestration can largely be split into two categories; size exclusion using a material with a suitable pore size to entrap a molecule of CO_2, or by chemical means through bonding a molecule of CO_2 to a adsorbent. Indeed, much research has been carried out in the area of CO_2 capture, absorption using liquid amine solutions, the current industry preferred method. This method does encounter many complications however, so improvement on performance of solid adsorbents is of high importance for the progression of carbon capture and storage (CCS). The majority of current research is aimed at finding a suitable solid adsorbent for CO_2 capture, that is both efficient in terms of the amount of CO_2 adsorbed per gram of material and cost effective to produce and regenerate.

After capture, CO_2 should then be either "stored" or transformed into other chemicals. Storage of CO_2 in a CCS aspect is widely seen as the transfer of the sequestered CO_2 to a designated reservoir for geological storage underground. On the other hand, carbon capture and utilisation (CCU) rather than storage of CO_2 can be seen as longer-term solution to rising CO_2 levels. Instead of being stored geologically, captured CO_2 can be used as a feedstock in industry on route to making more useful and useable materials. Although research in this area is not as mature as that of capture and sequestration, nonetheless this could prove to be an important step on the way to combat the ever increasing CO_2 emission levels.

1.2 Aim/Objectives

A full and comprehensive review of the current literature surrounding CO_2 adsorption, separation and conversion was undertaken here in order to effectively summarise current available techniques. This critical analysis of the current literature allowed for conclusions to be drawn on the criteria for an ideal solid state CO_2 adsorbent. The main aim of this study was to identify through critical evaluation of the current literature, what progress has been made towards finding suitable and sustainable nanoporous materials for CO_2 capture, sequestration and conversion. Furthermore, the potential applications of these nanomaterials for CCU purposes will also be investigated, with a specific emphasis placed on the catalytic conversion of CO_2.

1.3 Findings

1.3.1 CO_2 Capture: State-of-the-Art Methods and Their Limitations

The current actively used carbon capture technique in industry was found to be sequestration by chemical means using alkanolamine solutions, mainly monoethanolamine (MEA) and diethanolamine (DEA). Although these liquids/solutions readily isolate CO_2 from flue gas or natural gas by an acid-base neutralisation mechanism, the process of absorption and regeneration is far from ideal. One of the main drawbacks to this method was identified to be the large amount of energy required to regenerate the liquid alkanol adsorbent. As much as 70 % of the cost of running a CO_2 capture plant was associated with regeneration of the absorbent. Other complications to be considered when using liquid amines include corrosion of equipment, degradation of the absorbent through oxidation and the introduction of flow problems due to an increase in viscosity during absorption. Although the use of liquid amines is the current preferred CO_2 capture technique in industry due to the simplicity of the chemistry and relative ease of retrofitting to existing sites, it was determined that there is certainly room for improvement with respect to cost reduction and absorption efficiency.

1.3.2 Solid State CO_2 Adsorbents

Nanoporous materials were identified as a more sustainable adsorbent for CO_2 as they have the ability to combine both physical adsorption and chemical adsorption methods in the form of a solid adsorbent. Solid adsorbents are also easier to handle and have fewer problems associated with corrosion when compared to liquid amine adsorbents, identifying them as better materials for CO_2 sorption on a purely process handling basis. This property/advantage coupled with high surface areas and pore volumes associated with nanoporous materials also, allows for significant enhancement in adsorption capacity.

Zeolites are aluminosilicate minerals with ordered, nanoporous structures. The physical properties of zeolites make them ideal candidates for either CO_2 adsorption or gas separation applications. These materials generally have a high surface area (e.g. 571 m^2g^{-1} for zeolite 13X) and a pore size ranging between 3 and 12 Å (0.3-1.2 nm).

These physical properties allow zeolites to accommodate not only CO_2 but also other small molecules commonly found in the flue gas stream such as N_2, O_2, H_2O, H_2 or CH_4. It was found from the literature that the selectivity of the zeolite materials could be fine tuned towards CO_2 by adjusting the type and number of cationic sites (e.g. Cs^+, Rb^+, K^+, Na^+ and Li^+) within the zeolite framework. Another method of CO_2 separation using zeolites was via a so called "trapdoor mechanism". This involved the trapping of a molecule of CO_2 within the cavities of the zeolite by interaction of the cation and CO_2 directly. The strong interaction of the acidic CO_2 and the cationic species would close the pore by movement of the cation and thus not allowing the CO_2 molecule to leave. This also acts as another mechanism to improve selectivity to CO_2, as weakly interacting species such as N_2 or CH_4 would just pass through the cavity. Although these zeolite materials can be selective to CO_2 with large adsorption capacities [1.1, 1.2, 1.3], they could be quickly deactivated by the presence of water, leading to a reduction in the CO_2 adsorption efficiency. Water is an inevitable component of the flue gas stream, with an average of 8-14 %v/v, therefore, without an efficient regeneration step, zeolites would be unfeasible for CO_2 capture in industry.

Another family of nanoporous materials tested for CO_2 capture are metal organic frameworks (MOFs). MOFs are constructed using a mixture of inorganic and organic components. The inorganic component is usually a transition metal or cluster of transition metals. The organic component (the ligand) commonly contains aromatic rings, for rigidity, and are capped by functional groups capable of interacting with the transition metal atoms. Crucially, due to the large variety of inorganic and organic components available, MOFs can isolate CO_2 by physical or chemical means depending on how they are customised. The pore size within the MOF can easily be adjusted by varying the length of the organic ligands. The chemical selectivity towards CO_2 can also be improved by the addition of polarising groups within these pores. According to data from the literature MOFs were able to outperform zeolites in terms of selectivity towards CO_2 and adsorption capacity, thanks to their highly customisable structure. Although in some cases they are superior over zeolites, MOF materials are far from an ideal candidate for carbon capture. One major drawback is that MOFs are difficult to produce on an industrial scale with a typical synthesis being on the *ca.* 1g scale. However, recently there have been advancements in production of MOFs on an industrial scale [1.4]. Although, the production of MOFs on an industrial scale is

feasible, the MOFs under investigation may not be applicable to CO_2 adsorption applications. These issues, coupled with the use of toxic transition metals and ligands also has environmental implications.

Functionalised mesoporous silicas were also investigated for their use in CO_2 capture. Ordered mesoporous silicas have a high surface area (*ca.* 1000 m^2g^{-1}), high pore volume (*ca.* 1 cm^3g^{-1}) and a large pore size (>2 nm). This larger pore size when compared to zeolites and MOFs as well as the slightly acidic nature of the mesoporous silica surface, suggests that without modification these materials would perform poorly in CO_2 capture regarding selectivity. Commonly, the surface of the mesoporous silicas are functionalised using alkoxysilanes to introduce amine functional groups to the silica surface, allowing for selectivity towards acidic groups such as CO_2. Once functionalised, mesoporous silicas are able to achieve high CO_2 adsorption capacities (0.5 to 2.0 $mmolg^{-1}$ at 25°C and 1 atm). Unlike MOFs and zeolites, some amine functionalised mesoporous silicas can actually increase their CO_2 adsorption capacity when exposed to water, namely (3-aminopropyl)triethoxysilane (APTES) modified SBA-15 [1.5]. This is achieved through the formation of protonated ammonium ions and carbonates. It is also possible to further boost the adsorption capacity of these materials by utilising the unused space within the large pore network by coating the pores in a suitable aminated polymer, such as polyethyleneimine (PEI). These polymer/silica composite materials were observed to improve the CO_2 adsorption capacity, SBA-15 impregnated with PEI was observed to have an adsorption capacity of 4.89 $mmolg^{-1}$ [1.6]. However, complete immobilisation of the water-soluble PEI polymer was proved difficult. Overall, functionalised mesoporous silicas proved a good candidate for combating rising CO_2 levels, with large-scale production of mesoporous silicas already available. However, mesoporous silicas are not without their disadvantages. The template used during synthesis has to be either calcined at high temperature, requiring a lot of energy or extracted using solvent, generating a large amount of solvent waste. Adding to this issue is the uncertainty around the use of amine moieties and their potential environmental impact in the future.

The effect of water on the of CO_2 capture process has so far been either positive or negative depending on the adsorbent material used. If using amine based materials,

the presence of water can be beneficial where an increase in adsorption capacity has been observed. Without this specific chemical interaction of water and an amine species, water usually reduces CO_2 adsorption capacity of an adsorbent due to competition for adsorption sites. In cases such as this a hydrophobic surface for adsorption could lead to an increase in adsorption capacity by eliminating the competition with water molecules. Nanoporous carbon materials, including activated carbons, carbon fibers and ordered mesoporous carbons are naturally hydrophobic. Similar to the many other adsorption materials investigated, the adsorption of CO_2 is not entirely selective without the introduction of functional groups to aid selectivity. This can be achieved through either grafting to the surface or by using the hydrophobic surface to support a suitable polymeric material for CO_2 adsorption. Both methods were observed to improve the adsorption capacity of the carbon supports. Mesoporous carbon materials are synthesised by using mesoporous silica materials as a template, as a result they suffer from the same drawbacks. They also produce further waste during the removal of the mesoporous silica template using a strong base or hydrofluoric acid. APTES functionalised carbon nanotubes were observed to have a similar adsorption capacity when compared to other APTES functionalised materials. Although some of this research was based on simulated data due to the large expense involved in synthesising carbon nanotubes. Activated carbon materials can be produced in bulk using waste sources including plant wastes, such as nutshells and wood, or other bulk sources (e.g., peat and coal). However, this process does require a large amount of heat energy, with temperatures of up to 900°C required in the absence of oxygen. Furthermore, in order to introduce CO_2 selectivity, amination at temperatures up to 800°C is also required [1.7]. Suggesting that these materials are not the best candidate for CO_2 adsorption in the long term.

There also exists a group of porous organic nanomaterials which show potential in the area of selective CO_2 adsorption. Organic cage frameworks (OCF), covalent organic frameworks (COFs) and supramolecular organic frameworks (SOFs) are similar to MOFs but consist of only organic material without the need of a transition metal. Like MOF materials the size of the cages can be adjusted by altering the length of the organic components and selectivity introduced by coupling of amine containing compounds. The lack of transition metals within the structure, while better for the environment also has the added benefit of the materials being substantially less dense.

Simulated results for these materials look promising with the aim of CO_2 capture although the research in this area is in its infancy and has not yet been extensively studied.

1.3.3 Catalytic Conversion of CO_2

The ultimate goal of carbon capture is not the geological storage of the isolated CO_2 but the conversion into a more useful feedstock. Due to the chemical stability of carbon dioxide, the process of conversion usually requires the use of a catalyst. Homogeneous catalysis processes for the conversion of CO_2 with alkenes and alkynes has been well established. However, these homogeneous catalytic processes are usually linked to high energy consumption due to high temperatures and pressures required, produce a lot of waste and with poor recyclability. Heterogeneous catalysts can be used to avoid several key issues encountered when using homogeneous catalysts. However, heterogeneous catalysts generally have a poorer selectivity and lower reaction rate. Further research into new heterogeneous catalysts for CO_2 conversion is required in order to progress the CCU process.

The nanoporous catalysts investigated for carbon capture, namely zeolites, MOFs, functionalised mesoporous silicas and carbon nanotubes have also been investigated for their potential in CO_2 conversion. Zeolites have been investigated in the production of syngas by using CO_2 and CH_4 by supporting nickel on the zeolite surface along with a suitable promoter [1.8]. This removes not only CO_2 but also CH_4, which has a greenhouse effect *ca.* 25 times greater than CO_2. Although this process removes two greenhouse gases, this reformation process does require temperatures of up to 600-800°C to give effective conversion rates. Zeolites have also been studied as catalysts for the formation of methanol using a zeolite membrane reactor, as well as in a cycloaddition process with epoxides.

MOFs have also been studied for their potential use in catalytic conversion of CO_2. Transition metal centres are known to be catalytically active [1.9], suggesting that MOF materials may be used for catalytic processes. It was found in the literature that MOF-5 with the co-catalyst n-Bu_4NBr was effective at cycloaddition of CO_2 to

propylene oxide and styrene oxide. Where the Zn_4O transition metal centre in the MOF acts as a Lewis acid by interacting with the epoxide oxygen, while the Bu_4N^+ ion opened the epoxide ring. Although the MOF-5 material can be reused, the Bu_4N^+ ions are not so easily recovered, raising questions about the sustainability of this process. Similar experiments using Co-MOF-74 to add CO_2 onto styrene oxide without the use of a co-catalyst were successful, with 96% conversion observed after 4 hours. Unfortunately, high temperature and pressure were required (100°C and 20 atm) as well as the use of a toxic solvent, chlorobenzene.

Literature on the use of functionalised mesoporous silicas for catalysis is already readily available. The large pore dimensions (>1 nm) make them ideal candidates for catalysis as they can accommodate larger molecules than zeolites or MOFs. Opening the doors to potentially more complex catalytic conversions involving CO_2 in the future. TiO_2 photocatalyst was successfully supported onto the surface of MCM-41 and MCM-48 for the conversion of CO_2 into methane and methanol (3:1 ratio) in selectivity. The supported TiO_2 was able to overcome the low activity and selectivity of the bulk material. However, TiO_2 only absorbs radiation in the UV region, meaning doping with other transition metals (e.g. copper) is required in order to absorb energy in the visible region. Functionalised mesoporous silicas can also be used for the catalytic addition of CO_2 to epoxides as discussed for zeolites and MOFs. One advantage being that the co-catalyst (e.g. Bu_4N^+) can be grafted to the silica surface through silanisation. Using this method, imidazolium ions were grafted to the surface of an MCM-41 support and found to be active at cyclic carbonate formation from epoxides. Upon recycling, minimal deactivation of the catalyst was observed. However, as with the MOF systems studied, high pressures of 7-40 atm were required for these reactions, again questioning their feasibility.

1.4 Conclusion

Solid nanoporous materials can be employed for CO_2 capture over traditional liquid amines and outperform them in terms of CO_2 sorption capacity [1.10]. However, the initial cost for these materials to initially be produced can be perceived as a major limitation to their implementation for CCS. Ultimately the process of carbon capture and storage was determined to be a short-term to mid-term solution to increasing CO_2

levels in the environment. On the other hand, utilisation of the captured CO_2 may serve as a longer-term solution until humanity can relinquish its dependence on fossil fuels.

1.5 Impact on Literature and Research

In order to advance research within any given field, the availability of concise and accurate information is crucial. This review paper has outlined the parameters required for an ideal CO_2 adsorbent and brought together information on the best candidates possible within the research available. It has also summarised the current available pathways for conversion of CO_2 into more useful feedstock materials. This review has been cited in a wide range of publications within the areas of carbon capture and utilisation, including: using MOFs not only for CO_2 capture [1.11] but also the catalytic conversion of CO_2 [1.12, 1.13], studying the structural changes within trapdoor zeolites during CO_2 adsorption [1.14], using carbon based adsorbents for CO_2 capture [1.15, 1.16] and using metal organic polymers for heterogeneous catalytic addition of CO_2 to epoxides [1.17].

1.6 References

[1.1] J. Shang, G. Li, R. Singh, Q. Gu, K. M. Nairn, T. J. Bastow, N. Medhekar, C. M. Doherty, A. J. Hill, J. Z. Liu, P. A. Webley, *Discriminative Separation of Gases by a "Molecular Trapdoor" Mechanism in Chabazite Zeolites*, J. Am. Chem. Soc., **134**, 19246-19253 (2012)

[1.2] J. Shang, G. Li, R. Singh, P. Xiao, J. Z. Liu, P. A. Webley, *Determination of Composition Range for "Molecular Trapdoor" Effect in Chabazite Zeolite*, J. Phys. Chem. C, **117**, 12841-12847 (2013)

[1.3] M. M. Lozinska, E. Mangano, J. P. S. Mowat, A. M. Shepherd, R. F. Howe, S. P. Thompson, J. E. Parker, S. Brandani, P. A. Wright, *Understanding Carbon Dioxide Adsorption on Univalent Cation Forms of the Flexible Zeolite Rho at Conditions Relevant to Carbon Capture from Flue Gases*, J. Am. Chem. Soc., **134**, 17628-17642 (2012)

[1.4] M. Gaab, N. Trukhan, S. Maurer, R. Gummaraju, U. Mueller, *The progression of Al-based metal-organic frameworks – From academic research to industrial production and applications*, Microporous Mesoporous Mater., **157**, 131-136 (2012)

[1.5] A. Danon, P. C. Stair, E. Weitz, *FTIR Study of CO_2 Adsorption on Amine-Grafted SBA-15: Elucidation of Adsorbed Species*, J. Phys. Chem. C., **115**, 11540-11549 (2011)

[1.6] W. J. Son, J. S. Choi, W. S. Ahn, *Adsorptive removal of carbon dioxide using polyethyleneimine-loaded mesoporous silica materials*, Microporous Mesoporous Mater., **113**, 31-40 (2008)

[1.7] P. Chingombe, B. Saha, R. J. Wakeman, *Surface modification and characterisation of a coal-based activated carbon*, Carbon, **43**, 3132-3143 (2005)

[1.8] J. S. Chang, S. E. Park, H. Z. Chon, *Catalytic activity and coke resistance in the carbon dioxide reforming of methane to synthesis gas over zeolite-supported Ni catalysts*, Appl. Catal. A Gen., **145**, 111-124 (1996)

[1.9] J. Y. Lee, O. K. Farha, J. Roberts, K. A. Scheidt, S. T. Nguyen, J. T. Hupp, *Metal–organic framework materials as catalysts*, Chem. Soc. Rev., **38**, 1450-1459 (2009)

[1.10] C-H. Yu, C-H. Huang, C-S. Tan, *A Review of CO_2 Capture by Absorption and Adsorption*, Aerosol and Air Quality Research, **12**, 745–769 (2012)

[1.11] M. G. Frysali, E. Klontzas, E. Tylianakis, G. E. Froudakis, *Tuning the interaction strength and the adsorption of CO_2 in metal organic frameworks by functionalization of the organic linkers*, Microporous Mesoporous Mater., **227**, 144-151 (2016)

[1.12] A. Mahmood, W. Guo, H. Tabassum, R. Zou, *Metal-Organic Framework-Based Nanomaterials for Electrocatalysis*, Adv. Energy Mater., **6**, (2016)

[1.13] Y. Li, H. Xu, S. Ouyang, J. Ye, *Metal-organic frameworks for photocatalysis*, Phys. Chem. Chem. Phys. **18**, 7563-7572 (2016)

[1.14] A. G. Greenaway, J. Shin, P. A. Cox, E. Shiko, S. P. Thompson, S. Brandani, S. B. Hong, P. A. Wright, *Structural changes of synthetic paulingite (Na,H-ECR-18) upon dehydration and CO2 adsorption*, Z. Kristallogr.-Cryst. Mater., **230**, 223-231 (2015)

[1.15] R. A. Fiuza-Jr, R. C. Andrade, H. M. C. Andrade, *CO_2 capture on KOH-activated carbons derived from yellow mombin fruit stones*, J. Env. Chem. Eng., **4**, 4229-4236 (2016)

[1.16] Y. K. Kim, G. M. Kim, J. W. Lee, *Highly porous N-doped carbons impregnated with sodium for efficient CO_2 capture* J. Mater. Chem. A, **3**, 10919-10927 (2015)

[1.17] Z. Zhou, C. He, J. Xiu, L. Yang, C. Duan, *Metal-Organic Polymers Containing Discrete Single-Walled Nanotube as a Heterogeneous Catalyst for the Cycloaddition of Carbon Dioxide to Epoxides*, J. Am. Chem. Soc., **137**, 15066-15069 (2015)

DECLARATION

As primary author of this publication, I can confirm the majority of the work to be my own, with additional contributions from Dr Alex Greenaway in the areas of zeolites and molecular organic frameworks.

Signature: _____

PUBLICATION 1

The Potential Applications of Nanoporous Materials for the Adsorption, Separation and Catalytic Conversion of Carbon Dioxide

Gregor Sneddon, Alex Greenaway, and Humphrey H. P. Yiu

DOI: 10.1002/aenm

Advanced Energy Materials, **2014,** Volume 4, 1301873

Abstract

Carbon Capture and Storage (CCS) technologies aiming at tackling CO_2 emission have attracted much attention from scientists of various backgrounds. Most CCS systems require an efficient adsorbent to remove CO_2 from sources such as fossil fuels (pre-combustion) or flue gas from power generation (post-combustion). Research on developing efficient adsorbents with a high capacity, high stability and good recyclability has grown rapidly in the past decade. Because of their high surface area, highly porous structure and high stability, various nanoporous materials have been viewed as good candidates for this challenging task. In this progress report, recent developments in several classes of nanoporous materials (zeolites, metal organic frameworks MOFs, mesoporous silicas, carbon nanotubes and organic cage frameworks) for CCS are examined, as well as possible future directions for CCS technology. The main criteria for a sustainable CO_2 adsorbent for industrial use are also rationalized. Moreover, catalytic transformations of CO_2 to other chemical species using nanoporous catalysts and their potential for large scale Carbon Capture and Utilization (CCU) processes are also discussed. Application of CCU technologies not only avoids any potential hazard associated with CO_2 reservoirs but also allows possible recovery of some running cost for CO_2 capture by manufacturing valuable chemicals.

1. Introduction

The emission of CO_2 from industry and power plants has become a worldwide problem with its strong link to global warming. It has been predicted by the International Panel for Climate Change (IPCC) that by the year 2100, the mean global temperature could rise by as much as 1.9°C.[1] Increasing our reliance on renewable energy sources and refining the energy production processes using fossil fuels have provided some hope on reducing these problems associated with greenhouse gases, but they may not be enough to avert the rise in CO_2 levels, which has recently reached a landmark of 400 ppm level.[2] Therefore, development of CO_2 capture, storage and utilization (CCSU) techniques seems to be one obvious solution.[1] However, one of the main problems associated with carbon capture and storage (CCS) is the fact that the process itself requires a certain amount of energy consumption, which leads to further emission of CO_2.[3] Therefore, the aim of CCS is that through the development of more advanced CO_2 adsorption/absorption and adsorbent regeneration techniques this energy offset can be reduced, leading to a net reduction in CO_2 emission.

The energy sector accounts for the largest contributor to CO_2 emission (e.g. ca. 40% of the total emission in the UK in 2011).[4] Utilizing post-combustion CO_2 capture is important in order to lower the CO_2 emissions from large point sources of CO_2 such as power stations. To achieve this, an adsorption unit filled with a material (adsorbent) of high CO_2 absorption capacity can be integrated into the design of a new power plant or retro-fitted into suitable existing power stations. The captured CO_2 will then be either transported to designated CO_2 reservoirs for storage or converted into other chemicals via carbon capture and utilization (CCU) technologies, which are still yet to be developed on an industrial scale.

In this Progress Report, several families of nanoporous solids (including both "*microporous*" and "*mesoporous*" according to IUPAC's definition) will be introduced. These materials all have a high surface area and pore volume for CO_2 adsorption, with a number of examples showing the selective adsorption towards CO_2 from a mixture of gases. The critical characteristics of the materials for an efficient CO_2 adsorbent will be laid out and the advantages and limitations of these materials to be used on an industrial scale will be discussed. The potential of CCU technologies associated with nanoporous materials as catalysts will also be highlighted.

2. Criteria for CO_2 Adsorbent Materials

At a low pressure, carbon dioxide behaves similar to many other gases (e.g. N_2 and Ar) in terms of adsorption onto a surface of a non-porous solid, following closely to the Langmuir model. Therefore, in theory, a solid-state adsorbent with a high surface area will have a high CO_2 adsorption capacity, but also a high adsorption capacity toward other gases (e.g. N_2) due to non-specific adsorption. As such, the adsorption efficiency of an adsorbent for CO_2 will be significantly reduced when the CO_2 content is low in a mixture of gases because of competitive adsorption against other major gaseous components. In a typical flue gas from a power station, CO_2 content is only ca. 13 % (coal-fired stations) to 8 % (gas-fired stations).[5] As a result, in order to achieve a high CO_2 adsorption efficiency, the adsorbent for post-combustion capture needs to have a high selectivity towards CO_2 over other gases present in the gas stream notably N_2 and H_2O. To design efficient adsorbents for CO_2, two common strategies are currently used, one targeting the physical property of CO_2 in terms of molecular dimensions and the other exploiting its chemical properties.

2.1 CO_2 Capture by Size Exclusion

To separate CO_2 from other gases in a mixture, a technology termed size exclusion can be used, based on the difference in molecular dimensions of the components in the mixture.[6] Size exclusion exploits the permeability theory but it is largely used to separate larger molecules in liquid phase, such as dialysis for the purification of biomolecules. The principle of separation for CO_2 relies strongly on the size, shape, connectivity and even the topography of the pores of an adsorbent material to create a stronger interaction towards one specific component in the mixture due to the close proximity of the surface to the target gas molecules.[6] Zeolites, a family of microporous crystalline materials, have been widely used for this purpose due to their distinctive pore size/structure. Providing that they have distinctive pore dimensions, other microporous materials (e.g. carbon nanomaterials, metal organic frameworks) should also be capable for such separation.

2.2 Carbon Capture by Acid-Base Neutralization

Chemical properties of CO_2 can also be exploited for selective adsorption. Carbon dioxide can be considered as a weak acid and thus react readily with a base to form carbamates and carbonates, following the equations:

$$CO_2 + 2MOH \rightarrow M_2CO_3 + H_2O \quad (1)$$

$$CO_2 + 2R^1R^2NH \rightleftharpoons R^1R^2NCOO^- + R^1R^2NH_2^+ \quad (2)$$

$$CO_2 + H_2O + R^1R^2NH \rightleftharpoons HCO_3^- + R^1R^2NH_2^+ \quad (3)$$

where MOH is an inorganic base (metal hydroxide) and R^1R^2NH is an organic base, e.g. an amine.[7] Since most other components (N_2, H_2O, unreacted O_2 and hydrocarbons) in the flue gas are neutral, use of an adsorbent of a basic nature can selectively adsorb acidic gas like CO_2. However, there are two major issues to be considered for using a base as an adsorbent for CO_2. First, CO_2 is not the only acidic component in the flue gas. The other major acidic gas sources are SO_2 (if the flue has a high sulfur content) and NO_x. Increasing the concentration of these two acidic gases will reduce the efficiency of the CO_2 adsorption. Also, the adsorption force of CO_2 onto these basic adsorbent cannot be too strong so that the downstream removal of CO_2 and regeneration of active sites for adsorption is possible. For example, inorganic bases, such as calcium oxide CaO, have a high affinity towards CO_2, as well as other acidic species, but regeneration of these adsorbent is problematic (e.g. low regeneration efficiency) and energy intensive.[8] For example, regeneration of CaO requires a high temperature of 900 °C and at this temperature, the surface area of the adsorbent is likely to reduce due to sintering, hence reducing the adsorption capacity and efficiency. Therefore, much research is currently directed towards the use of organic bases, which tend to be easier in regeneration at a low temperature but retain a high degree of affinity towards acid gases such as CO_2.[9]

Aliphatic amines are among the most popular choice of organic bases as adsorbents for CO_2 adsorption via neutralization to form carbamates (see **Figure 1**). These can be free amine molecules,[10] supported polyamine polymers,[11] and grafted amine groups on a support material.[12] Regardless of the form of amine, the principle of neutralization is essentially the same. For supported amine adsorbents, the adsorption efficiency highly depends on the basicity, the concentration of these basic sites and their accessibility, which can also be influenced by the structure of the support materials such as porosity and pore connectivity of the support.

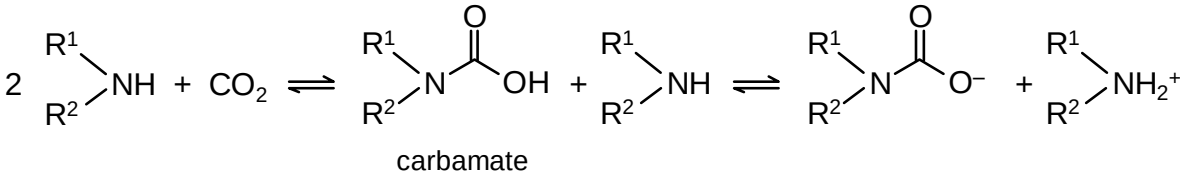

Figure 1. A 2-step formation of carbamate from amines and CO_2.

2.3 Measuring the Capacity and Efficiency of a Sorbent for CO_2

To compare adsorption capacity and efficiency, standard methods with comparable parameters (reaction conditions including temperature and pressure) have been established. For solid adsorbents, it is common to measure the CO_2 adsorption capacity from a standard adsorption-desorption isotherm using pure CO_2. This can be carried out at 25 °C (298 K), 0 °C (273 K) or -78.5 °C (194.5 K) and a pressure of 1 atm (760 mmHg) or higher (*ca*. 5 atm). In general, the lower the adsorption temperature, the higher the adsorption capacity will be. However, some works report experiments carried out at a higher temperature (e.g. 75 °C) to mimic the flue gas condition or at higher pressures. **Table 1** provides a comparison on the properties of various nanoporous adsorbent types considered to be suitable for CO_2 adsorption.

Nanoporous material	Typical range of capacity [mmol g^{-1}] at 1 bar, 25°C	Adsorption mechanism	Quantity produced per batch	Reference
Zeolites	1.5 – 4.0	Interaction with metal ions (e.g. K^+, Na^+)	Tonnes	[13]
MOFs	1.0 – 7.0	Physisorption and chemisorption	100 – 500 mg	[14]
Mesoporous silica	1.0 – 2.0	chemisorption onto basic groups (e.g. amines)	1 – 5 g	[13]
Carbons (CNT, mesoporous carbon)	0.5 – 3.0	Physisorption (except amine-functioanlized CNT)	< 1 g	[13]
Organic cage framework (OCFs)	1.0 – 5.0	Physisorption and chemisorption	< 1 g	[15]

Table 1. Comparison on the CO_2 adsorption properties among nanoporous materials

For basic adsorbents using neutralization, the maximum CO_2 adsorption capacity can also be estimated stoichiometrically, assuming 100% efficiency. For instance, the CO_2 adsorption capacity of calcium oxide CaO can be estimated to be *ca.* 17.86 mmol g^{-1} using the following equations:

$$CaO + CO_2 \rightarrow CaCO_3 \quad (4)$$

$$CO_2 \text{ adsorption capacity (in mmol g}^{-1}) = \frac{\text{sorbent/CO}_2 \text{ stiochiometric ratio}}{\text{formular weight of sorbent}} \times 1000 \quad (5)$$

Using this method, we can estimate the maximum capacity of all bases, liquids or solids. Therefore, ammonium hydroxide solution (ca. 30 % w/w) will have a maximum CO_2 adsorption capacity of 8.8 mmol g^{-1}, while that of BeO solid can be as high as 37.0 mmol g^{-1}, which is probably the material available with the highest theoretical CO_2 adsorption capacity *via* neutralization. Unfortunately, this estimation assumes a 100 % stoichiometric reaction and it is unlikely to happen, particularly for solid, non-porous adsorbents such as CaO, due to the accessibility of sites. Therefore, the experimental data are usually much lower than these values. For amine adsorbents, normally it is assumed that two amine groups will react with one CO_2 molecule to form the more stable carbonate species (see **Figure 1**). Therefore, the N/CO_2 ratio provides a certain degree of indication on how efficient an amine-based adsorbent is. On the other hand, the efficiency of CO_2 adsorption for an adsorbent can be derived from the experimental and theoretical maximum adsorption capacity as follows:

$$\text{adsorption efficiency (\%)} = \frac{\text{experimental capacity}}{\text{theoretical maximum capacity}} \times 100\ \% \quad (6)$$

This value indicates how many basic sites, such as the number of amine groups on a polymer, are engaging with CO_2 molecules.

2.4 Other Considerations

In addition to the adsorption characteristic, there are several factors regarding practicality for a material to be a suitable adsorbent for CCS applications. For example, (i) the adsorbent material needs to be easily regenerated, and reusable, (ii) the material should be stable (physically and chemically) under the operational conditions; this includes thermal stability and moisture sensitivity, (iii) the material needs to be readily available and economically viable (e.g. BeO shows a high theoretical adsorption

capacity but beryllium is a rare element, so large-scale applications become unlikely), (iv) the manufacture of adsorbent can be scaled up, and (v) the material has to be of low toxicity, easy to handle and harmless to the environment upon disposal. All these factors are also influenced by the size of the operation, type and design of the power station, and other environmental factors.

3. Current CO_2 Capture Technology in Industries

In the industrial sector, the most widely applied CO_2 separation technology would be chemical *absorption* (instead of adsorption on solids) with an aqueous solution of alkanolamines such as monoethanolamine (MEA) and diethanolamine (DEA). These amine solvents reacts readily with acidic gases including CO_2, making them popular CO_2 absorbents.[10] However, complications associated with the use of liquid amines such as corrosion on equipment, oxidative degradation of absorbents, flow problems caused by increasing viscosity with fast-reacting amines and relatively high energy consumption[16] suggest that this method is far from ideal. In addition, since most CO_2 absorption systems are designed as stripping columns, the overall efficiency of the conventional stripping tower is subject to mass-transfer limitations (See **Figure S1**).

Among these amine solvent systems, the most extensively used in CO_2 absorption is the MEA absorption process, e.g. post-combustion removal of CO_2 from the flue gas stream in the natural gas industry. In this absorption process, the MEA solution is required to be contacted with the flue gas in an absorber column, reacting with CO_2 to form MEA carbamate in solution. The CO_2-rich MEA solution is then sent to a stripper where the solution is reheated to release pure CO_2.[17] However, this is an expensive process as it requires an intensive energy input for absorbent regeneration and large process units. In the literature, it estimated that the heating cost during solvent regeneration constituted up to 70 % of the total operating costs in a CO_2 capture plant.[18] Considering all these problems associated with amine solvent absorptions, the next generation of CO_2 capture systems are rapidly required for advancing CCS technologies.

4. Nanoporous Materials for CO_2 Capture

One possible solution to overcome the limitations of current liquid amine processes is using solid adsorbents instead. Generally, solids are easier to handle and impose fewer problems associated with corrosion. In order to maximize the adsorption capacity, these

solids need to possess a high specific surface area (surface area per mass of material, in m^2g^{-1}). Because of this reason, nanoporous materials will be among the most suitable solid adsorbents for CO_2. These materials usually have a high specific BET surface area (500 – 2000 m^2g^{-1}) and a high pore volume (0.5 – 1 cm^3g^{-1}), leading to a high theoretical adsorption capacity. **Figure 2** shows an illustrative comparison on the pore size for selected nanoporous materials. Also, many of these materials (e.g. carbon and silica based materials) are thermally stable up to 150 – 200 °C, an essential property for post-combustion capture as the discharged flue gas from a power plant can be at an elevated temperature (40 – 120 °C).

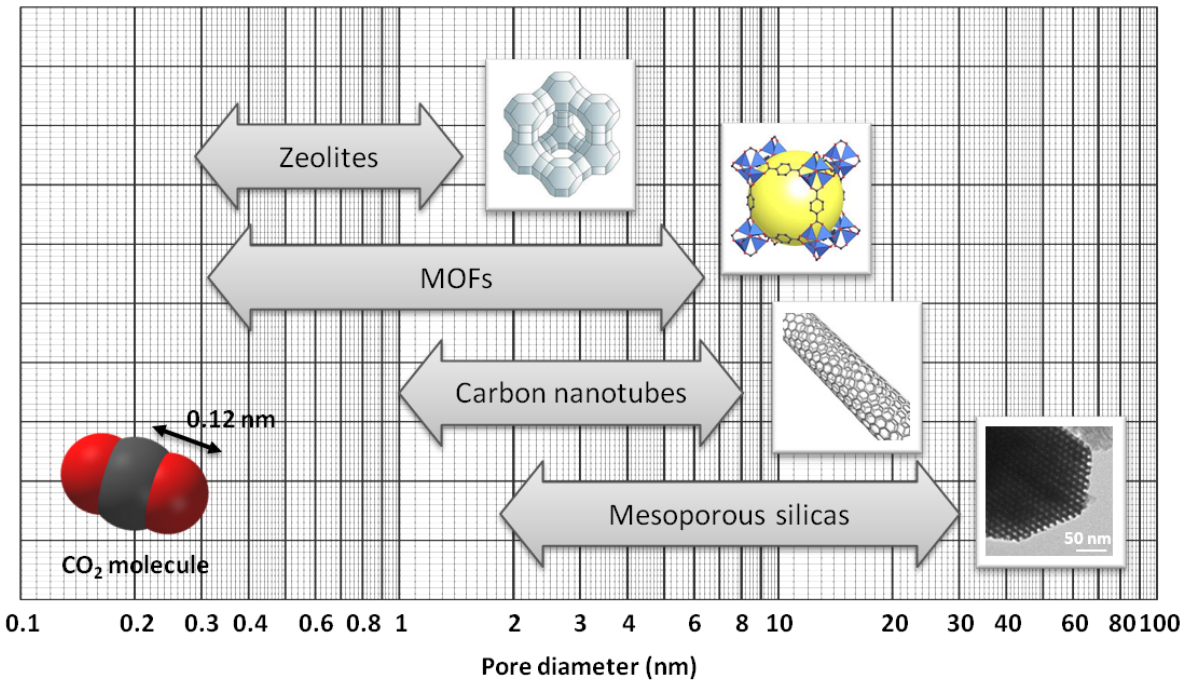

Figure 2. Illustrative comparison on the pore size of several common nanoporous materials.

4.1. Zeolites

Zeolites are aluminosilicate minerals with ordered, nanoporous structures. They can be found naturally, prepared industrially or synthesized in laboratories. Because of their high surface area (e.g. 571 m^2g^{-1} for zeolite 13X), specific porous structures and availability in large quantities, zeolites have been widely used in industry as adsorbents and catalysts. The pore size of zeolites is usually ranging from 3 – 12 Å (0.3 – 1.2 nm). Inside the smaller pores, guest molecules (adsorbates) of a comparable size can strongly interact with the walls of the pores. Structures of selected zeolites (X, Y, A, and rho)

are shown in **Figure 3a**. Considering the size of a CO_2 molecule (ca. 5.4 Å in length and 3.1 Å in diameter), zeolites with a pore size of 4 – 5 Å can be highly affinitive to CO_2. However, similar attractive forces can also be seen towards other gaseous adsorbates such as N_2 and H_2O. Therefore, the basicity of zeolites becomes the key property for selective adsorption of CO_2 over N_2 and H_2O.

The basicity of a zeolite can be created by ion exchanging with cations of alkali metals (Group 1A). Usually, the basic strength increases following the order: $Cs^+ > Rb^+ > K^+ > Na^+ > Li^+$.[19] However, this trend does not always reflect the CO_2 adsorption capacity of a cation exchanged zeolite. For example, a study on cation exchanged ZSM-5 zeolites showed the CO_2 adsorption capacity with the order of $Li^+ > Cs^+ = Rb^+ > K^+ = Na^+$ at 303 K (30 °C) and $Rb^+ > K^+ > Na^+ > Li^+ > Cs^+$ at 333 K (60 °C), both measured at 200 kPa (*ca*. 2 atm).[20] This is because the size of cation affects their distribution in the pores of zeolites while their polarity also affects the polarization of adsorbed CO_2.[21] Another factor influencing the CO_2 adsorption capacity of a zeolite is the Si/Al ratio, which is also related to the total cation exchange capacity, leading to the total amount of cations in the structure. A lower Si/Al ratio (see Note in SI) gives a higher cation exchange capacity and therefore more cations will be available for interacting with the CO_2 molecules, hence a higher adsorption capacity. Moreover, the pore size of zeolites also has an effect on the CO_2 adsorption capacity, as well as the rate of adsorption. At a low pressure, such as ambient pressure, smaller pores tend to show a higher affinity to CO_2 over N_2 and O_2, based on a study using zeolites A, X and Y as the adsorbents.[22]

Recently it has been discovered that some small pore zeolites show an enhanced ability to selectively adsorb CO_2 over N_2 or CH_4 due to a "molecular trapdoor" mechanism.[23] Zeolites exhibiting this molecular trapdoor mechanism contain super cages that are accessible through eight-membered rings (8MR)[24] or double eight-membered rings (d8MR).[25] The windows formed by the 8MR or d8MR are large enough to allow small molecules such as N_2, O_2, CO_2 and CH_4, to pass through, but these windows become effectively blocked by cations which adopt the energetically most favorable position at the center or face of the window. For a molecule to pass through the window the cation has to first move away from its position and this is achieved by a favorable interaction between the cation and certain guest species.

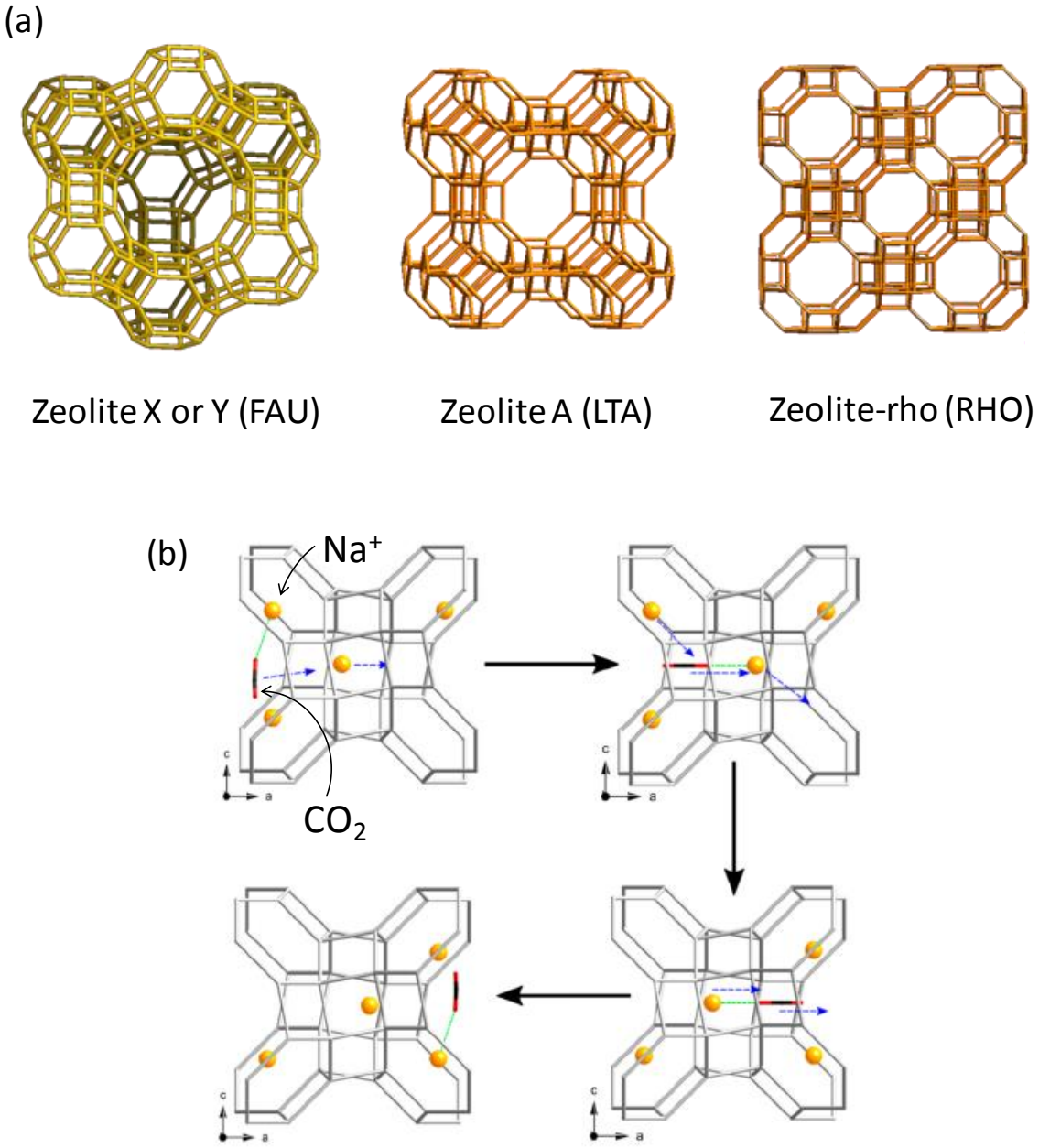

Figure 3. (a) Structures for zeolite X and Y (both have the same faujasite FAU structure), zeolite A, and zeolite-rho (structures from IZA Structure Commission, www.iza-structure.org). (b) Postulated cooperative mechanism by which CO_2 molecules (represented by red and black sticks) could pass through a window site between a-cages in zeolite Na-rho, where a Na^+ cation (yellow sphere) occupies one of the S8R sites in the window. Reproduced with permission.[25] Copyright 2012, American Chemical Society.

This temporary and reversible trapdoor mechanism starts as a closed gate becoming opened when the "gate keeping" cation interacts favorably with a guest species causing a reduction in the energy barrier and moving away from the center of the window. When the cation is situated at the "open" position, guest species molecules are capable to pass through the window and move into the next cavity within the zeolite structure. As the guest molecules diffuse into the adjacent cages inside the zeolite, the force holding the cation at the open position decreases and the cation moves back to its original position, closing the gate (See **Figure 3b**). This trapdoor mechanism will only occur with guest species that can interact strongly and favorably with the gate keeping cations, such as CO_2 with K^+, and it will not occur with weakly interacting species such as N_2 and CH_4 as the energy barrier is too high to cause the cation to move away from the gate keeping site. Since such selectivity depends on the interaction between the gate keeping cation and guest species (CO_2 in this case) rather than the size of the guest species, molecular trapdoor zeolites allow for the possibility of inverse size discrimination so should be viewed as an independent selection mechanism that is separated from the molecular sieving (or size exclusion) mechanism. The high levels of selectivity exhibited by the molecular trapdoor zeolites reported so far suggest that other zeolites that contain 8MR or d8MR such as zeolite A (LTA)[26] and ZK-5[27] may also exhibit similar adsorption properties.

The conventional method to analyze the performance of a zeolite sample, as well as most newly developed adsorbent materials, as a potential CCS material is to acquire gas isotherms at a set of relevant temperatures and pressures for the gases present in the mixture from which CO_2 is to be removed. However, as has been suggested, relevant temperatures and pressures for different systems can vary widely. For example, conditions for post-combustion capture, where the major separation is between CO_2 and N_2, are significantly different from that for pre-combustion capture, where CO_2 is to be separated out from H_2 or CH_4. Indeed even among post-combustion capture systems at different power stations there can be subtle differences, such as the CO_2 concentration in flue gas from a gas-fired station to that from a coal-fired station as discussed earlier. These issues coupled with the advanced synthesis methods to rapidly generate a variety of cation exchanged species (e.g. K^+ and Na^+) of many different zeolites mean that a large quantity of gas adsorption isotherm data need to be collected for a comprehensive analysis on one single type of materials.[25] Therefore a significant bottle-neck for CO_2 adsorption studies using new zeolite-based adsorbent materials is the availability of

access to efficient gas adsorption instrumentation. As a result instrument manufacturers are attempting to develop automated high throughput gas adsorption analyzing units. One notable example of which is a volumetric technique that can analyze 28 samples in parallel recently developed by Wildcat Discovery Technology Inc.[28] This apparatus has recently been demonstrated in a high throughput study of cation exchanged forms of zeolites Na-A (LTA) and Na-X (FAU) for use in CCS, with the results acquired from the high throughput analyzer validated against data acquired from a conventional Micromeretics ASAP® 2020 gas adsorption analyzer.[29]

Zeolites have already been widely used in many industrial processes. However, their application in CO_2 capture from power plant flue gas has not been as successful. This is likely because zeolites can be deactivated by moisture, leading to a significant reduction in CO_2 adsorption capacity. One possible explanation for this phenomenon is that water can reduce the strength of the local electric field on the cation sites.[30] Since water is an inevitable product from combustion, cation exchanged zeolites are considered to be ineffective unless the moisture content is removed prior to CO_2 adsorption, or prevented from entering the zeolite by some other means. There are, for example, several reported attempts at forming a "water proof" coating for zeolites which have had a highly hydrophobic surface layer chemically bound to the zeolite crystallites in a post-synthetic process.[31]

4.2. Metal-organic Frameworks (MOFs)

Metal organic frameworks (MOFs) are ordered structures constructed with both inorganic and organic species. In general, MOFs are comprised of transition metal ions, free or in clusters, interconnected with organic 'struts', or ligands.[32] These organic ligands are usually molecules with aromatic groups (providing rigidity) terminated with functional groups capable of coordinating to these metal ions (coordination bonds). The functional groups can be carboxylic acid groups [33] or heterocyclic aromatic rings incorporated with nitrogen atoms (e.g. pyridine),[34] but other coordinating functional groups such as phosphonates have also been used to form MOFs.[35] Many MOF systems show nanoscale porosity, resulting in a large internal surface area, with a variety of window sizes.[32] Similar to zeolites, these properties can lead to a wide range of applications, including: drug delivery, chemical sensing, ion exchange, chemical catalysis, molecular separations and gas storage.[32] One of the major advantages of MOFs over other solid porous adsorbent materials is the possibility to

tune systems to carry out a particular task by varying the size and nature of the components used in the synthesis. For example, the pore size of a MOF system can be controlled by changing the length of the struts. The ability to generate a whole series of MOFs sharing the same type of connectivity is known as "isoreticular" synthesis and notable examples include the MOF-5 (structure shown in **Figure 4a**)[36] and NOTT-11 series.[37] Such unique structural tunability of MOFs enables them to be considered as promising candidate materials as adsorbents for CCS applications, and therefore, many studies in this area can be found in the literature.[38-41]

For instance, MOFs have been studied for selective CO_2 adsorption over N_2. As pointed out previously, in post-combustion CO_2 capture the primary gas separation occurs between CO_2 and N_2 at a slightly elevated temperature of around 40 °C (313 K) and at ambient pressure. The composition of the flue gas varies depending on the hydrocarbon source, but a typical composition is 15 % CO_2, 75 % N_2, 7 % H_2O with the remainder being made up with contaminants such as SO_x, NO_x, O_2 and CO. For the purpose of post-combustion CO_2 capture, an idealized material would exhibit a high selectivity to CO_2 over N_2 as well as a good volumetric and gravimetric uptake of CO_2. With these requirements, several MOFs performed well, with the isomorphous CPO-27 series showing very high levels of uptake with a good selectivity[42] while HKUST-1 (structure shown in **Figure 5b**) giving one of the best selectivities,[43] calculated by dividing mass of CO_2 at 0.15 bar by mass of N_2 at 0.75 bar.[44]

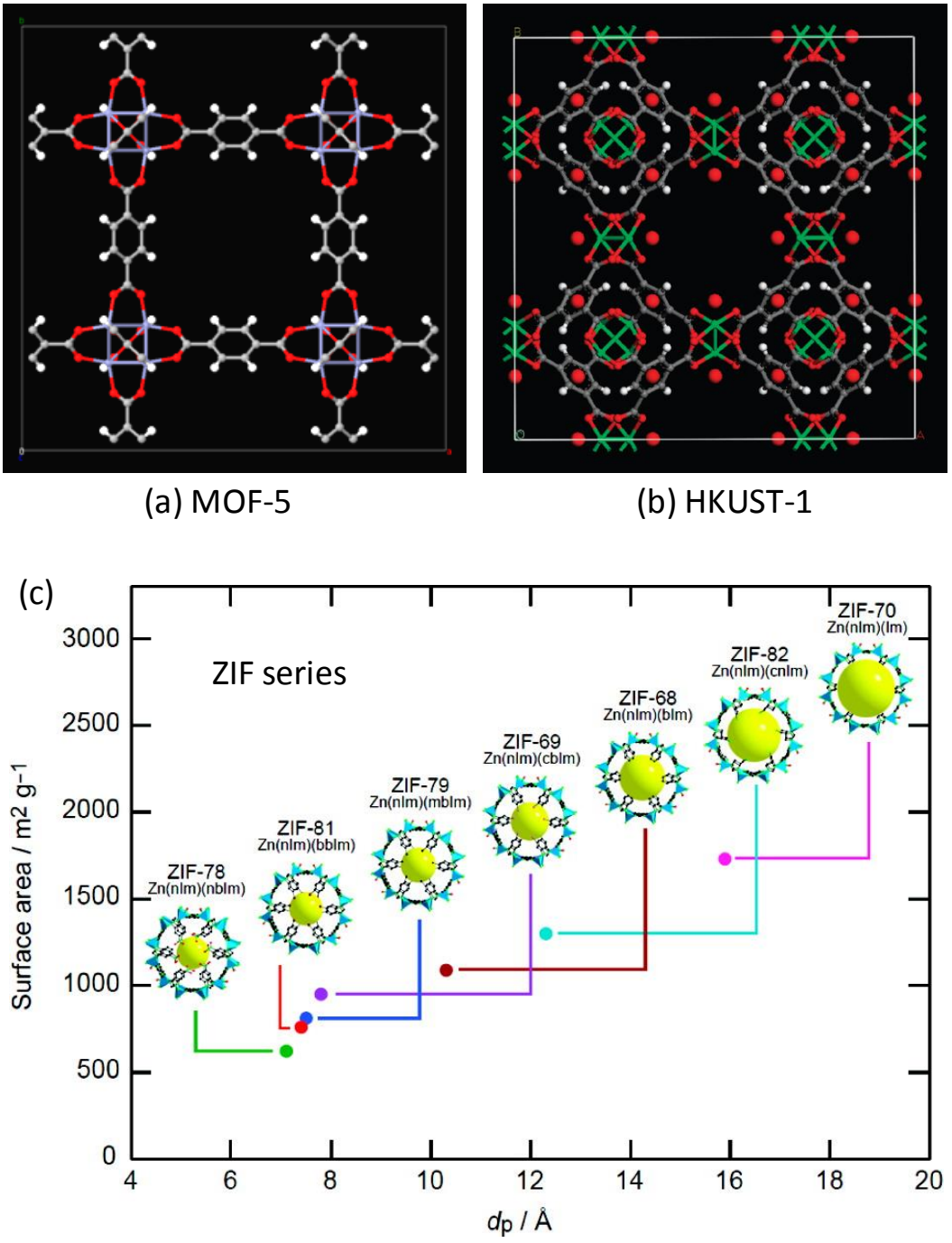

Figure 4. The structure for (a) MOF-5 (structure from MOFomics structure simulation website) and (b) HKUST-1 (reproduced with permission [55]). (c) Plot of pore diameter (d_p) *vs.* surface area for the ZIF series, indicating a nearly linear relationship. Among them, ZIF-78 showed the highest selectivity for CO_2 over N_2 (S = 396), see **Table 2**. To illustrate the variation of the poresize and functionality, the *kno* cage of each ZIF is shown in yellow(reproduced with permission [53]).

One method that has been investigated in detail as a route to improve CO_2 against N_2 selectivity is to generate MOFs with functionalized pores, as the addition of polarizing groups enhances interactions with the CO_2 molecules. For example, a study on using cobalt adeninate bio-MOF's for selective adsorption of CO_2 was reported by An et al. With the multiple nitrogen Lewis base groups, adenine showed a high capacity for CO_2 uptake. The basic nature of the coordinating ligand allowed a CO_2:N_2 selectivity of 81:1 at 0 °C and 75:1 at 25 °C, with a total CO_2 adsorption capacity of 6 mmol g^{-1} and 4.1 mmol g^{-1} at 0 °C and 25 °C respectively.[39] Other example of MOFs, triazolate-bridged systems functionalized with ethylenediamine, were also studied for selective CO_2 adsorption at low pressure.[40] These MOF systems showed excellent stability in moist and acidic conditions, an advantage over most zeolite adsorbents. Combined with the improved low-pressure performance over the standard triazolate-bridged MOFs, they are ideal for dealing with real flue gas environments. At pressures of up to 0.06 bar (6 kPa, *ca*. 0.06 atm) CO_2 the ethylenediamine modified MOFs showed an enhanced capacity of 0.366 mmol g^{-1} from 0.277 mmol g^{-1} for the standard sample, an improvement of over 30 %.[40]

MOFs with small pores showing selectivity based upon a molecular sieving principle are less common as the pore dimension needs to be finely tuned to allow CO_2 but not N_2 or CH_4 to diffuse into the framework. However, a recent investigation into the functionalized forms of Sc_2BDC_3 (scandium terephthalate) yielded interesting results for the -NO_2 (nitro) functionalized framework.[45] Interestingly, the single crystal structure of -NO_2 functionalized Sc_2BDC_3 suggested that it does not appear to contain any pores large enough to allow CO_2 or N_2 to adsorb. Nonetheless, it does show appreciable CO_2 uptake (*ca*. 1.0 mmol g^{-1} at 25 °C) while it adsorbs a negligible amount of N_2, making it an extremely selective MOF system for CO_2 against N_2. The possible explanation for such selectivity exhibited is a size exclusion process in which the -NO_2 groups effectively block the pores to the bulbous N_2 molecules while the longer more polarizing CO_2 molecules are able to manipulate the -NO_2 groups enough to move through the pores and become adsorbed inside the MOF structure.

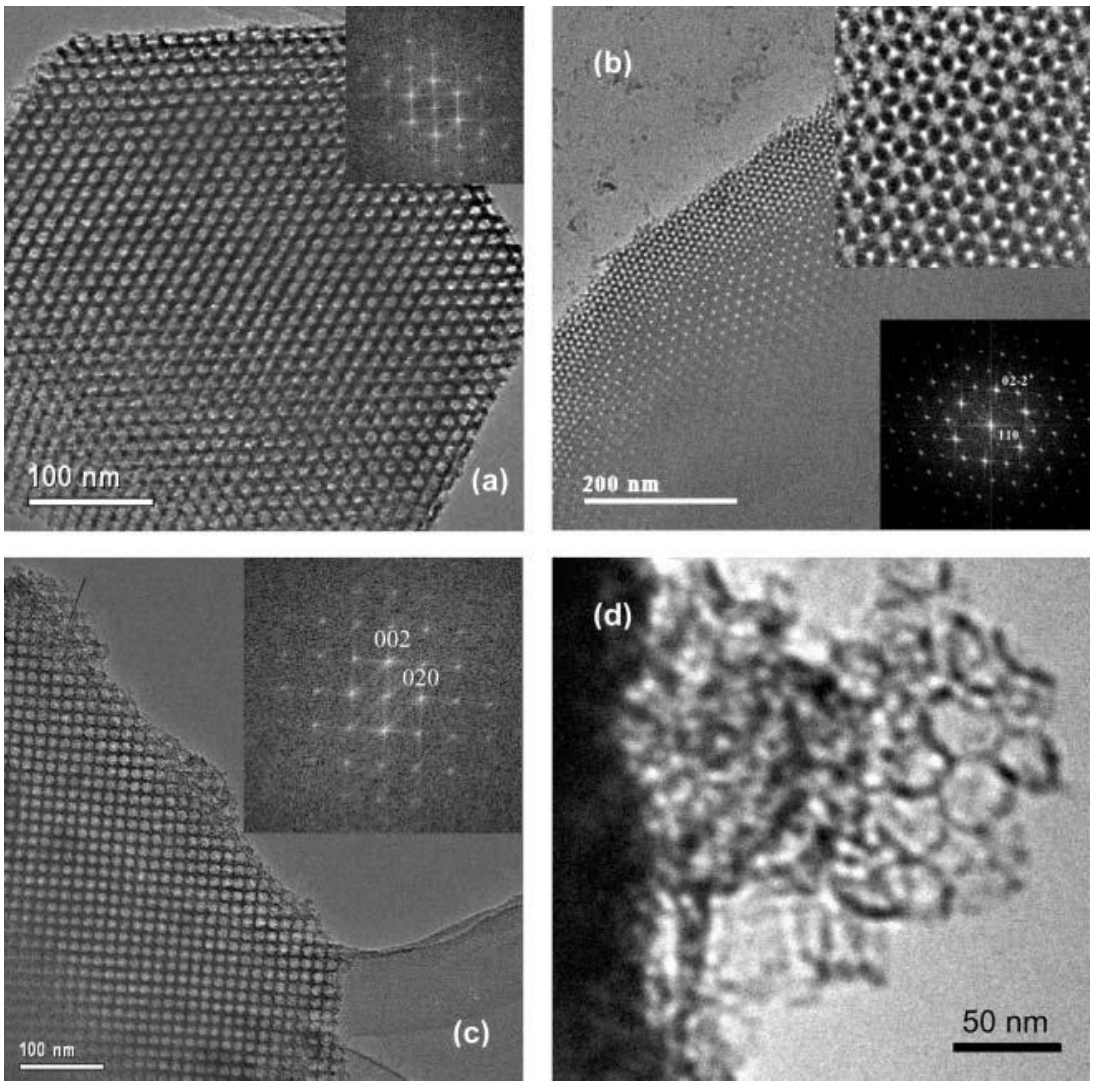

Figure 5. TEM micrographs showing structures of (a) SBA-15 (*p6mm*), (b) FDU-5 (*Ia*$\bar{3}$*d*), (c) FDU-12 (*Fm3m*) and (d) MCF. Reproduced with permission.[64] Copyright 2005, Royal Society of Chemistry.

For pre-combustion CO_2 separation, the primary gas separation required is different from that in post-combustion CCS, and therefore the requirements/properties of the adsorbents also changes. For example, in pre-combustion, the major separation is between CO_2 and H_2 and arises after a hydrocarbon source having undergone a syngas shift followed by a wet syngas transformation. The conditions for measuring the optimal adsorbent performance should be at approximately 40 $^{\circ}$C and between 5 and 40 bar pressure. It is likely that a pressure swing adsorption mechanism for the removal of adsorbed CO_2 would be most applicable to a pre-combustion CCS system. Therefore a material showing a low initial uptake can be beneficial as it would not require the system to undergo a significant pressure drop to release the stored CO_2.[46]

As we can appreciate, the ability for selective CO_2 adsorption in a gaseous mixture determine whether a MOF system is a suitable candidate for use in CCS, as well as having a scalable synthesis and ability to adsorb/desorb CO_2 in a rapid timescale. However, experimentally it has been difficult to directly measure adsorption selectivity, between CO_2 and N_2 for example, and methods to study adsorption-desorption cycles on small samples have been lacking. Recently, there has been some progress made in both of these areas, enabling more thorough investigation of MOFs for use in CCS. Similar to assessing zeolites, CO gas adsorption at a chosen temperature is commonly used for studying the CO_2 adsorption property for MOFs. Such studies can be carried out either gravimetrically (in which the mass of the sample is measured as it increases due to adsorbed gas) or volumetrically (in which the sample is exposed to a certain dose of the adsorbate gas and the difference between the equilibration pressure is measured, yielding the amount of the gas adsorbed). Unfortunately, gas adsorption isotherms can only be measured using single gas components as it is impossible to deconvolute results obtained when a multi-component system is used. As mentioned previously, adsorption selectivity for simulated post combustion systems is often estimated indirectly by dividing the uptake of CO_2 at 0.15 bar by the uptake of N_2 at 0.75 bar.[44] This method could lead to uncertainty and inaccuracy as the adsorption behavior of an adsorbent can be different at a multi-component gaseous environment.

Recently scientists working on MOFs have reported a "breakthrough" (the course for a gas to go pass a bed of adsorbent) experiment for studying the separation of CO_2 from mixtures in N_2 or CH_4.[47,48] During this new experiment a column was packed with pelletized sample, which is then purged with an inert gas (e.g. He) to remove any water or other adsorbed species. The sample was then exposed to a stream of gaseous mixture, such as 15 % CO_2 with 85 % N_2. The composition of the gas flow exiting the column was then monitored by mass spectrometry. As such, it was possible to calculate retention times of the gas components exposed to the sample and therefore their relative adsorption properties (see **Figure S2**). By conducting a series of these breakthrough experiments, van Baten *et al.* compared the CO_2 capture characteristics of several MOFs and zeolites.[47] Among the MOFs tested, only Mg-MOF-74 consistently outperformed the majority of the zeolites selected for the study.

One of the major advantages for using these breakthrough experiments over commercial volumetric or gravimetric adsorption techniques is the much shorter time

required to run a dynamic separation from a mixed gas composition. Depending on the sample and experiment protocol, a breakthrough separation can occur on a few minutes timescale (as opposed to approximately a day to complete an adsorption-desorption isotherm), which allows for repeated experiments to be conducted after a regeneration period, usually at elevated temperatures under inert gas flow (e.g. 150 °C under flowing He). This also allows two further critical performance criteria to be investigated. First, regeneration capacities of the sample can be studied as a function of temperature or number of cycles. Furthermore the level of humidity present in the gas streams can be regulated enabling studies on any potential loss of adsorption performance due to water. For example, Remy *et al.* have reported that the performance of Mg-MOF-74 decreased upon the cycling of humid CO_2 in a linear manner as the number of cycles increased, a result which could have important ramifications for the suitability of Mg-MOF-74 as a potential CCS adsorbent.[48]

Another selectivity study has also been carried out by collating data from many reports on using MOF systems for CO_2 specific adsorption.[41] During separation of CO_2 from the flue gas stream using a vacuum-swing adsorption (VSA) regeneration process, MOFs were also found to be less efficient than zeolites. At specific conditions such as a 10:90 mixture of CO_2:N_2 with an adsorption pressure of 1 bar (*ca*. 1 atm) and desorption pressure of 0.1 bar (*ca*. 0.1 atm), generally, MOFs were found to have a lower CO_2 adsorption capacity than zeolites but a greater potential for regenerability. One parameter used for evaluation of the MOFs was the *sorbent selection parameter* (*S*),[49] which is a combination of the adsorption selectivity and working capacity, and is defined as

$$S = \frac{\Delta q_1}{\Delta q_2}\left(\frac{q_{m1} b_1}{q_{m2} b_2}\right) \qquad (7)$$

where q_i is the amount adsorbed (in mmol g^{-1}); q_{mi} is the monolayer saturation amount (in mmol g^{-1}); and b_i Langmuir parameter (atm^{-1}).

The *S* values of selected zeolites and MOF materials are summarized in **Table 2**. Based on these *S* values, the most promising MOF materials for CO_2 adsorption using these criteria were found to be the zeolitic imidazolate frameworks (ZIF's) as well as Ni-MOF-74. Although the CO_2 adsorption capacities for these materials were relatively low in comparison to the zeolites, their *S* values were similar. In particular ZIF-78

showed a large *S* value indicating its suitability towards flue gas treatment. **Figure 5c** shows the relationship between the surface area and the pore diameter of the ZIF series. Results from **Table 2** also suggested that both zeolite samples out performed MOFs in terms of selectivity towards CO_2, except ZIF-78. Recently, a series of MOF systems built with SiF_6^{2-} anions (SIFSIX) showed an outstanding selectivity towards CO_2 (up to1700 at 1 bar) over N_2, over 4 times higher than that of zeolite 13X.[56] Moreover, their selectivities for CO_2 over CH_4 and H_2 (350 and 1800 respectively) were also remarkable, making these SIFSIX materials suitable for both pre- and post-combustion CO_2 capture. Therefore, SIFSIX MOFs can be considered as a showcase adsorbent for carbon capture.

Absorbent	Pore size [nm]	BET surface area [m^2 g^{-1}]	CO_2 adsorption capacity [mmol g^{-1}][a)]	Sorbent selection parameter (*S*)[b)]		Reference
				CO_2:N_2 = 1:9	CO_2:CH_4 = 1:1	
Zeolite-5A	0.5	506	3.5	163	-	[50]
Zeolite-13X	0.11	616	2.49 (3.97)	128	19.1	[51]
ZIF-78	0.38	620	0.58	396	-	[52]
ZIF-79	0.4	810	0.26	83	-	[52]
ZIF-81	0.39	760	0.27	101	-	[52]
ZIF-82	0.81	1300	0.41 (1.42)	105	20.5	[52]
Mg-MOF-74	1.11	1542	(7.23)	-	23.5	[53]
Ni-MOF-74	1.11	1218	4.34 (6.23)	83.5	21.0	[53]
HKUST-1	0.35	1571	(0.62)	-	19.8	[54, 55]

a) CO_2 adsorption capacity measured at 1 atm (CO_2:N_2 = 1:9) and 25°C, values in brackets indicate CO_2:CH_4 = 1:1 conditions.

b) Using a vacuum swing adsorption process. Adsorption pressure = 1 bar, desorption pressure = 0.1 bar.

Table 2. Selectivity (sorbent selection parameters, *S*) of selected examples of zeolites and MOF systems for CO_2 against nitrogen or methane.

One of the disadvantages of using breakthrough experiments for selectivity measurements is the requirement for a relatively large quantity of sample (around 5 g) which can be troublesome to achieve for certain MOFs. Therefore to test the regeneration capabilities of MOFs on a much smaller sample size a new technique based on thermogravimetric analysis (TGA) has been successfully reported.[50] In this

work, a sample of 10% $Ni(OAc)_2/H_3PO_3$-modified Mg-MOF-74 was repeatedly cycled (10 times) in alternating flowing argon at 493 K (220 °C) and CO_2 at 313 K (40°C) in a TGA instrument, during this time the mass gain and loss for the sample was measured and used to calculate a working uptake capacity for CO_2 of 6.1 mmol g^{-1}.

In many reports, MOFs have been regarded as some of the best candidates for the ultimate task of CO_2 capture due to their high adsorption capacity, selectivity and recyclability. However, at the moment, use of MOFs for large scale processes, such as industrial catalysis and CCS, is still far from feasible. One major limitation to using MOFs is that only small quantities, usually < 1 g per batch, of the active material can be synthesized although production of a MOF material at an industrial scale has been reported.[57] Moreover, probably the least considered factor, the environmental impacts of MOFs cannot be ignored, particularly if they are to be used on an industrial scale. Many MOF systems are built using toxic transition metals (Co, Ni, Mn, Cu) and ligands (aromatic and/or heterocyclic compounds) and these materials may cause serious environmental issues upon disposal. Unfortunately, research on the environmental impacts of MOFs has been widely overlooked.

4.3. Functionalized Mesoporous Silicas

In the early 1990s, the discovery of ordered mesoporous silica materials (MCM-series, SBA-series and MCFs, structures shown in **Figure 5**)[58] opened up many new research directions in separation,[59] catalysis,[60] even biotechnology.[61] Because of their high surface area (ca. 1000 m^2 g^{-1}) and high pore volume (ca. 1 cm^3 g^{-1}), these mesoporous silicas have been used as a sorbent for many species including gases,[62] organic pollutants[63] and biomolecules.[64] Unlike zeolites and MOFs, the larger pore size (>2 nm or >20 Å in diameter) of mesoporous silicas implies that, without modification, the intrinsic interaction between the guest molecules and the adsorbent is weaker, particularly at low pressure. Moreoever, selective chemisorption of CO_2 is also difficult as the surface of mesoporous silica is covered with mildly acidic silanol groups (-Si-OH). Therefore, surface modification is required if mesoporous silicas are to be used for CO_2 capture. Generally, two possible modification routes are used for this purpose; impregnation of basic nano-sized crystals (alkaline or alkaline earth metal oxides) and grafting organic groups with basic characters such as amines.

Mesoporous silicas have been used to support transition metal oxide particles (e.g. iron oxides,[65] titania TiO_2,[66] and zirconia ZrO_2[67]) for catalytic purposes, and alkaline earth metal oxide particles (CaO[68] and MgO[69]) to provide a basic surface for CO_2 chemisorption. Although a good CO_2 capacity has been shown from these composite materials (up to 10 mmol g^{-1}), the sustainability of these composite materials is questionable. Firstly, they were synthesized from calcium and magnesium salts, which are likely to be manufactured from carbonates ($CaCO_3$ or $MgCO_3$, both are common natural minerals) with a substantial CO_2 emission, at a stoichiometric ratio of 1, in addition to the energy required to decompose the carbonates or to manufacture the strong acids (e.g. HNO_3) required for the preparation of these basic adsorbents. Secondly, regenerating materials requires a high temperature (700 – 900 °C) due to the high thermal stability of $CaCO_3$ and $MgCO_3$. Unless the source of CO_2 for capture has a high temperature and requires a thermally stable adsorbent, these materials are unlikely to be practical for most CCS applications.

Since the associated energy consumption of using purely inorganic mesoporous silicas, modified with CaO or MgO, for CCS is too high to be realistic, organic-inorganic hybrid mesoporous silicas were developed for this purpose. As early as mid-1990s, silanization methods have been introduced for the synthesis of organic-inorganic hybrid mesoporous silica, using functionalized alkoxysilanes.[70] One of the most commonly used alkoxysilanes, 3-aminopropyltriethoxysilane or APTES, has been used for grafting amine groups onto the mesoporous silica surface.[71] These basic amine groups can also provide strong affinity towards CO_2 and other acidic gases. Depending on the conditions of measurement and the preparation method, the CO_2 adsorption capacity of amine-functionalized mesoporous silica (NH_2-MCM-41, NH_2-SBA-15 or NH_2-MCF) varies from 0.5 to 2.0 mmol g^{-1} at 25 °C and 1 atm. Results from selected publications using amine functionalized mesoporous silica for CO_2 adsorption are summarized in **Table 3**. In general, the CO_2 adsorption capacity increases when the water content (either on the adsorbent surface or the gas) increases due to the formation of the protonated ammonium ions and carbonates.[87] This observation is opposite to that from cation exchanged zeolites, which can be easily deactivated by water. For post-combustion CO_2 capture from flue gas where high moisture content is likely, this could be a distinctive advantage. Furthermore, such resistance to deactivation due to water has the added benefit that supported amines on mesoporous silicas could be used in a temperature swing adsorption (TSA) CCS system based on a steam heating

regeneration cycle. This is unlikely to be applicable to either MOFs or zeolites since both can rapidly degrade in the presence of moisture.

Mesoporous silica type	Amine groups[a)]	Functionalization method	BET surface area [m^2 g^{-1}]	Pore volume [cm^3g^{-1}]	N concentration [mmol g^{-1}]	CO_2 adsorption capacity [mmol g^{-1}]	Temp [°C]	Reference
MCM-48	mono	post synthesis	-	-	2.3	2.05	25	[72]
MCM-48	penta + diethanolamine	impregnation	572	0.41	-	0.4	25	[73]
MCM-48	PEI (600)	post synthesis[b)]	58.4	0.02	5.2	0.4	25	[74]
MCM-41	mono	post synthesis	17	0.04	2.48	1.15	30	[75]
MCM-41	mono	post synthesis	239	0.04	3.0	0.57	25	[76]
MCM-41	mono	post synthesis	727	0.22	2.35	0.83	25	[77]
MCM-41[c)]	tri	post synthesis	429	1.05	7.8	2.28[d)]	25	[78]
MCM-41	PEI (423)	impregnation	11	0.03	15.5[e)]	2.03	75	[79]
MCM-41	PEI[f)]	impregnation	4.2	0.011	15.5[e)]	4.89[g)]	75	[80]
SBA-12	mono	post synthesis	416	-	2.13	1.04	25	[76]
SBA-15	mono	post synthesis	134	-	2.72	1.54	25	[76]
SBA-15[f]	mono	post synthesis	374	0.54	2.61	0.66	60	[81]
SBA-15[f]	di	post synthesis	250	0.40	4.61	1.36	60	[81]
SBA-15[f]	tri	post synthesis	183	0.29	5.80	1.80	60	[81]
SBA-15	PEI (423)	impregnation	80	0.20	15.5[e)]	3.18	75	[79]
MSU-1	penta	impregnation	0.72	0	13.23	3.87	75	[82]
KIT-6	PEI (600)	impregnation	86	0.18	17.3	1.79	25	[77]
MCF	mono	post synthesis	289	1.85	2.55	0.78	45	[83]
MCF	mono	post synthesis	407	1.3	3.4	0.8	75	[84]
MCF	di	post synthesis	183	1.21	2.46	1.25	45	[83]
MCF	tri	post synthesis	139	0.7	4.0	1.3	75	[74]
MCF	penta	impregnation	12	0.1	12.9	4.5	75	[74]
MCF	PEI (423)	impregnation	70.8	0.46	15.5[e)]	3.45	75	[85]
MCF	PEI (800)	impregnation	201	1.54	6.25	1.26	45	[83]
MCF	PEI (3335)	aziridine polymerization	350	2.12	3.48	0.51	23	[86]

Table 3. Selected studies on using functionalized mesoporous silica as the adsorbent for CO_2. All CO_2 adsorption measurements were recorded at 1 atm.

Footnotes for Table 3

[a)]key for functional groups:

mono = Pr–NH_2 (3-aminopropyl);

di = Pr–NH–CH_2–CH_2–NH_2 (N-(2-aminoethyl)-3aminopropyl);

tri = Pr–NH–CH_2–CH_2–NH–CH_2–CH_2–NH_2 (3-[2-(2-aminoethylamino) ethylamino]propyltrimethoxysilane or diethylene amine, DETA)

penta = NH_2–CH_2–CH_2–NH–CH_2–CH_2–NH_2–CH_2–CH_2–NH–CH_2–CH_2–NH_2 (tetraethylenepentamine)

PEI = –(NH–CH_2–CH_2)$_n$– (polyethyleneimine)

[b)]PEI grafted onto a propylchloride-functionalized MCM-48

[c)]pore-expanded MCM-41 using postsynthesis hydrothermal treatment with *N*,*N*-dimethyldecylamine (DMDA) at a temperature of 120 °C for 72 h.

[d)]measured at 5% CO_2 in N_2, 1 atm

[e)]estimated from 50 w/w% PEI

[f)]M_w of PEI not provided

[g)]calculated from 215 mg CO_2 g^{-1} PEI

In theory, the CO_2 adsorption capacity of an amine-functionalized mesoporous silica sample should be proportional to the amine content; at a ratio of $N:CO_2 = 2:1$, assuming that all CO_2 molecules form carbonates. Therefore, if the amine groups are to be extended to diamine or triamine groups, the adsorption capacity should be doubled or even tripled. Also, a propylamine group on APTES is relatively small (*ca.* 0.5 nm in length) when compared with the diameter of mesopores (*ca.* 2 – 10 nm). There are unused space inside these "monoamine" functionalized mesoporous silicas. Consequently, scientists had been exploiting this space by using polyamine groups, $–(CH_2CH_2NH)_n–$, to create a surface with multilayered amines for further enhancing the CO_2 adsorption capacity.[88] Unfortunately, the increase in capacity was much lower than expected.[89] There are several possible reasons. First of all, these groups can be closely packed on a concave surface with approximately 0.7 nm between groups (see **Figure 6**), while a CO_2 molecule is about 0.23 nm wide. At such a comparable dimension, the CO_2 molecules adsorbed to the amines on the outer layer may block the others from interacting with the inner amine groups. Moreover, when the density of amine groups increases, the competition for protons in a "moist" environment also increases.[90] This results in a fraction of amine groups being un-protonated (or less basic) and reduces their affinity towards CO_2.

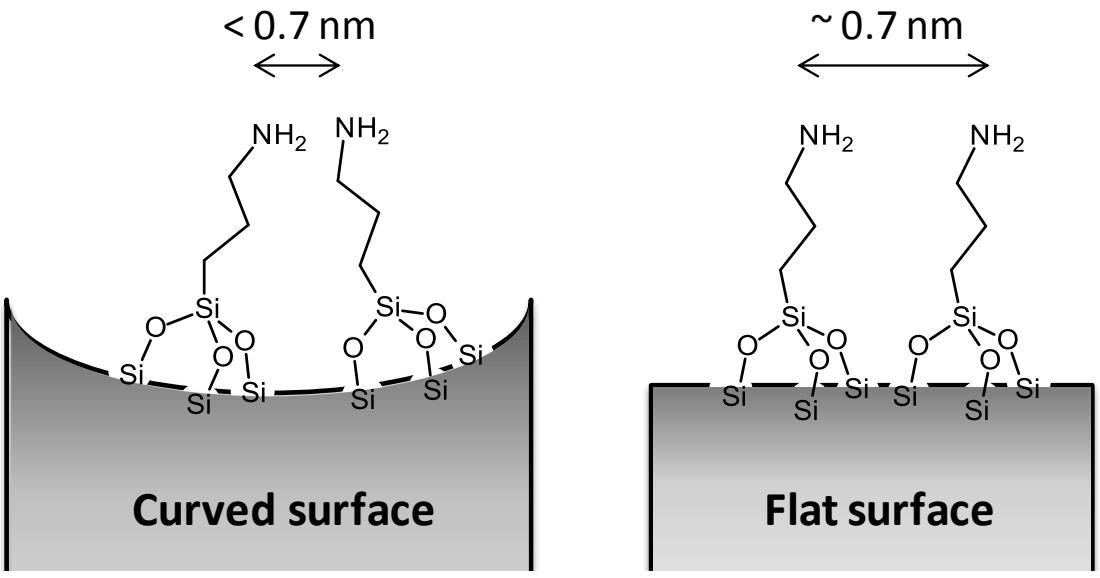

Figure 6. Schematic illustration on the distance between propylamine groups on a flat and curved silica surface.

Nevertheless, scientists still attempted to fill these mesopores with polyamines to maximize the CO_2 adsorption capacity, notably using polyethyleneimine (PEI). For example, PEI has been immobilized onto SBA-15 via the wet impregnation method and the resultant composite material show an enhanced CO_2 adsorption capacity of 4.89 mmol g^{-1}.[91] However, PEI is a water soluble polymer and these composite materials can be unstable to gas streams with a high moisture content, particularly for prolong use. Therefore, an alternative method for PEI immobilization is necessary to produce a PEI-mesoporous silica composite which is stable under a high moisture environment. For example, Drese et al. reported a procedure to prepare PEI-mesoporous silica composite *via* polymerization of aziridine inside the mesopores.[92] Although the composite material showed a good adsorption capacity, aziridine is a highly toxic and penetrative chemical and therefore, the method is rather unsustainable. Kumar et al. grafted PEI onto a MCM-48 support functionalized with propylchloro groups (Pr-Cl) but a low CO_2 adsorption capacity (0.4 mmol g^{-1}) was recorded due to pore blockage.[93]

As with both MOFs and zeolites, for a supported amine adsorbent to be considered suitable for use in CCS on an industrial scale it has to be able to be fully regenerated and be able to undergo adsorption-desorption on a rapid timescale. In general these supported amine adsorbents with a full desorption of CO_2 can be regenerated by selecting the right desorption conditions, usually at a lower temperature (70 – 150 °C) and atmospheric pressure, which circumvent the regeneration problems associated with the CaO- or MgO-modified mesoporous silicas (at > 700 °C). Moreover, Chaffee *et al.* have shown that propylamine-functionalized hexagonal mesoporous silicas (HMS) can be regerenated at a temperature as low as 20 °C (293 K) under a fully anhydrous argon purge. [94]

Unlike MOFs, research on scaling up the production of mesoporous silica has seen much progress. First, mesoporous silicas can be prepared at room temperature and pressure;[95] this helps in scaling up the synthesis. Moreover, continuous synthesis of mesoporous silica with a highly ordered 2-D hexagonal (*P6mm*) structure has also been reported.[96] Large scale production of mesoporous silica for industrial use is therefore possible. In terms of environmental impact, functionalized mesoporous silicas do not rely on toxic metals or ligands for the adsorption of CO_2. However, one concern will be on the tethered amine groups; the environmental impact of these groups is still

unknown. Moreover, and more importantly, the template used for preparing mesoporous silica cannot be ignored. It can only be removed either by calcination or solvent extraction. A considerable amount of CO_2 is to be emitted upon calcination while extraction of template generates unwanted solvent waste. Therefore, in order to lower the carbon footprint for using mesoporous silica, template-free synthesis should be considered.[97]

4.4. Carbon Nanotubes and Ordered Mesoporous Carbon

Nanoporous carbon materials, including activated carbons and carbon fibers, have also been considered as adsorbents for CO_2, because of their hydrophobic nature and high surface area;[98] both properties make them suitable for CCS purpose. Moreover, many carbon materials are light in weight and relatively cheap to manufacture (except carbon nanotubes).[99] Therefore, they have many industrial uses including water purification and decolorization.[100] Among all carbon materials, carbon nanotubes (CNT, single-wall or multi-wall) have been extensively studied as an adsorbent for carbon dioxide. For example, multi-walled carbon nanotubes have shown a CO_2 adsorption capacity of ca. 0.5 mmol g^{-1} (22.7 mg CO_2 g^{-1}) with an increase to ca. 0.9 mmol g^{-1} after grafting with amine groups using APTES.[101] However, silanization using APTES could be wasteful for this expensive carbon material because such a CO_2 adsorption capacity can be easily achieved by other APTES functionalized materials, e.g. mesoporous silica (see Section 4.3) or even commercial fumed silica. Furthermore, many of the CO_2 adsorption studies using carbon nanotubes are based on computer simulations rather than real adsorption experiments.[102] One reason is that, unlike other bulk nanoporous carbon materials, carbon nanotubes are expensive to prepare although continuous production has been reported.[103] This is also likely to be the main obstacle for carbon nanotubes to be used as a CO_2 adsorbent on an industrial scale.

Another family of nanoporous carbon materials is the ordered mesoporous carbon, prepared from mesoporous silica templates. By carbonizing ordered mesoporous silicas and then removing the silica templates using a strong base (KOH or NaOH) or HF, a mesoporous carbon material with an “inverse” structure of the template itself can be formed.[104] In terms of adsorption chemistry, these materials have similar characters to carbon nanotubes. Therefore, they have been used for CO_2 adsorption and separation. For example, the CO_2 adsorption capacity of mesoporous carbon CMK-3 (template with SBA-15) and CMK-8 (template with KIT-6) were

recorded at 2.4 and 2.1 mmol g^{-1} (25°C and 1 atm) respectively.[105] An enhanced CO_2 adsorption capacity was demonstrated by a treatment using KOH followed by heating. However, details for the chemical effects on the material surface due to this treatment were not discussed in this report. Similar to mesoporous silicas, in order to enhance the CO_2 adsorption capacity, polymers with basic characters have been immobilized inside the pores of mesoporous carbon.[106] It was found that PEI-loaded CMK-3 composites showed a maximum adsorption capacity of 3.13 mmol g^{-1}, compared with 1.55 mmol g^{-1} recorded from a pure carbon CMK-3 sample. As shown from both mesoporous silica and mesoporous carbon, polyamine-loaded composite materials are promising candidates for CCS purpose.

Although scaling up production of these ordered carbon nanomaterials at a possible kilogram-scale production has been reported,[107] the more suitable candidate among this group of carbon materials for CO_2 adsorption is still microporous activated carbon. This is mainly because their production cost and scale of preparation are much more realistic for large scale applications. Activated carbons can be prepared from various plant wastes, such as nutshells and wood, or other bulk sources (e.g. peat and coal) by heating (or carbonizing) the precursors at a high temperature (up to 900 °C) in the absence of oxygen. Usually, a surface area of 200 – 500 m^2 g^{-1} can be achieved for most activated carbon. However, since these carbon-based materials are neutral or mildly acidic on surface, they need further chemical modification to be made selective for CO_2 adsorption. Amination of activated carbon is one popular method for modifying the surface in order to enhance the selectivity towards CO_2 due to the improved surface basicity.[108] Unfortunately, the extend of amination depends on the reaction temperature and extensive heat (up to 800 °C) is usually required. These two energy-intense steps (carbonization and amination) for preparing basic activated carbon are likely to hamper their sustainable, long-term use for CO_2 capture.

4.5. Other Nanoporous Materials for CO_2 Capture

In the past few years, new types of porous organic nanomaterials have caught the attention of many research groups. Organic cage framework (OCF) materials consist of repeated units of cage-like ordered structures, similar to MOF systems.[109] Unlike MOFs, these OCFs are purely organic without any metal component. The specific cage size seems to have a significant effect on the separation of CO_2 from other gases, such as nitrogen. For instance, the OCF material formed from 1,3,5-tris(4-

aminophenyl)benzene and isophthaldehyde showed a high CO_2 adsorption capacity of 2.71 mmol g^{-1} (60.7 cm^3g^{-1}) at 0°C, as well as a high CO_2 selectivity over N_2.[110] Moreover, many of these OCF materials are prepared by coupling amine compounds, which can provide a large number of binding sites for CO_2.

Covalent organic frameworks (COFs), another class of porous organic nanomaterials, are frameworks formed from molecules which are able to react with one another via strong covalent bonds. As with MOF synthesis the building blocks used for COFs are designed to interact with one another in a way to promote a propagation of the framework, and is achieved though using rigid building blocks with divergent functionalities, for example tetra(4-dihydroxyborylphenyl)methane (TBPM), and its silane analogue (TBPS), both rigid tetrahedral molecules containing 4 boronic acid groups. These molecules are able to either to undergo a self-condensation reaction to form a structured framework, or a co-condensation reaction with a different building unit such as hexahydroxytriphenylene (HHTP), which has a rigid triangular shape, thus leading to a different COF system.[111] It has been shown that COFs can contain similar sized pores (0.9 nm – 3.2 nm) to many MOFs and indeed both COF-105 and COF-108 were shown to have a very low density (as low as 0.17 g cm^{-3}), which is lower than many highly porous MOFs. While there are still relatively few experimental gas adsorption studies on COFs it has been shown by simulation studies that large CO_2 adsorption capacities may be achievable with certain COFs.[112]

Recently another type of purely organic framework, known as a supramolecular organic framework (SOF), has been reported to show interesting reversible gas adsorption properties.[113] A SOF system is a crystalline porous material stabilized through exploiting non-covalent interactions such as hydrogen bonds and π-π stacking interactions. However, because these interactions are inherently weaker than co-ordinate or covalent bonds, few target molecules have been discovered that can successfully form a framework that is stable to solvation. Nonetheless, as with OCFs and COFs, the ability to eliminate the need of a source of metal in the synthesis of SOFs offers the possibility to develop some extremely low-density solid adsorbents.

Despite their considerable potential, research in OCF, COF and SOF systems is still relatively in its infancy compared to the much more widely studied systems of zeolites, MOFs and supported amines. Therefore additional effort is still required to

make any of these porous organic frameworks a realistic candidate for CO_2 capture on an industrial scale. As with other adsorbent materials discussed earlier, production of these materials has to be scalable while the environmental impact of these organic materials has to be scrutinized carefully.

5. Catalytic Conversions of CO_2 as New Pathways for Carbon Capture and Utilization (CCU)

As research on adsorbents for CCS has been expanded rapidly in recent years, many nanoporous materials with excellent adsorption capacity, selectivity and stability have been reported. However, CCS technologies based on adsorbents are still limited by their adsorption capacity. Instead of just simple "capture and storage", CO_2 can be transformed into important chemical products via various CO_2 activation reactions. As such, the "capture process" is not limited by the adsorption capacity of the adsorbents, which is now approaching saturation. Since CO_2 is a very stable compound thermodynamically, catalysts are usually required to activate CO_2 molecules to form other compounds, mainly organics. In nature, one notable catalytic process has been regulating the CO_2 content in our atmosphere; photosynthesis is a very efficient catalytic process to convert CO_2 into carbohydrate. Unfortunately, under the current CO_2 emission rate, photosynthesis from plants simply cannot cope, and it is further hampered by continuous global deforestation. Therefore, scientists have also been actively investigating other catalytic processes for CO_2 transformations, or commonly termed as "carbon capture and utilization" (CCU).

5.1. Catalytic Activation of CO_2

Despite its chemical stability, there are several pathways for catalytic CO_2 activation showing some potential in tackling the CO_2 problem. For example, CO_2 has been reacted with various unsaturated hydrocarbons (alkenes and alkynes) to form carboxylic acids and esters in presence of homogeneous catalysts such as $Ni(acac)_2$ (nickel(II) acetylacetonate) and $Ni(cod)_2$ (bis(cyclooctadiene)nickel) via a reductive carboxylation reaction.[114] This includes the synthesis of an important chemical, acrylic acid, from CO_2 and ethylene. Another homogeneous catalyst (Zn complexes) has been used to catalyze the synthesis of polycarbonates from CO_2 and epoxides.[115]

However, these examples involve use of homogeneous catalysts, which are usually associated with high energy consumption, high waste emission and poor

recyclability. Use of heterogeneous catalysts for CO_2 conversion can circumvent many problems associated with homogeneous catalysis but usually shows a lower reaction rate and poorer selectivity. For instance, a mesoporous adenine-modified Ti-SBA-15 catalyst was shown to be active for the conversion of CO_2 to cyclic carbonates in presence of an epoxide but high pressure (6.9 atm) was required.[116]

In industry, large scale catalytic processes involving the use of CO_2 as a feedstock are also available. One classic example is the conversion of CO_2 with H_2 to form CO and H_2O in a low-temperature water-gas shift reaction, which is widely used in the fuel industry.[117] A supported copper on zinc oxide catalyst, with a Cu:Zn molar ratio = 1:2, is considered as the most suitable for this reaction.

$$CO_2 + H_2 \rightarrow CO + H_2O \qquad \Delta H = -164.9 \text{ kJ mol}^{-1} \qquad (8)$$

Alternatively, use of photocatalysts can convert CO_2 to various simple compounds including methanol, CO and methane.[118] Although photocatalysis resembles the preferred photosynthesis process, these products are far from ideal for consideration by industries, where much more efficient processes are available for the production of methanol and CO. On the other hand, methane is usually not industrially manufactured because of the abundant natural gas available globally. Also, methane is considered as another greenhouse gas with a greenhouse effect 25 times higher than CO_2. Therefore, transforming CO_2 to methane does not really solve our greenhouse gas problem.

While many of the large-scale CO_2 conversion processes have already been well optimized in terms of choice of catalysts, reaction temperature and pressure, operational cost, and reactor/process design, new catalysts are being developed for small laboratory-scale conversions but the products need to be of a high value or high importance for justification. Therefore, it could be challenging to develop new nanoporous catalysts to outperform these commercial catalysts when all these operational parameters need to be considered. Nonetheless, Figure 7 highlights five classes of CO_2 conversion reactions that could involve the use of nanoporous catalysts.

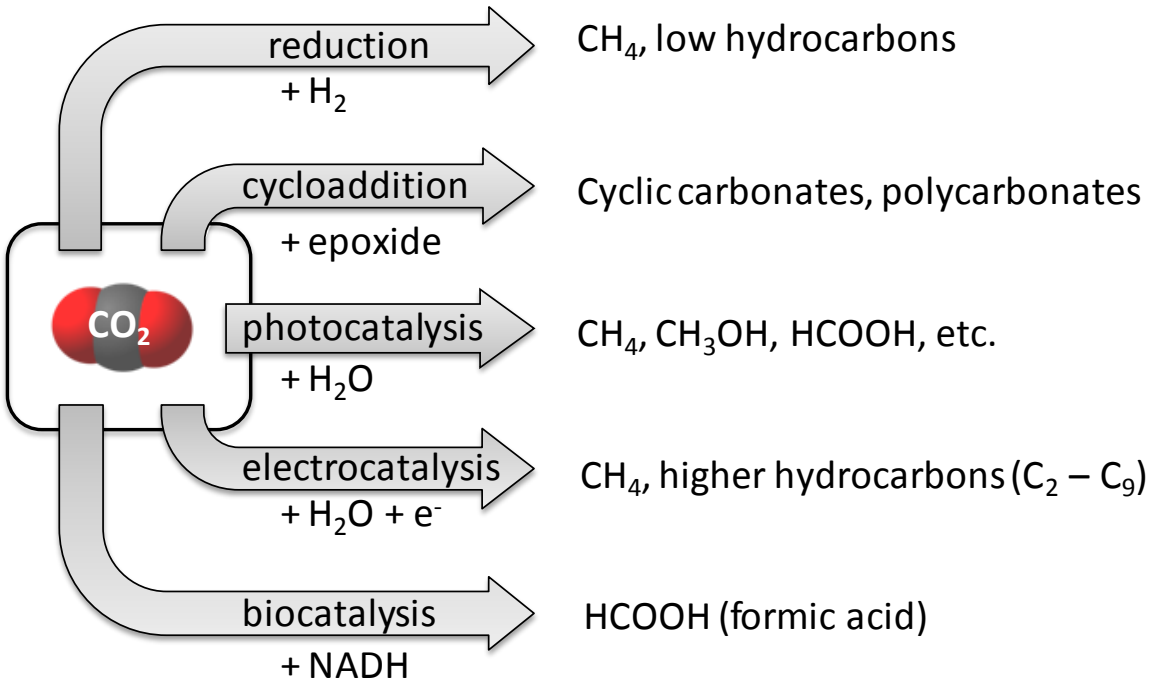

*cycloaddition of CO_2 onto epoxide to form cyclic carbonate:

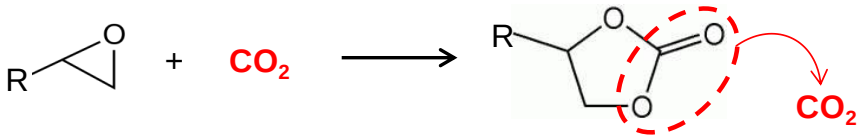

Figure 7. Summary on available pathways for catalytic conversions of CO_2 to various chemicals suitable for CCU purpose.

5.2. Nanoporous Catalysts for CO_2 Conversion

Many nanoporous materials have been widely used as heterogeneous catalysts. Notably, zeolites such as ZSM-5 and zeolite-Y (faujasite, FAU) are commonly used as solid acid catalysts for hydrocarbon cracking and isomerization.[119] On the other hand, research on the catalytic applications of MOFs[120] and functionalized mesoporous silicas[60] can also be found in the literature. As discussed in Section 4, nanoporous materials usually have a high BET surface area, which is a positive feature for heterogeneous catalysis. Such advantage is of course beneficial to CO_2 conversion reactions.

5.2.1. Zeolites for CO_2 conversion

Because of their established applications in petroleum industries, the catalytic properties of zeolites have been tested on a number of hydrocarbon formation reactions using CO_2,

notably reformation of methane. In this methane reforming reaction, hydrogen (H_2) is produced as well as CO (see equation 9), which are the components for syngas.

$$CO_2 + CH_4 \rightarrow 2CO + 2H_2 \quad (9)$$

A supported Ni catalyst is commonly used for this reaction, sometimes with a promoter, such as Al_2O_3, CaO, MgO or CeO_x. For example, Ni supported on zeolite, with CaO and K_2O promoters, has shown a high activity as well as a high resistance to coke formation.[121] Selected examples of methane reformation studies using zeolite catalysts are summarized in Table 4. This process represents a possible "reverse" mechanism for the combustion of fossil fuels by converting CO_2 back to fuels (H_2 and CO). However, the high energy consumption for methane reforming must be considered due to the high temperature (600 – 800 °C) for process operation. Other examples of using zeolites in CO_2 conversion to bulk chemicals include CO_2 hydrogenation to form methanol in a zeolite (zeolite A) membrane reactor [133] and, by further reacting with in situ formed methanol, to produce dimethyl ether over a Cu–ZnO–ZrO_2/H-ZSM5 catalyst.[134]

In addition to industrial processes for bulk chemicals, modified zeolites, acting as base catalysts, have also shown ability to promote cycloaddition of CO_2 to epoxides. Potassium exchanged zeolite X (or KX) loaded with Cs^+ ions have shown a high activity for adding CO_2 onto ethylene oxide to form ethylene carbonate (reaction equation shown in Figure 5),[135] which is a useful chemical as a plasticizer as well as an electrolyte in lithium batteries. However, because of the small pore size of zeolite X ($\leq$1.2 nm), the activity for converting larger reactants such as epoxypropylbenzene was much lower. This is a common limitation for using zeolites as catalysts as only small molecules of both reactants and products are applicable.

Nanoporous support	Catalyst components	Mass of catalyst [mg]	GHSV[a] [$cm^3\ h^{-1}\ g_{cat}^{-1}$]	Temp [°C]	P [atm]	CO_2:CH_4	CO_2 conversion	References
Zeolites								
Silicate-1	Ni	200	30,000	700	1	1:1	80-84%	[122]
BEA	Ni/Rh	200	30,000	700	1	1:1	77-78%	[123]
BEA	Ni/Pt	70	85,700	640	1	1:1	26-31%[b]	[124]
Y	Ni/Pt	70	85,700	640	1	1:1	26%[b]	[124]
Y	Ni	200	30,000	700	1	1:1	90%	[125]
ZSM-5	La_2NiO_4	100	48,000	800	1	1:1	77%	[126]
Mesoporous oxides								
SBA-15	Ni/MgO-Al_2O_3	300	12,000	800	1	1:1	85%	[127]
SBA-15	Ni/MgO	100	36,000	550-800	1	1:1	25-83%	[128]
SBA-15	$LaNiO_3$	100	36,000	550-800	1	1:1	30-80%	[129]
MCM-41	$LaNiO_3$	100	36,000	550-800	1	1:1	30-80%	[129]
SBA-16	Ni/CeO_2	20	25,500	700	1	1:1	68-72%	[130]
Mesoporous Al_2O_3	Ni/CeO_2	100	36,000	550-800	1	1:1	38-85%	[131]
Mesoporous Al_2O_3	Ni/MgO	100	15,000 - 60,600	600-800	1	1:1	95%	[132]

[a] GHSV = gas hourly space velocity

[b] CO_2 conversion data was not supplied, figures shown were CH_4 conversions.

Table 4. Selected examples of methane reforming with CO_2 using supported metal on zeolite and mesoporous oxide catalysts for producing syngas.

5.2.2. MOFs as catalysts

Catalysis using MOFs is not as common as zeolites due to the lower thermal stability of the MOFs. Unlike zeolites, the metal centers of MOFs, particularly those constructed with transition metals, can act as catalytic active sites for organic transformation reactions. Regarding using CO_2 as a feedstock, several MOF systems have been found active for cycloaddition reactions with epoxides. For example, MOF-5 was shown to be active in the cycloaddition of CO_2 onto propylene oxide and styrene oxide at 4 atm and 50 °C, in presence of a quaternary ammonium salt, e.g. n-Bu_4NBr.[136] Indeed, the proposed mechanism suggested that the metal center (Zn_4O) of MOF-5 acted as a Lewis

acid for interacting with the epoxide oxygen while the Bu_4N^+ ion opened the epoxide ring. Therefore, the quaternary ammonium can be viewed as a co-catalyst and the activity seemed to have a direct relationship to its solubility in the epoxide reactant. Although the MOF-5 solid can be reused, the Bu_4N^+ ions are unlikely to be recovered easily, raising a real question over sustainability. Co-MOF-74 has also been tested in a similar reaction, addition of CO_2 onto styrene oxide, but without a co-catalyst.[137] A 96 % conversion was observed in 4 hours but the reaction was operated at elevated pressure and temperature (20 atm and 100 °C). Also a toxic solvent, chlorobenzene, is required. This research group has also compared the activity of selected MOF systems for the cycloaddition of CO_2 onto styrene oxide and among them, UIO-66-NH_2 MOF was found to be the most active, with 70 % conversion in 1 h.[138] However, the reaction conditions remained at high pressure and temperature with the use of a toxic solvent.

There are other examples showing the catalytic activity of MOFs (Ni(salphen)-MOF,[139] Mg-MOF-74,[140] ZIF-8[141] and MIXMOF-5[142]) as catalysts for cycloaddition of CO_2 onto an epoxide. Compared with zeolite catalysts, the larger pores of MOF catalysts did promote cycloaddition of CO_2 on larger epoxides, but most of these systems were operated at high pressure (>5 atm) and temperature (100 – 140 °C), with quarternary ammonium ions as co-catalysts in some cases. Despite the superiority in selective CO_2 adsorption, MOFs' potential as catalysts for CCU still seems rather limited.

5.2.3. Functionalized mesoporous silica catalysts

Catalytic applications using functionalized mesoporous silicas is widely available in the literature [60], partly due to their large pore dimensions available for accommodating larger organic reactants and products, as well as facilitating their diffusion into and out of the catalyst. For CO_2 conversions, this property is advantageous because the target products are mostly larger organic molecules (>1 nm) which may block smaller pores of zeolites and MOFs.

For example, dry reformation of methane with CO_2 using nickel nanoparticles supported on mesoporous silica catalysts have been reported as early as 2006.[143] Table 4 summarizes several selected examples published since 2013. Although many of these catalysts showed good resistance to deactivation over a long period of continuous

use (e.g. 80 h), there was a lack of direct comparison on the catalytic performance among these mesoporous catalysts. It is difficult to pinpoint which is the best composition for methane reformation or which parameters are critical for an efficient process. In industry, dry reformation of methane is still not commonly used due to the coke formation and subsequent catalyst deactivation,[144] which was shown to be minimized using these mesoporous silica-based catalysts. Therefore, more research in this area may lead to some breakthrough for methane reformation using CO_2 in industry.

Mesoporous silicas have also been used as a support for photocatalysts (e.g. TiO_2) for the conversion of CO_2 to methane and methanol. For example, Ti-doped MCM-41 and MCM-48 were found to be active in the conversion of CO_2 in water to form both methane and methanol, at a 3:1 ratio;[145] this is in contrast to the low activity and low selectivity towards methanol shown from bulk TiO_2. A photocatalyst prepared by impregnating TiO_2 nanoparticles into the cages of FSU-16 mesoporous silica was also active in converting CO_2 to a mixture of methane and methanol.[146] However, it is well-known that TiO_2 species only adsorb UV radiation while doping with other transition metals, such as Cu, is required for the adsorption of visible energy.

In addition to conversion to simple molecules such as methane and methanol, cycloaddition can also be catalyzed using catalysts supported on mesoporous silica. The reactions are essentially the same as those presented previously for catalysis using MOFs. Similar to some MOF systems for this reaction, a positively charged species (e.g. Bu_4N^+) is required to activate the epoxide ring. In these mesoporous silica systems, positively charged groups can be grafted onto the silica surface via silanization. For example, imidazolium ions have been supported onto the MCM-41 surface via a 3 step-grafting method.[147] This catalyst was shown to be active for the formation of cyclic carbonate from epoxides (styrene oxide and allyl glycidyl ether) and recycling of catalysts showed insignificant deactivation. However, also similar to the MOF systems, a high pressure of CO_2 (7 – 40 atm) was required for the reactions. Therefore, the sustainability of these processes is once again questionable.

5.3.4. Modified carbon nanotubes for CO_2 conversions

Although carbon materials have been widely used as supports for metal catalysts (e.g. Pd/C and Pt/C), use of carbon nanotubes (CNTs) for catalysis is rare because of the high

cost associated with production. In many cases, other carbon materials, such as activated carbon and carbon nanofibres, are preferred materials for supporting metal catalysts.[148] Nonetheless, use of CNTs as a support for catalysts is still possible, including use in catalytic conversion of CO_2. For example, transition metal (Ni and Fe) supported on multi-walled CNTs (MWCNTs) have been used to convert CO_2 into hydrocarbons, including methanation reaction.[149] Ni/MWCNTs (10 % Ni) have shown a conversion (< 50 %) of CO_2 with nearly 100 % selectivity towards methane at 500°C in presence of H_2. Addition of La (1 %) has shown an increase in conversion up to 60 %. However, the study did not include comparison on activity with other activated carbon-based catalysts. Therefore, it would be difficult to assess the advantage of using CNT as a catalyst support material. O'Byrne et al. showed that a Fe/MWCNT catalyst prepared by growing the CNT support on Fe nanoparticles was active for CO_2 conversion, in presence of H_2, with selectivity towards higher-order hydrocarbons, with 24.3 % $C_2 - C_4$ hydrocarbon formed.[150] The formation of higher hydrocarbons is certainly encouraging but this study also lacks comparison with other conventional carbon-based catalysts.

Multi-walled CNT supported TiO_2 catalysts have also been used as photocatalysts for the reduction of CO_2 with water.[151] In this study, the catalyst preparation was found to have a significant influence on the product selectivity; TiO_2/CNT prepared from a sol-gel/precipitation method is selective towards the formation of ethanol while formic acid is the main product from the catalyst prepared via a hydrothermal method. This is because the TiO_2 formed from sol-gel/precipitation was mainly anatase while an increased amount of rutile phase was found in the sample prepared from the hydrothermal method. When compared with use of activated carbon support, only a marginal improvement was observed from using CNT as catalyst support. Such result raises a question mark over using this CNT-supported catalyst for a large scale CO_2 conversion.

Compared with other nanoporous materials, CNTs are superior in terms of electroconductivity. Therefore, it can be used as materials for electrodes in electrocatalytic conversion of CO_2. Genovese et al. have found the formation of higher hydrocarbon (up to $C_8 - C_9$) using electrodes based on Fe nanoparticles supported on CNT.[152] Further enhancement was achieved by doping the CNT with nitrogen.

There is no evaluation on the electricity consumption presented in this report so it is difficult to assess the viability of this method as a carbon dioxide re-utilization.

6. Concluding Remarks and Future Outlook

The current CCS landscape is still heavily directed to capture followed by geological storage. For example, "concentrated" CO_2 from post-combustion capture is transported to designated reservoirs and stored underground. However, these CO_2 reservoirs are not simple ecological panaceas as industrial accidents and natural leaks could cause disasters similar to that at Lake Nyos, Cameroon in 1986[153] can happen. Moreover, these capture-storage coupling projects are costly, estimated to around 150 – 200 GBP (*ca.* 250 – 330 USD)/MWh,[154] although this figure is likely to reduce when full-scale CCS facilities are to be built in the next few decades. Considering such a high operational cost for these CCS technologies, using nanoporous materials as CO_2 adsorbents could only further increase this financial burden and therefore they are unlikely to be practical until a significant reduction in cost for preparing these adsorbents is available. These are considered as non-recoverable costs and likely to be loaded onto the already high production cost for energy in many countries. Sustainability of the whole capture and storage process is therefore somehow dubious.

On the other hand, if CCU technologies are mature for large-scale operations, the potential hazard of CO_2 reservoirs can be avoided. Furthermore, the products formed from catalytic conversions of CO_2 can be sold and therefore can compensate part of the operational cost for CO_2 capture. Since many of these reactions are operated with a pure CO_2 feed or at a high CO_2 content, sorbent materials may still be required to capture CO_2 from flue gas for pre-concentration. Therefore, the catalytic reactor may have to be constructed near a power station fitted with CO_2 capture facilities. This may cause some engineering challenges. In economical terms, although some cost can be recovered, bulk products such as methanol and hydrocarbons are unlikely to provide financial security for the operation. Consequently, CCU processes towards fine chemical products, such as organic carbonates, will be much more likely to succeed.

Despite the large amount of research, CCS and CCU technologies are still regarded as short-term to mid-term solutions for tackling ever increasing CO_2 emission into the environment. Ultimately, our society has to move away from the reliance on fossil fuels for energy generation. Renewable energy sources, such as solar energy,

wind energy, hydropower, and wave energy, are all considered to have potential. However, we should still be cautious before rapidly implementing any new technology as all implications, particular in the long-term, should be considered to prevent any unexpected damaging and potentially irreversible effects, such as the over-plantation of oil palms for bio-diesel and the subsequent massive deforestation.[155] Nonetheless, current and future CCS systems could act as an important stop gap while scientists continue the intense research required to fully develop new sustainable technologies for low carbon power generation to tackle the global problem of anthroprogenic climate change.

Acknowledgements

This work is supported by EPSRC, UK (EP/F034482/1 and EP/J02077X/1) and the Scottish Carbon Capture and Storage (SCCS).

References

[1] L. Li, N. Zhao, W. Wei, Y. Sun, *Fuel* **2013**, *108*, 112.

[2] R. Williamson, *Carbon Manage.* **2013**, *4*, 241.

[3] H. Yang, Z. Xu, M. Fan, R. Gupta, R. B. Slimane, A. E. Bland, I. J. Wright, *J. Environ. Sci.- China* **2008**, *20*, 14.

[4] Statistical data released by the Department of Energy and Climate Change, UK, 2013. https://www.gov.uk/government/uploads/system/uploads/attachment_data/file/193414/280313_ghg_national_statistics_release_2012_provisional.pdf (accessed September 2013).

[5] M. M. F. Hasan, R. C. Baliban, J. A. Elia, C. A. Floudas, *Ind. Eng. Chem. Res*. **2012**, *51*, 15642

[6] R. Krishna, J. M. van Baten, *J. Membrane Sci.* **2010**, *360*, 323.

[7] E. R. Bobicki, Q. Liu, Z. Xu, H. Zeng, *Prog. Energy Combust. Sci.* **2012,** *38*, 302.

[8] A. Iizuka, K. Hashimoto, H. Nagasawa, K. Kumagai, Y. Yanagisawa, A. Yamasaki, *Sep. Purif. Technol.* **2012**, *101*, 49.

[9] L. M. Romeo, I. Bolea, J. M. Escosa, *Appl. Therm. Eng.* **2008**, *28*, 1039.

[10] G. T. Rochelle, *Science* **2009**, *325*, 1652.

[11] S. Yuan, Z. Wang, Z. Qiao, M. Wang, J. Wang, S. Wang, *J. Membrane Sci.* **2011**, *378*, 425.

[12] R. A. Khatri, S. S. C. Chuang, Y. Soong, M. Gray, *Energy Fuels* **2006**, *20*, 1514.

[13] A. Samanta, A. Zhao, G. K. H. Shimizu, P. Sarkar, R. Gupta, *Ind. Eng. Chem. Res*. **2012**, *51*, 1438.

[14] Z. J. Zhang, Y. G. Zhao, Q. H. Gong, Z. Li, J. Li, *Chem. Commun.* **2013**, *49*, 653.

[15] Y. H. Jin, B. A. Voss, R. McCaffrey, C. T. Baggett, R. D. Noble, W. Zhang, *Chem. Sci.* **2012**, *3*, 874.

[16] P. Markewitz, W. Kuckshinrichs, W. Leitner, J. Linssen, P. Zapp, R. Bongartz, A. Schreiber, T. E. Müller, *Energy Environ. Sci.* **2012**, *5*, 7281.

[17] C. Stewart, M. A. Hessami, *Energy Conv. Manag.* **2005**, *46*, 403.

[18] R. Idem, M. Wilson, P. Tontiwachwuthikul, A. Chakma, A.Veawab, A. Aroonwilas, D. Gelowitz, *Ind. Eng. Chem. Res.* **2006**, *45*, 2414.

[19] M. M. Huang, S. Kaliaguine, *J. Chem. Soc., Faraday Trans.* **1992,** *88*, 751.

[20] M. Katoh, T. Yoshikawa, T. Tomonari, K. Katayama, T. Tomida, *J. Colloid Interface Sci.* **2000**, *226*, 145.

[21] R. Hernandez-Huesca, L. Diaz, G. Aguilar-Armenta, *Sep. Purif. Technol.* **1999**, *15*, 163.

[22] J. A. Dunne, M. Rao, S. Sircar, R. J. Gorte, A. L. Myers, *Langmuir* **1996**, *12*, 5896.

[23] J. Shang, G. Li, R. Singh, Q. Gu, K. M. Nairn, T. J. Bastow, N. Medhekar, C. M. Doherty, A. J. Hill, J. Z. Liu, P. A. Webley, *J. Am. Chem. Soc.* **2012**, *134*, 19246.

[24] J. Shang, G. Li, R. Singh, P. Xiao, J. Z. Liu, P. A. Webley, *J. Phys. Chem. C* **2013**, *117*, 12841.

[25] M. M. Lozinska, E. Mangano, J. P. S. Mowat, A. M. Shepherd, R. F. Howe, S. P. Thompson, J. E. Parker, S. Brandani, P. A. Wright, *J. Am. Chem. Soc.* **2012**, *134*, 17628.

[26] Q. Liu, A. Mace, Z. Bacsik, J. Sun, A. Laaksonen, N. Hedin, *Chem. Commun.* **2010**, *46*, 4502.

[27] Q. Liu, T. Pham, M. D. Porosoff, R. F. Lobo, *ChemSusChem* **2012**, *5*, 2237.

[28] B. Li, S. S. Kaye, C. Riley, D. Greenberg, D. Galang, M. S. Bailey, *ACS Comb. Sci*., **2012**, *14*, 352

[29] REF:- T. H. Bae, M. R. Hudson, J. A. Mason, W. L. Queen, J. J. Dutton, K. Sumida, K. J. Micklash, S. S. Kaye, C. M. Brown, J. R. Long, *Energy Environ. Sci.*, **2013**, *6*, 128.

[30] F. Brandani, D. M. Ruthven, *Ind. Eng. Chem. Res.* **2004**, *43*, 8339.

[31] P. A. Zapata, J. Faria, M. Pilar Ruiz, R. E. Jentoft, D. E. Resasco, *J. Am. Chem. Soc.* **2012**, *134*, 8570.

[32] O. K. Farha, J. T. Hupp, *Accounts Chem. Res.* **2010**, *43*, 1166.

[33] H. Li, M. Eddaoudi, M. O'Keeffe, O. M. Yaghi, , *Nature* **1999**, *402*, 276.

[34] J. H. Jia, H. S. Athwal, A. J. Blake, N. R. Champness, P. Hubberstey, M. Schroder, *Dalton Trans.* **2011**, *40*, 12342.

[35] M. T. Wharmby, J. P. S. Mowat, S. P. Thompson, P. A. Wright, *J. Am. Chem. Soc.* **2011**, *133*, 1266.

[36] M. Eddaoudi, J. Kim, N. Rosi, D. Vodak, J. Wachter, M. O'Keeffe, O. M. Yaghi, *Science* **2002**, *295*, 469.

[37] X. Lin, J. Jia, X. Zhao, K. M. Thomas, A. J. Blake, G. S. Walker, N. R. Champness, P. Hubberstey, M. Schroeder, *Angew. Chem. Int. Ed.* **2006**, *45*, 7358.

[38] a) Y. S. Bae, O. K. Farha, A. M. Spokoyny, C. A. Mirkin, J. T. Hupp, R. Q. Snurr, *Chem. Commun.* **2008**, *35*, 4135; b) Z. Zhang, S. Xian, H. Xi, H. Wang, Z. Li, *Chem. Eng. Sci.* **2011**, *66*, 4878; c) V. Finsy, L. Ma, L. Alaerts, D. E. De Vos, G. V. Baron, J. F. M. Denayer, *Microporous Mesoporous Mater.* **2009**, *120*, 221.

[39] J. An, S. J. Geib, N. L. Rosi, *J. Am. Chem. Soc.* **2010**, *132*, 38.

[40] A. Demessence, D. M. D'Alessandro, M. L. Foo, J. R. Long, *J. Am. Chem. Soc.* **2009**, *131*, 8784.

[41] Y. S. Bae, R. Q. Snurr, *Angew. Chem. Int. Ed.* **2011**, *50*, 11586.

[42] J. A. Mason, K. Sumida, Z. R. Herm, R. Krishna, J. R. Long, *Energy Environ. Sci.* **2011**, *4*, 3030.

[43] P. Aprea, D. Caputo, N. Gargiulo, F. Iucolano, F. Pepe, *J. Chem. Eng. Data* **2010**, *55*, 3655.

[44] K. Sumida, D. L. Rogow, J. A. Mason, T. M. McDonald, E. D. Bloch, Z. R. Herm, T. H. Bae, J. R. Long, *Chem. Rev.* **2012**, *112*, 724.

[45] J. P. S. Mowat, S. R. Miller, J. M. Griffin, V. R. Seymour, S. E. Ashbrook, S. P. Thompson, D. Fairen-Jimenez, A. M. Banu, T. Düren, P. A. Wright, *Inorg. Chem.* **2011**, *50*, 10844.

[46] Z. R. Herm, J. A. Swisher, B. Smit, R. Krishna J. R. Long, *J. Am. Chem. Soc.* **2011**, *133*, 5664.

[47] R. Krishna, J.M. van Baten, *Sep. Purif. Technol.* **2012**, *87*, 120.

[48] T. Remy, S. A. Peter, S. van der Perre, P. Valvekens, D. E. De Vos, G. V. Baron, J. F. M. Denayer, *J. Phys. Chem. C* **2013**, *117*, 9301.

[49] S. U. Rege, R. T. Yang, *Sep. Sci. Technol.* **2001**, *36*, 3355.

[50] J. Kahr ,R. E. Morris, P. A.Wright, *CrystEngComm* **2013**, *15*, 9779.

[51] J. H. Park, J. N. Kim, S. H. Cho, J. D. Kim, R. T. Yang, *Chem. Eng. Sci.* **1998**, *53*, 3951.

[52] S. Cavenati, C. A. Grande, A. E. Rodrigues, *J. Chem. Eng. Data* **2004**, *49*, 1095.

[53] R. Banerjee, H. Furukawa, D. Britt, C. Knobler, M. O'Keeffe, O. M. Yaghi, *J. Am. Chem. Soc.* **2009**, *139*, 3875.

[54] P. D. C. Dietzel, V. Besikiotis, R. Blom, *J. Mater. Chem.* **2009**, *19*, 7362

[55] Z. J. Liang, M. Marshall, A. L. Chaffee, *Energy Fuels* **2009**, *23*, 2785.

[56] P. Nugent, Y. Belmabkhout, S. D. Burd, A. J. Cairns, R. Luebke, K. Forrest, T. Pham, S. Q. Ma, B. Space, L. Wojtas, M. Eddaoudi, M. J. Zaworotko, *Nature* **2013**, *495*, 80.

[57] M. Gaab, N. Trukhan, S. Maurer, R. Gummaraju, U. Mueller, *Microporous*

Mesoporous Mater. **2012**, *157*, 131.

[58] J. S. Beck, J. C. Vartuli, W. J. Roth, M. E. Leonowicz, C. T. Kresge, K. D. Schmitt, C. T. W. Chu, D. H. Olson, E. W. Sheppard, S. B. McCullen, J. B. Higgins, J. L. Schlenker, *J. Am. Chem. Soc.* **1992**, *114*, 10834.

[59] S. A. El-Safty, *Trac-Trends Anal. Chem.* **2011**, *30*, 447.

[60] A. Corma, *Chem. Rev.* **1997**, *97*, 2373.

[61] F. Torney, B. G. Trewyn, V. S. Y. Lin, K. Wang, *Nat. Nanotechnol.* **2007**, *2*, 295.

[62] W. G. Lin, F. Wei, Q. Hou, T. Y. Zhang, Y. K. Wang, J. H. Zhu, *Microporous Mesoporous Mater.* **2012**, *156*, 233.

[63] A. Walcarius, L. Mercier, ***J. Mater. Chem.*** **2010**, *20*, 4478.

[64] H. H. P. Yiu, P. A. Wright, *J. Mater. Chem.* **2005**, *15*, 3690.

[65] H. H. P. Yiu, M. A. Keane, Z. A. D. Lethbridge, M. R. Lees, A. J. El Haj, J. Dobson, *Nanotechnology* **2008,** *19*, 255606.

[66] P. O. Vasiliev, B. Faure, J. B. S. Ng, L. Bergstrom, *J. Colloid Interface Sci.* **2008**, *319*, 144.

[67] C. L. Chen, T. Li, S. F. Cheng, N. P. Xu, C. Y. Mou, *Catal. Lett.* **2002**, *78*, 223.

[68] a) C. H. Huang, K. P. Chang, C. T. Yu, P. C. Chiang, C. F. Wang, *Chem. Eng. J.* **2010**, *161*, 129; b) J. Fernandez, F. Gonzalez, C. Pesquera, C. Blanco, M. J. Renedo, *Ind. Eng. Chem. Res.* **2010**, *49*, 2986.

[69] H. Zhao, W. Yan, Z. Bian, J. Hu, H. Liu, *Solid State Sci.* **2012**, *14*, 250.

[70] K. Moller, T. Bein, *Chem. Mater.* **1998**, *10*, 2950.

[71] A. S. M. Chong, X. S. Zhao, *J. Phys. Chem. B* **2003**, *107*, 12650.

[72] H. Y. Huang, R. T. Yang, D. Chinn, C. L. Munson, *Ind. Eng. Chem. Res.* **2003**, *42*, 2427.

[73] M. Anbia, V. Hoseini, S. Mandegarzad, *Korean J. Chem. Eng.* **2012**, *29*, 1776.

[74] S. Kim , J. Ida , V. V. Guliants , J. Y. S. Lin, *J. Phys. Chem. B* **2005**, *109*, 6287.

[75] M. R. Mello, D. Phanon, G.Q. Silveira, P. L. Llewellyn, C. M. Ronconi, *Microporous Mesoporous Mater.* **2011**, *143*, 174.

[76] V. Zelenak, D. Halamova, L. Gaberova, E. Bloch, P. Llewellyn, *Microporous Mesoporous Mater.* **2008**, *116*, 358.

[77] S. N. Kim, W. J. Son, J. S. Choi, W. S. Ahn, *Microporous Mesoporous Mater.* **2008**, *115*, 497.

[78] R. Serna-Guerrero, Y. Belmabkhout, A. Sayari, *Chem. Eng. Sci.* **2010**, *65*, 4166.

[79] X. Ma, X. Wang, C. Song, *J. Am. Chem. Soc.* **2009**, *131*, 5777.

[80] X. Xu, C. Song, J. M. Andresen, B. G. Miller, A. W. Scaroni, *Energy Fuels* **2002**, *16*, 1463.

[81] N. Hiyoshi, K. Yogo, T. Yashima, *Microporous Mesoporous Mater.* **2005**, *84*, 357.

[82] X. Wang, H. Li, H. Liu, X. Hou, *Microporous Mesoporous Mater.* **2011**, *142*, 564.

[83] W. Li, P. Bollini, S. A. Didas, S. Choi, J. H. Drese, C. W. Jones, *ACS Appl. Mater. Interface* **2010**, *2*, 3363.

[84] S. H. Liu, C. H. Wu, H. K. Lee, S. B. Liu, *Top. Catal.* **2010**, *53*, 210.

[85] X. Yan, L. Zhang, Y. Zhang, K. Qiao, Z. Yan, S. Komarneni, *Chem. Eng. J.* **2011**, *168*, 918.

[86] J. H. Drese, S. H. Choi, S. A. Didas, P. Bollini, M. L. Gray, C. W. Jones, *Microporous Mesoporous Mater.* **2012**, *151*, 231.

[87] A. Danon, P. C. Stair, E. Weitz, *J. Phys. Chem. C.* **2011**, *115*, 11540.

[88] Y. Belmabkhout, R. Serna-Guerrero, A. Sayari, *Ind. Eng. Chem. Res.* **2010**, *49*, 359.

[89] E. De Canck, I. Ascoop, A. Sayari, P. Van Der Voort, *Phys. Chem. Chem. Phys.* **2013**, *15*, 9792.

[90] H. H. P. Yiu, L. Bouffier, P. Boldrin, J. Long, J. B. Claridge, M. J. Rosseinsky *Langmuir* **2013**, *29*, 11354.

[91] W. J. Son, J. S. Choi, W. S. Ahn, *Microporous Mesoporous Mater.* **2008**, *113*, 31.

[92] J. H. Drese, S. Choi, R. P. Lively, W. J. Koros, D. J. Fauth, M. L. Gray, C. W. Jones, *Adv. Funct. Mater.* **2009**, *19*, 3821.

[93] P. Kumar, S. Kim , J. Ida , V. V. GuliantsInd. *Eng. Chem. Res.*, **2008**, *47* , 201.

[94] G. P. Knowles, J. V. Graham, S. W. Delaney, A. L. Chaffee, *Fuel Process. Technol.* **2005**, *86*, 1435.

[95] X. Liu, B. Tian, C. Yu, F. Gao, S. Xie, B. Tu, R. Che, L. M. Peng, D. Y. Zhao, *Angew. Chem. Int. Ed.* **2002**, *41*, 3876.

[96] J. Jammaer, T. S. van Erp, A. Aerts, C. E. A. Kirschhock, J. A. Martens, *J. Am. Chem. Soc.* **2011**, *133*, 13737.

[97] X. Wang, S. Cheng, J. C. C. Chan, J. C. H. Chao, *Microporous Mesoporous Mater.* **2006**, *96*, 321.

[98] C. Amorim, G. Yuan, P. M. Patterson, M. A. Keane, *J. Catal.* **2005**, *234*, 268.

[99] E. Frackowiak, *Phys. Chem. Chem. Phys.* **2007**, *9*, 1774.

[100] G. Mezohegyi, F. P. van der Zee, J. Font, A. Fortuny, A. Fabregat, *J. Environ. Manage.* **2012**, *102*, 148.

[101] C. Lu, H. Bai, B. Wu, F. Su, J. Fen-Hwang, *Energy Fuels* **2008**, *22*, 3050.

[102] J. C. Palmer, J. D. Moore, T. J. Roussel, J. K. Brennan, K. E. Gubbins, *Phys. Chem. Chem. Phys.* **2011**, *13*, 3985.

[103] L. S. Ying, M. A. B. Salleh, H. B. M. Yusoff, S. B. A. Rashid, J. B. Abd Razak, *J. Ind. Eng. Chem.* **2011**, *17*, 367.

[104] R. Ryoo, S. H. Joo, S. Jun, *J. Phys. Chem. B* **1999**, *103*, 7743.

[105] M. Sevilla, A. B. Fuertes, *J. Colloid Interface Sci.* **2012**, *366*, 147.

[106] C. C. Hwang, Z. Jin, W. Lu, Z. Sun, L. B. Alemany, J. R. Lomeda, J. M. Tour, *ACS Appl. Mater. Interfaces* **2011**, *3*, 4782.

[107] J. Wang, C. Xue, Y. Lv, F. Zhang, B. Tu, D. Y. Zhao, *Carbon* **2011**, *49*, 4580.

[108] P. Chingombe, B. Saha, R. J. Wakeman, *Carbon* **2005**, *43*, 3132.

[109] T. Tozawa, J. T. A. Jones, S. I. Swamy, S. Jiang, D. J. Adams, S. Shakespeare, R. Clowes, D. Bradshaw, T. Hasell, S. Y. Chong, C. Tang, S. Thompson, J. Parker, A. Trewin, J. Bacsa, A. M. Z. Slawin, A. Steiner, A. I. Cooper, *Nat. Mater.* **2009**, *8*, 973.

[110] C. Xu, N. Hedin, *J. Mater. Chem. A* **2013**, *1*, 3406.

[111] H. M. El-Kaderi, J. R. Hunt, J. L. Mendoza-Cortes, A. P. Cote, R. E. Taylor, M. O'Keeffe, O. M. Yaghi, *Science* **2007**, *316*, 268.

[112] R. Babarao, J. W. Jiang, *Energy Environ. Sci.*, **2008**, *1*, 139.

[113] W. Yang, A. Greenaway, X. Lin, R. Matsuda, A. J. Blake, C. Wilson, W. Lewis, P. Hubberstey, S. Kitagawa, N. R. Champness, M. Schroder, *J. Am. Chem. Soc.* **2010,** *132*, 14457.

[114] a) S. N. Riduan, Y. G. Zhang, *Dalton Trans.* **2010**, *39*, 3347; b) Y. G. Zhang, S. N. Riduan, *Angew. Chem. Int. Ed.* **2011**, *50*, 6210.

[115] D. J. Darensbourg, M. W. Holtcamp, G. E. Struck, M. S. Zimmer, S. A. Niezgoda, P. Rainey, J. B. Robertson, J. D. Draper, J. H. Reibenspies, *J. Am. Chem. Soc.* **1999**, *121*, 107.

[116] R. Srivastava, D. Srinivas, P. Ratnasamy, *J. Catal.* **2005**, *233*, 1.

[117] A. J. Morris, G. J. Meyer, E. Fujita, *Accounts Chem. Res.* **2009**, *42*, 1983.

[118] F. Boccuzzi, A. Chiorino, M. Manzoli, D. Andreeva, T. Tabakova, *J. Catal.* **1999**, *188*, 176.

[119] J. Weitkamp, P. A. Jacobs, J. A. Martens, Appl. Catal. **1983**, 8, 123.

[120] J. Y. Lee, O. K. Farha, J. Roberts, K. A. Scheidt, S. T. Nguyen, J. T. Hupp, *Chem. Soc. Rev.* **2009**, 38, 1450

[121] J. S. Chang, S. E. Park, H. Z. Chon, Appl. Catal. A Gen. **1996**, 145, 111

[122] P. Frontera, A. Macario, A. Aloise, F. Crea, P.L. Antonucci, J.B. Nagy, F. Frusteri, G. Giordano, *Catal. Today* **2012**, *179*, 52.

[123] P. Frontera, A. Aloise, A. Macario, P.L. Antonucci, F. Crea, G. Giordano, J.B. Nagy, *Topic Catal*. **2010**, *53*, 265.

[124] A. N. Pinheiro, A. Valentini, J. M. Sasaki, A. C. Oliveira, *Appl. Catal. A Gen*, **2009**, *355*, 156.

[125] A. Luengnaruemitchai, A. Kaengsilalai, *Chem. Eng. J.* **2008**, **144**, 96.

[126] W. D. Zhang, B. S. Liu, C. Zhu, Y. L. Tian, *Appl. Catal. A Gen.* **2005**, *292*, 138.

[127] Z. J. Zuo, C. F. Shen, P. J. Tan, W. Huang, *Catal. Commun*. **2013**, *41*, 132.

[128] N. Wang, X. P. Yu, K. Shen, W. Chu, W. Z. Qian, *Int. J. Hydrogen Energy*, **2013**, *38*, 9718.

[129] N. Wang, X. P. Yu, Y. Wang, W. Chu, M. Liu, *Catalysis Today*, **2013**, *212*, 98.

[130] S. H. Zhang, S. Muratsugu, N. Ishiguro, M. Tada, *ACS Catal.* **2013**, *3*, 1855.

[131] N. Wang, K. Shen, L. H. Huang, X. P. Yu, W. Z. Qian, W. Chu, *ACS Catal.* **2013**, 3, 1638.

[132] L. L. Xua, H. L. Song, L. J. Chou, *Int. J. Hydrogen Energy*, **2013**, *38*, 7307.

[133] F. Gallucci, L. Paturzo, A. Basile, *Chem. Eng. Process*. **2004**, *43*, 1029.

[134] G. Bonura, M. Cordaro, L. Spadaro, C. Cannilla, F. Arena, F. Frusteri, *Appl. Catal. B Environ*. **2013**, *140*, 16.

[135] M. Tu, R. J. Davis, *J. Catal.* **2001**, *199*, 85.

[136] J. L. Song, Z. F. Zhang, S. Q. Hu, T. B. Wu, T. Jiang, B. X. Han, *Green Chem*. **2009**, *11*, 1031.

[137] H. Y. Cho, D. A. Yang, J. Kim, S. Y. Jeong, W. S. Ahn, *Catal. Today* **2012**, *185*, 35.

[138] J. Kim, S. N. Kim, H. G. Jang, G. Seo, W. S. Ahn, *Appl. Catal. A Gen*. **2013**, *453*, 175.

[139] Y. W. Ren, Y. C. Shi, J. X. Chen, S. R. Yang, C. R. Qi, H. F. Jiang, *RSC Adv.* **2013**, *3*, 2167.

[140] D. A. Yang, H. Y. Cho, J. Kim, S. T. Yang, W. S. Ahn, *Energy Environ. Sci.*, **2012**, *5*, 6465.

[141] C. M. Miralda, E. E. Macias, M. Zhu, P. Ratnasamy, M. A. Carreon, *ACS Catal*. **2012**, *2*, 180.

[142] W. Kleist, F. Jutz, M. Maciejewski, A. Baiker, *Eur. J. Inorg. Chem*. **2009**, 3552.

[143] M. L. Zhang, S. F. Ji, L. H. Hu, F. X. Yin, C. Y. Li, H. Liu, *Chinese J. Catal.* **2006**, *27*, 777.

[144] C. J. Liu, J. Y. Ye, J. J. Jiang, Y. X. Pan, *ChemCatChem*, **2011**, *3*, 529.

[145] M. Anpo, , H. Yamashita, K. Ikeue, Y. Fujii, S. G. Zhang, Y. Ichihashi, D. R. Park, Y. Suzuki, K. Koyano, T. Tatsumi, *Catalysis Today*, **1998**, *44*, 327.

[146] K. Ikeue, H. Yamashita, M. Anpo, *Chem. Lett.* **1999**, 1135.

[147] a) S. Udayakumar, M. K. Lee, H. L. Shim, S. W. Park, D. W. Park, *Catal. Commun*. **2009**, *10*, 659; b) J. N. Appaturi, F. Adam, *Appl. Catal. B Environ.* **2013**, *136–137*, 150.

[148] P. Serp, M. Corrias, P. Kalck, *Appl. Catal. A Gen.* **2003**, *253*, 337.

[149] R. B. Zhang, L. Liang, X. R. Zeng, J. Y. Shang, T. Wang, J. X. Cai, *Acta Phys. Chim. Sin.* **2012**, *28*, 1951.

[150] J. P. O'Byrne, R. E. Owen, D. R. Minett, S. I. Pascu, P. K. Plucinski, M. D. Jones, D. Mattia, *Catal. Sci. Technol*. **2013**, *3*, 1202.

[151] X. H. Xia, Z. J. Jia, Y. Yu, Y. Liang, Z. Wang, L. L. Ma, *Carbon*, **2007**, *45*, 717.

[152] C. Genovese, C. Ampelli, S. Perathoner, G. Centi, *J. Energy Chem*. **2013**, *22*, 202.

[153] G. W. Kling, M. A. Clark, H. R. Compton, J. D. Devine, W. C. Evans, A. M. Humphrey, E. J. Koenigsberg, J. P. Lockwood, M. L. Tuttle, G. N. Wagner, *Science*, **1987**, *236*, 169.

[154] J. Chapman, W. Goldthrope, J. Overton, P. Dixon, P. Hare, S. Murray, The Potential For Reducing the Costs of CCS in The U.K. Final Report, published by CCS Cost Reduction Taskforce and the Department of Energy and Climate Change, U.K. 2013.

[155] M. K. Lam, K. T. Tan, K. T. Lee, A. R. Mohamed, *Renew. Sust. Energ. Rev*. **2009**, *13*, 1456-1464.

Supporting Information

The Potential Applications of Nanoporous Materials for the Adsorption, Separation and Catalytic Conversion of Carbon Dioxide

Gregor Sneddon, Alex Greenaway, and Humphrey H. P. Yiu

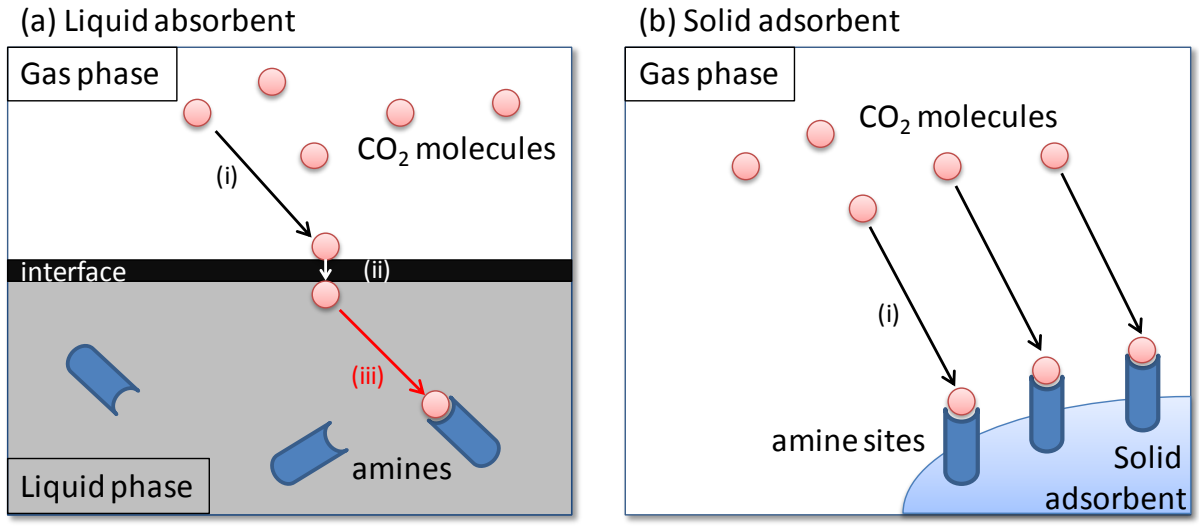

Figure S1. Schematic illustration for CO_2 chemisorption system using (a) a liquid phase absorbent and (b) a solid adsorbent. Arrows represent the mass transfer processes (i) diffusion in gas phase, (ii) solvation at gas-liquid interface driven by solubility, and (iii) diffusion in liquid phase.

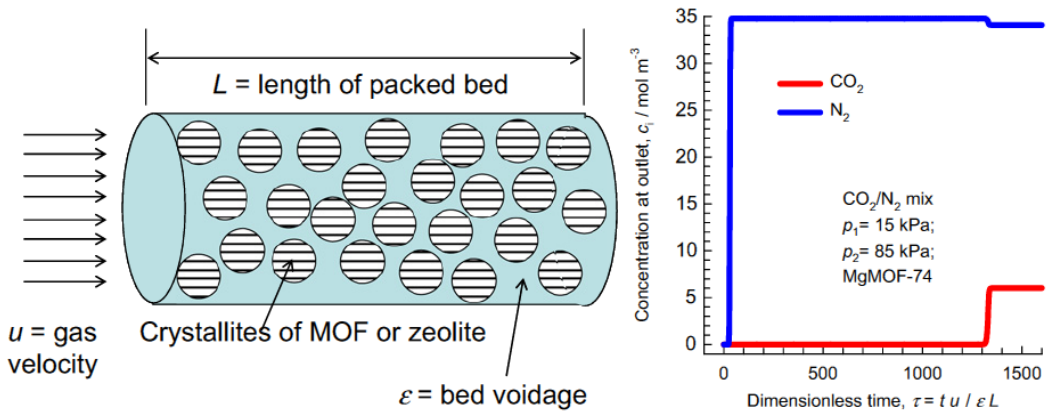

Figure S2. Schematic of packed bed adsorber, along with data on the breakthrough characteristics of an adsorber packed with MgMOF-74 crystallites with feed of CO_2(1)/N_2(2) mixture with p_1= 15 kPa, p_2= 85 kPa. (reproduced from [47])

Note S1.

The cation exchange capacity of zeolites, aluminosilicate minerals, is due to the aluminium substitution on the silica framework, causing a charge deficiency. In **Figure S3**, a proton (positively charged) is on the framework to balance this charge deficiency. However, this proton can be easily exchanged with other cations, notably alkali metal ions (Li^+, Na^+, K^+ etc.). Such phenomenon has been widely used in daily products including domestic water purifier for softening hard water. This cation exchange capacity is determined by the Si/Al ratio in the framework structure; the lower the Si/Al ratio of an aluminosilicate zeolite, the more the cation exchange sites will be available, hence the higher the cation exchange capacity.

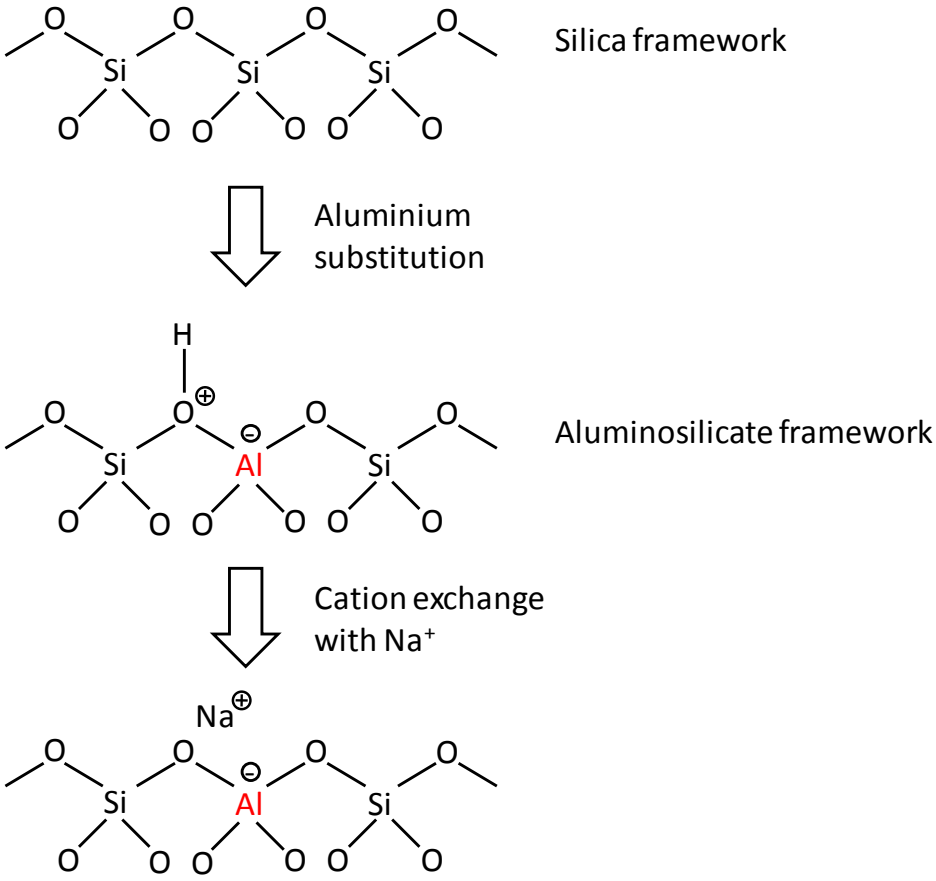

Figure S3. Graphical illustration for the cation exchange capacity of a zeolite.

CHAPTER 2

Sustainable CO_2 Adsorbents Prepared by Coating Chitosan onto Mesoporous Silicas for Large Scale Carbon Capture Technology

2.1 Background

Chitin is the major structural component of the shells of shrimp and other marine crustaceans and is a major waste product from the seafood industry. Chitosan is a copolymer derived from chitin comprised of randomly distributed *N*-acetyl-*β*-D-glucosamine and D-glucosamine units, Figure 2.1. Chitosan can be produced from chitin by either enzymatic hydrolysis with chitin deacetylase, or by reacting chitin with concentrated NaOH in a heterogeneous reaction [2.1]. Deacetylation using these methods is usually not complete but the material can be considered chitosan when >60 % deacetylation has been achieved. Chitosan has been widely studied in the literature with applications in food and agriculture, catalysis and biomedical applications [2.2]. Chitosan contains one NH_2 group per D-glucosamine unit, meaning the adsorption of one molecule of CO_2 would require the two D-glucosamine units. As discussed in Chapter 1, basic groups such as amines are essential to provide adsorption selectivity towards acidic groups such as CO_2. Chitosan as a solid adsorbent without any modification was measured to have a low CO_2 adsorption capacity of 0.02 $mmolg^{-1}$, therefore may not be a suitable adsorbent for CO_2. Although chitosan can be selective towards CO_2 due to the presence of amine groups within the structure, such a low adsorption capacity would need to be improved in order to make chitosan a suitable adsorbent. Limited literature is available on the use of chitosan as a CO_2 adsorbent. Yoshida et al. [2.3, 2.4] used chitosan deposition into the pores of the basic anion-exchange resin HPA 25 to maximise the available CO_2 adsorption capacity of the resin, a maximum capacity of 0.06 $mmolg^{-1}$ was measured for this material. This low capacity, although three times that of chitosan alone, was likely explained by the low surface area of the resin itself of 23-25 m^2g^{-1}.

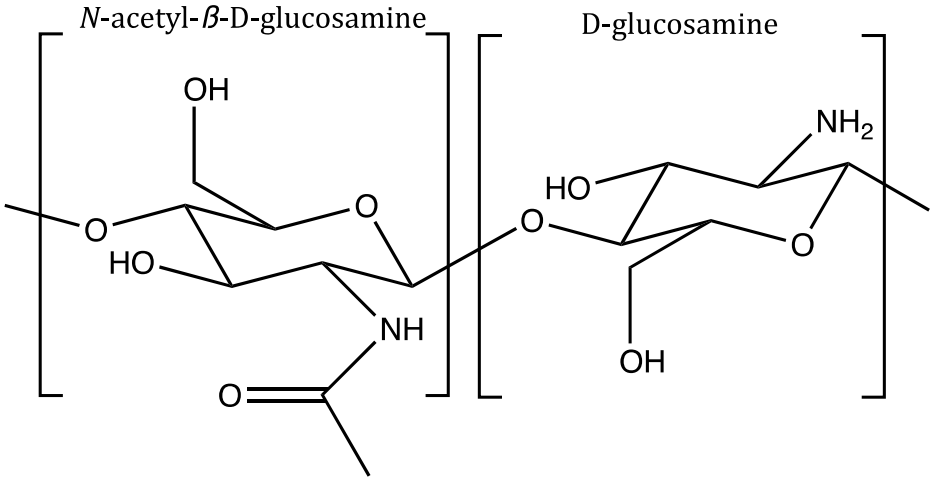

Figure 2.1 *N*-acetyl-*β*-D-glucosamine and D-glucosamine units of chitosan

2.3 Aim/Objectives

The main aim of this study was to demonstrate that chitosan can be used for the sustainable adsorption of CO_2, through deposition of chitosan into the pores of mesoporous silicas. The deposition into the large mesopores of fumed silica, SBA-15 and MCFs 3, 6 and 10 acted to increase the availability of NH_2 groups for CO_2 adsorption by increasing the overall available chitosan surface area. The presence of chitosan within these composite materials was confirmed by elemental analysis, TG/DSC and FTIR, with Raman spectroscopy used to determine the distribution of chitosan within the samples.

2.2 Methodology/Synthesis of Materials

Chitosan/mesoporous silica composites were prepared and tested as the CO_2 adsorbents in this chapter. The preparation procedure in general consists of 2 steps; preparation of support materials and chitosan deposition. The adsorbent samples were then characterised using FTIR spectroscopy, Raman spectroscopy, CHN elemental analysis, thermogravimetric analysis/differential scanning calorimetry (TGA/DSC), and BET surface area measurement.

2.2.1 Synthesis and Characterisations for SBA-15 and MCF Mesoporous Silicas

SBA-15 support material was prepared using a procedure selected for consistent repeatability [2.5]. In general, Pluronic 123 was used as the surfactant template and TEOS as the silica source. The gel was acidified using HCl and allowed to age for 24, prior to a hydrothermal treatment at 100°C in a PTFE bottle for 72 h. The resulting white precipitated SBA-15 material was filtered dried, and then calcined in air at 550°C for 6 h to remove the surfactant template.

Mesocellular foam (MCF) support materials were prepared using the same procedure as for SBA-15 but with the added use of the pore expanding agent TMB [2.6]. Three TMB/P123 ratios (0.3, 0.6 and 1.0) were chosen in order to generate support materials of a range of pore size for investigation on the relationship between pore structure and CO_2 adsorption capacity.

2.2.2 Coating Chitosan on Silica Supports

Initial experiments were carried out using fumed silica as support material in order to determine an optimum chitosan/silica support ratio. Deposition was achieved by dissolving chitosan in acetic acid solution (20mL, 0.2M) and mixing with fumed silica (1.0g). The chitosan/silica solution was allowed to sonicate for 1 hour to degas the composite material before drying in a petri dish to increase the evaporation rate of acetic acid. The composite was then dried at 50°C at a pressure of ≈ 20 mbar overnight the remove any residual acetic acid. The samples were finally ground using a mortar and pestle.

Based on the information from chitosan/fumed silica experiments, chitosan was supported on other mesoporous silica supports at a 19% w/w chitosan loading (0.24g chitosan with 1.0g silica support) which exhibited the highest CO_2 adsorption capacity. Samples were prepared as above substituting fumed silica for one of 4 mesoporous silica supports previously prepared, namely SBA-15, MCF-3, MCF-6 and MCF-10. Again, 1 g of these silica supports was mixed with 0.24g of chitosan in an acetic acid solution (20mL, 0.2M).

2.2.3 Adsorbent Sample Characterisation

The support SBA-15, MCF and fumed silica materials as well as the composite materials were analysed by nitrogen adsorption/desorption isotherms using a Micromeritics Gemini VII 2390p unit. The isotherms were recorded at -196°C and revealed information about the BET surface area, pore size distribution and pore volumes of the support and composite materials. The support materials were further characterised by transmission electron microscopy (TEM) using a Tecnai T20 microscope (200 keV). TEM analysis was carried out by Colin How, University of Glasgow physics department. TEM images were recorded to investigate the surface characteristics of the support materials and in the case of SBA-15 to ensure a highly ordered hexagonal porous array. Chitosan/mesoporous silica composite materials were characterised by TGA/DSC using a TA Instruments SDT Q600 thermobalance. TGA/DSC experiments were carried out in air to confirm the mass of organic material within the composite through oxidative decomposition of the chitosan component. CHN elemental analysis was carried out on the chitosan/mesoporous silica samples using a CE 440 Elemental Analyser to determine the percentage content of carbon, hydrogen and nitrogen within the samples. CHN analysis was carried out by Brian Hutton, Heriot-Watt University chemistry department. FTIR spectra were recorded of the chitosan/mesoporous silica composite materials using a Perkin Elmer Spectrum 100 spectrophotometer. These experiments were carried out to determine the vibrational spectrum of the composite material and identify the chitosan material within the composite by comparison with the vibrational spectrum of unsupported chitosan. Raman spectroscopy was additionally carried out on the chitosan/fumed silica composite materials using a Horriba LabRam-HR spectrometer. Raman spectroscopy was employed to determine the distribution of chitosan within the composite material to ensure even deposition within the pore structure. Raman spectroscopy was carried out by Dr Alexey Ganin, University of Glasgow chemistry department.

2.2.4 Measuring the CO_2 Adsorption Capacities

Two methods were used for measuring the CO_2 adsorption capacity; volumetric and gravimetric method. The volumetric CO_2 adsorption capacity of the composite materials was measured using the Micromeritics Gemini VII 2390p unit. This was achieved by

measuring the CO_2 adsorption isotherm at 25°C in a closed system for the composite materials using 100% CO_2 between a P/P_o = 0–760 mmHg.

The gravimetric method was carried out using the SDT Q600 unit with a cyclic custom programme. In a typical measure, a sample was activated at 75°C overnight prior to adsorption studies. After activation, the sample was cooled down to 25°C and a 50:50 v/v gaseous mixture of CO_2:N_2 was purged through the sample for 90 min once the weight stabilised. After 90 min of exposure, the temperature was raised to 75°C at a rate of 5°C min^{-1} and held at 75°C for a further 30 min to allow CO_2 desorption and hence regeneration of samples to complete. The temperature was then decreased to 25°C for the second adsorption loop. This procedure was repeated for four cycles to test the regeneration of the adsorption medium. Figure 2.2 showed a typical adsorption-desorption loop of CO_2 on an adsorbent sample. CO_2 adsorption capacity was determined based on the increase in the sample weight after introduction of CO_2 to the adsorbent material using Equations 1 and 2.

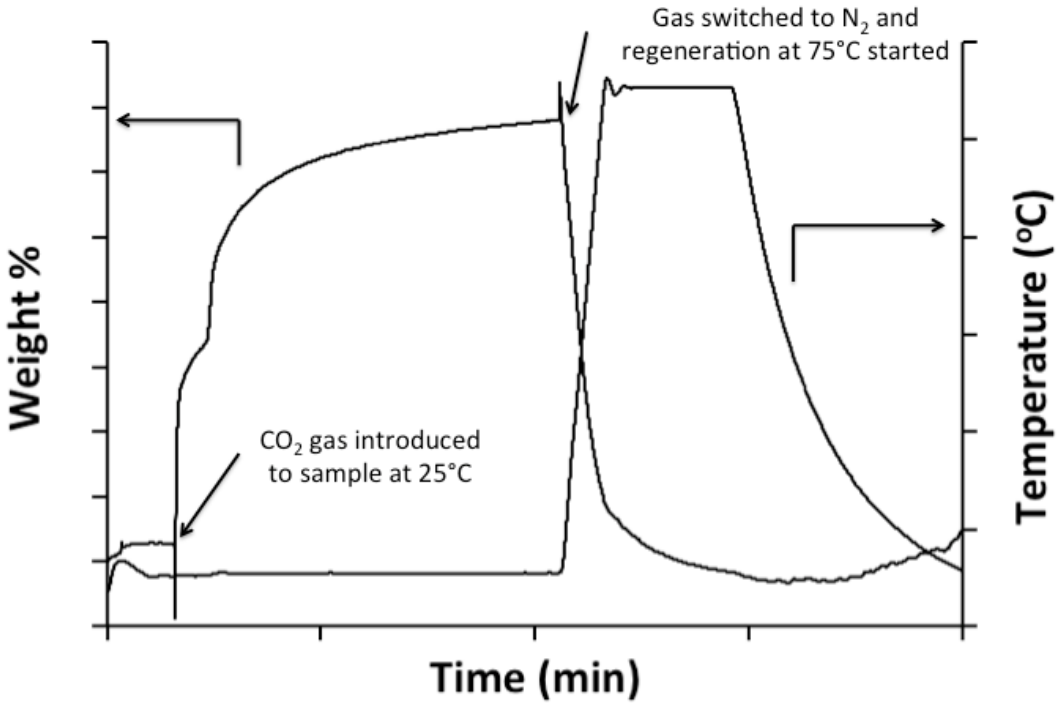

Figure 2.2 Results of a typical gravimetric CO_2 adsorption experiment by TGA/DSC. The increase in mass observed upon switching to a CO_2:N_2 atmosphere is used to calculate the CO_2 adsorption capacity. CO_2 adsorption is carried out at 25°C for 90 minutes and desorption carried out at 75°C for 30 minutes.

$$Moles\ CO_2\ Adsorbed\ (mol) = \frac{Mass\ Gained\ by\ TGA\ (g)}{MW\ CO_2\ (gmol^{-1})} \quad (1)$$

$$CO_2\ Adsorption\ Capacity\ (mmolg^{-1}) = \frac{Moles\ CO_2\ Adsorbed\ (mol)}{Mass\ of\ adsorbent\ (g)} \times 1000 \quad (2)$$

2.4 Findings

Chitosan was initially deposited onto the fumed silica support at loadings of 7.4, 14, 19, 24, 29 and 32 wt%. The assigned FTIR spectrum of chitosan was successfully used to confirm the presence of chitosan in the composite material. The organic content of the composite material was confirmed by TGA and elemental analysis, with both methods of analysis in good agreement. Raman spectroscopy was used to probe the relative dispersion of chitosan within the pores of the fumed silica. Raman of a 19 wt% loaded composite indicated the chitosan to be evenly dispersed within the fumed silica pore network. The series of composite materials, as well as the unmodified fumed silica and a control sample of fumed silica treated with acetic acid only were analysed with BET surface area analysis. The surface area data indicated no change in surface area between the unmodified fumed silica and the control sample but a steady decrease in the surface area as the chitosan content increased. Closer inspection of the pore volumes of the composite materials, indicated that upon deposition of 7.4 wt% chitosan there is a decrease in the number of pores with pore volume <8 nm but an increase in pores with pore volume >10 nm when compared to the unmodified fumed silica. This phenomenon was thought to be due to the interconnection of larger pores after chitosan deposition. A chitosan loading of 19 wt% was determined to have both a high pore volume (0.33 cm^3g^{-1}) while still maintaining a relatively high surface area (123 m^2g^{-1}), for this reason a 19 wt% loading was chosen as the benchmark loading for this work.

Chitosan was also coated onto the mesoporous silica supports SBA-15, MCF-3, MCF-6 and MCF-10 at a 19 wt% loading, see Table 2.1 for organic content determination by TG/DTA and CHN analysis. Even deposition of chitosan was observed within the pore structure of these materials, with a 30-50% loss of pore volume in both the 4-10 nm and >10 nm ranges. High surface areas were also maintained for these samples between 187 and 376 m^2g^{-1}. The maintaining of a high surface area and pore volume is indicative of deposition into the pore network and not

just onto the surface of the mesoporous support. If deposition had occurred onto only the surface of the mesoporous silica, larger losses would be observed in surface area and pore volume due to pore blockage. BET surface area analysis of all chitosan/silica composite materials indicated a loss in surface area and pore volume in the N_2 adsorption/desorption isotherms after deposition of chitosan.

CO_2 adsorbent	Expected organic content (wt%)	Organic Content from TGA thermal decomposition (wt%)	Organic content from CHN analysis (wt%)
Chitosan/fumed silica	19	16	17
Chitosan/SBA-15	19	20	19
Chitosan/MCF-3	19	17	20
Chitosan/ MCF-6	19	19	16
Chitosan/ MCF-10	19	18	20

Table 2.1. Organic content of composite samples from TGA and CHN analysis

A CO_2 adsorption capacity of 0.29 $mmolg^{-1}$ was measured volumetrically and 0.09 $mmolg^{-1}$ measured gravimetrically for the chitosan/fumed silica composite material with 19 wt% chitosan. The differences observed in adsorption capacities are attributed to the methods used. The volumetric method can be considered a static closed system using 100% CO_2, whereas the gravimetric method is a dynamic flow system using a 50:50 CO_2:N_2 gas stream. Crucially, the unmodified fumed silica material showed no apparent uptake using a gravimetric method, with no increase in mass observed when switching between 100% nitrogen and a CO_2 containing atmosphere. This represents an increase in capacity up to 0.47 $mmolg^{-1}_{chitosan}$ when considering only the chitosan content of the composite material. This is a fair comparison to make since it has been proven that unmodified fumed silica shows no uptake of CO_2 in gravimetric methods.

CO_2 adsorption experiments were performed on the chitosan/mesoporous silica composite materials both using a volumetric and gravimetric method. As with the

chitosan/fumed silica composite material, a *ca.* 3 times higher CO_2 adsorption capacity was measured when using a volumetric method compared to a gravimetric method. The highest CO_2 adsorption capacity was measured for the chitosan/MCF-3 composite material at 0.98 $mmolg^{-1}$ by a volumetric method and 0.34 $mmolg^{-1}$ by a gravimetric method. The other chitosan/mesoporous silica composites studied recorded volumetric CO_2 adsorption capacities within the 0.75-0.8 $mmolg^{-1}$ range and gravimetric CO_2 adsorption capacities within the 0.26-0.32 $mmolg^{-1}$ range. It would be expected that the composite material with the largest surface area and pore volume would have the greatest potential for CO_2 adsorption when considering physisorption alone. However, this is not the case with this series of chitosan/silica composite materials, as the Chitosan/MCF-3 material had the lowest surface area and pore volume with the exception of chitosan/fumed silica. When comparing all CO_2 adsorption data for the chitosan/silica composite materials, there is no direct correlation drawn from the physical characteristics of the surface and the CO_2 adsorption capacity. This suggests a complex relationship between the structural parameters of the surface (pore volume and surface area) and the CO_2 adsorption capacity.

Gas composition analysis was also carried out for the Chitosan/MCF-3 composite material by varying the percentage of CO_2 in the gas stream during gravimetric adsorption experiments. The gas compositions studied were 100, 50, 13 and 8% of CO_2 in an N_2 gas stream. Gas streams containing CO_2 at levels of 13% and 8% were used to mimic the CO_2 content of the flue gas from coal-fired and gas-fired power stations respectively. When using 100% CO_2 a maximum adsorption capacity of 0.42 $mmolg^{-1}$ was achieved quickly, within 30 minutes of exposure to CO_2. Using 50% CO_2 the maximum adsorption of 0.34 $mmolg^{-1}$ was achieved after *ca.* 90 minutes. When using both 13% and 8% CO_2 content in the gas stream a maximum adsorption capacity of 0.10 $mmolg^{-1}$ was measured in each case after *ca.* 90 minutes. This valuable information suggests that these waste polymer containing composite materials could, realistically be used as a CO_2 adsorbent with a reasonable CO_2 adsorption capacity to adsorb CO_2 from the flue gas stream. Another key component of the flue gas stream is water (6-15%). As discussed previously in this thesis, water can prove problematic for some solid adsorbents such as zeolite or MOF materials, which can be quickly deactivated by water. The surface amine adsorption mechanism of these chitosan/silica adsorbents means that deactivation by water would be unlikely. Furthermore, these

adsorbents were produced from an aqueous acetic acid solution initially, suggesting water content of the flue gas would have little effect on adsorption capacity.

Regeneration studies were also performed using the Chitosan/MCF-3 composite material. Adsorption was carried out at 25°C using a 50% CO_2 in N_2 gas stream for 90 minutes. Desorption/regeneration was carried out at 75°C for 30 minutes in a 100% N_2 stream, with a maximum of 4 regeneration cycles performed. CO_2 Adsorption capacities of 0.34, 0.30, 0.30 and 0.29 $mmolg^{-1}$ were achieved for cycles 1 to 4 respectively. This equates to an overall drop in capacity of less than 15% after 4 regeneration cycles and a minimum retention of capacity of 88% between cycles. Interestingly, there is a step-wise decrease in weight after every adsorption cycle. This is due to residual strongly bound water and acetic acid leaving the adsorbent at 75°C during CO_2 desorption. This loss of this bound solvent has no effect on the adsorption of the material during the next adsorption cycle. The relatively low regeneration temperature required for these composite materials demonstrates great improvement over other adsorbent materials, thanks to decrease in the cost of the high energy regeneration step.

2.5 Conclusion

Chitosan/mesoporous silica materials were successfully produced and their suitability to the application of CO_2 adsorption proven, with a maximum volumetric CO_2 adsorption capacity of 0.98 $mmolg^{-1}$ determined at 25°C. These materials are also thermally (up to 200°C) and chemically stable and importantly, regenerable at a low temperature of 75°C with 85 % capacity retained after 4 regeneration cycles. When compared to other solid state adsorbents such as aminated mesoporous silicas, carbon nanotubes or MOFs, the method for synthesis is substantially more "green". No toxic solvents are used and preparations occur at room temperature and pressure. The ease of synthesis and low energy required for regeneration is beneficial for applications in industry, especially when compared to the high energy regeneration process associated with the used of monoethanolamine (MEA) solutions.

Furthermore, the use of a major food waste such as chitosan is advantageous, as it uses one major waste material to tackle another environmental problem. Fumed silica is already heavily used in industry, suggesting chitosan/fumed silica composites could be used in the short term in industry to tackle rising CO_2 levels. Once more environmentally friendly ways of producing high surface area silicas such as SBA-15 and MCF-3 become available, these materials could then be used for CO_2 adsorption. Indeed, any suitable non-silica support with a surface area and pore structure similar to that of MCF-3 could prove adequate for deposition of chitosan.

2.6 Impact On Literature and Research

This novel research is of significant benefit to the ever-expanding research area that is carbon capture. The use of sustainable chitosan/silica composite materials for CO_2 adsorption provides a suitable alternative to specifically designed state-of-the-art adsorbents. Prior to the undertaking and publishing of this body of work, very little research existed in the literature pertaining to the use of chitosan or indeed natural polymers as an adsorbent for CO_2. The works that did utilise chitosan within the literature did not use chitosan as the primary adsorbent. Chitosan was used to deposit into the macroporous pore network as a method for boosting CO_2 adsorption capacity of an already established adsorbent rather than as the primary adsorbent itself. This work has provided evidence that with an increase in available surface amines, through deposition on a suitable support material, chitosan can be used for the solid-state adsorption of CO_2. Chitosan is not only suitable for CO_2 adsorption after modification but can also do so on a level comparable to specifically designed adsorbents. This publication was an invited article, submitted at the request of the Energy Technology journal. Additionally this paper was highlighted as the inside cover of the issue it was published in.

2.7 References

[2.1] M. Rinaudo, *Chitin and chitosan: Properties and applications*, Prog. Polym. Sci., **31**, 603-632 (2006)

[2.2] J. Berger, M. Reist, J. M. Mayer, O. Felt, N. A. Peppas, R. Gurny, *Structure and interactions in covalently and ionically crosslinked chitosan hydrogels for biomedical applications*, Eur. J. Pharm. Biopharm., **57**, 19-34 (2004)

[2.3] H. Yoshida, S. Oehlenschlaeger, Y. Minami, M.Terashima, *Adsorption of CO_2 on Composites of Strong and Weak Basic Anion Exchange Resin and Chitosan*, J. Chem. Eng. Japan., **35**, 32-39 (2002)

[2.4] H. Yoshida, S. Oehlenschlaeger, Y. Minami, M. Terashima in *Adsorption Science and Technology* (Ed. D.D. Do), World Scientific Publishing, Singapore, 693-697 (2000)

[2.5] H. H. P. Yiu, M. A. Keane, Z. A. D. Lethbridge, M. R. Lees, A. J. El Haj, J. Dobson, *Synthesis of novel magnetic iron metal–silica (Fe–SBA-15) and magnetite–silica (Fe_3O_4–SBA-15) nanocomposites with a high iron content using temperature-programed reduction*, Nanotechnology, **19**, 255606 (2008)

[2.6] P. Schmidt-Winkel, C. J. Glinka, G. D. Stucky, *Microemulsion Templates for Mesoporous Silica*, Langmuir, **16**, 356-361 (2000)

DECLARATION

As primary author of this publication, I can confirm the majority of the work to be my own, with TEM, CHN and Raman spectroscopy sample analysis carried out by other parties as outlined in Section 2.2.3.

Signature: _____

PUBLICATION 2

Sustainable CO_2 Adsorbents Prepared by Coating Chitosan onto Mesoporous Silicas for Large Scale Carbon Capture Technology

Gregor Sneddon, Alexey Y. Ganin, Humphrey H. P. Yiu

DOI: 10.1002/ente.201402211

Energy Technology **2015**, 3, 249

Abstract

In this article, we report a new sustainable synthesis procedure for manufacturing chitosan/silica CO_2 adsorbents. Chitosan is a naturally abundant material and contains amine functionality, which is essential for selective CO_2 adsorptions. It is, therefore, ideally suited for manufacturing CO_2 adsorbents on a large scale. By coating chitosan onto high-surface area mesoporous silica supports, including commercial fumed silica (another economical and accessible reagent) and synthetic SBA-15 and MCF silicas, we have prepared a new family of CO_2 adsorbents, which are fully characterised with nitrogen adsorption isotherms, TGA/DSC, TEM, FTIR and Raman spectroscopy. These adsorbents have achieved a significant CO_2 adsorption capacity of up to 0.98 mmol g^{-1} at ambient conditions (1 atm and 25°C). The materials can also be fully regenerated/recyclable on demand at temperature as low as 75°C with a >85% retention of adsorption capacity after 4 cycles, making them promising candidates for advanced CO_2 capture, storage and utilisation (CCSU) technology.

1. Introduction

Despite impressive development of renewable energy sources for power generation, the progress is insufficient for tackling the worldwide problem of increasing "greenhouse gas" emission from industry, in particular the energy sector [1]. For example, with only a 4% growth predicted for the electricity generated from renewable sources over the next 30 years [2], CO_2 carbon capture storage (CCS) remains the only viable solution. With the world's first commercial CCS plants already in operation [3] and there has been a strong demand for development of the current CCS technology, enabling the additional utilisation step of CO_2. Current CCS technology in power generation industry employs amine solutions, such as 30% monoethanolamine in water, for eliminating CO_2 from the flue gas stream [4]. Despite high recovery rate of CO_2 up to 98% shown for these solutions [5], there are numerous disadvantages associated with this technology. These include: (1) high energy consumption required for regenerating the aqueous amine absorbent; (2) degradation of the amine by other flue gas components e.g. SO_2, NO_2, HCl and oxygen; (3) corrosion of equipment and (4) high toxicity.[6-9] Consequently, new solid state adsorbents for CO_2 with a high specificity and enhanced energy efficiency, handling and regeneration capabilities are needed for fully advancing the CCSU technology.[10]

Several types of solid adsorbents have been proposed for CCSU including nanoporous carbons, metal organic frameworks (MOFs), aminated mesoporous silicas and microporous organic polymers [11-13]. Take aminated mesoporous silica (NH_2-SBA-15 or NH_2-MCM-41) as an example, this adsorbent shows a good CO_2 capacity adsorption typically of 1.0 to 3.6 mmol g^{-1} at 1 atm and 25°C [14-16]. However, the synthesis of aminated mesoporous silica involves grafting of toxic 3-aminopropyltriethoxysilicate (APTES), which is destructive to the mucous membranes and the upper respiratory tract of human body, and the use of toluene as solvent in a ca.100-times quantity (1 g of silica in 100 mL toluene) [17]. For industrial scale productions of adsorbents, excessive use of aromatic solvents and toxic reagents should be avoided.

Chitosan is a natural polysaccharide which contains randomly distributed D-glucosamine units (see **Figure 1**) and has been widely used in various biomedical

applications [18], indicating its benign nature to humans. Similar to other amine-based adsorbents, CO_2 adsorption can take part on the free amine groups of the D-glucosamine units by the cooperative adsorption of one CO_2 molecule with two adjacent amine groups [19]. Chitosan is a sustainable reagent because it occurs naturally as chitin which is a major waste of seafood industry [20]. Such mass scale availability presents an ultimate opportunity to create a viable platform for carbon storage on demand if problems associated with the low surface area of chitosan and, hence, low adsorption properties, could be resolved. This challenge, however, could be addressed by coating chitosan onto an appropriate support material with a high surface area. For example, Yoshida et al. have coated chitosan onto the macropores of a basic anion exchange resin HPA 25 and achieved an adsorption capacity of 0.06 mmol g^{-1} using a 27% w/w chitosan/HPA 25 composite [21, 22]. However, such a low capacity was linked to the low surface area of the HPA 25 resin, only 23 – 25 m^2g^{-1}. To maximise the potential of chitosan as a CO_2 adsorbent, a support material with a much higher surface area will be required.

To address the challenge of finding a highly specific, high-surface area and low-cost CCSU adsorbent, while capable of releasing CO_2 on demand at low temperatures, we employed a strategy by coating high surface area silicas such as SBA-15 and mesocellurar foams MCF's with chitosan. Porous silica materials have a good thermal stability and high porosity and have been widely used as industrial adsorbents.[23] This enabled us to develop an efficient, sustainable CO_2 adsorbent which can lead to a significant advancement towards a large-scale production, overcoming one major obstacle of CCSU technologies for practical industrial use.

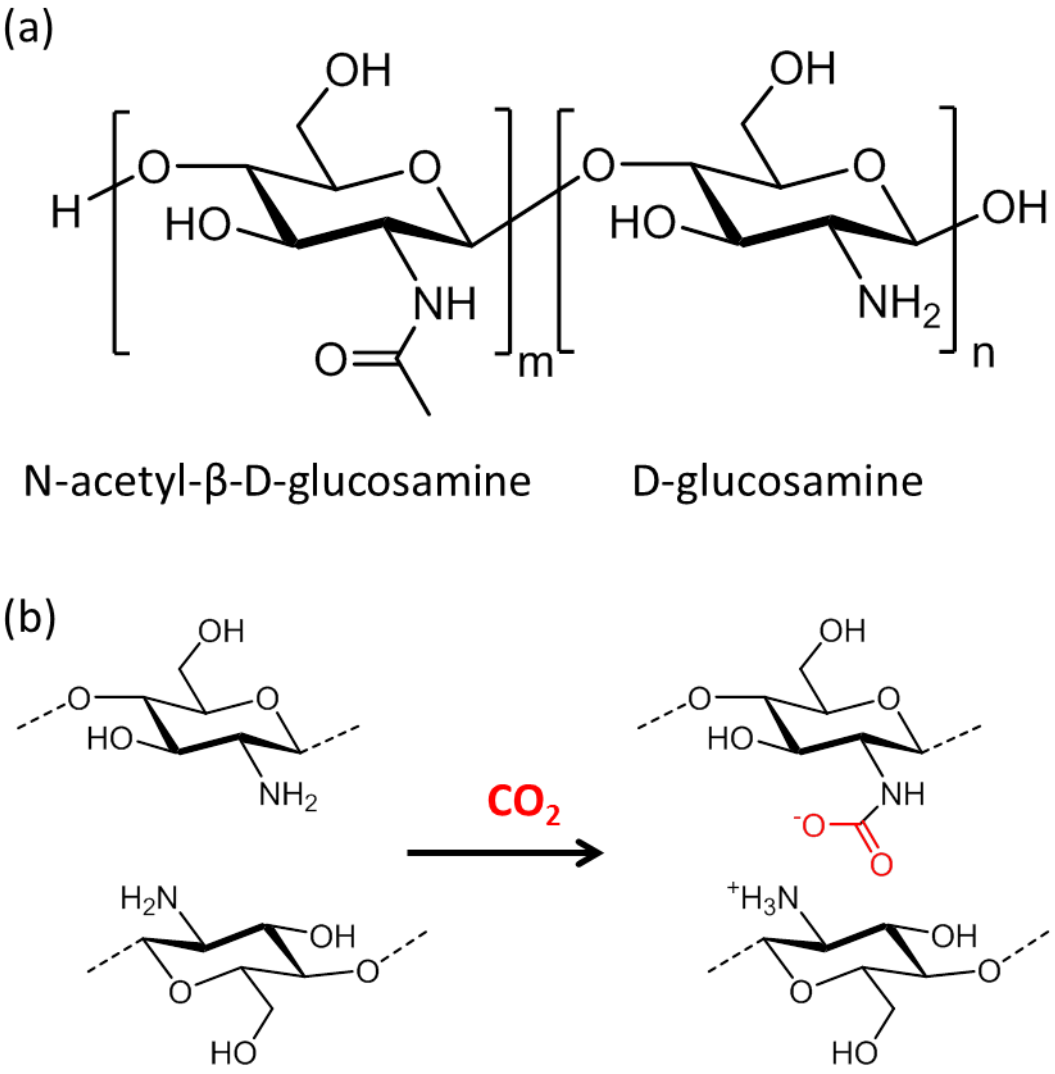

Figure 1. (a) structure of chitosan, showing the N-acetyl-β-D-glucosamine and D-glucosamine units, (b) The cooperative adsorption of one CO_2 molecule by two D-glucosamine units of the chitosan.

2. Experimental

2.1 Materials

Low molecular weight chitosan (75-85% deacetylated), fumed silica with a BET surface area ca. 200 $m^2\ g^{-1}$ (data provided by supplier), glacial acetic acid (99.7%), tetraethyl orthosilicate (TEOS, 98%) and 1,3,5-trimethylbenzene (TMB, or mesitylene, 98%) were all purchased from Sigma Aldrich. Concentrated hydrochloric acid (37%) was supplied by Fisher Scientific. Pluronic P123 surfactant ($EO_{20}PO_{70}EO_{20}$, M_w = 5800) was kindly donated by BASF. Deionised water was used in all experimental

procedures. All chemicals were used as received without further purification. All gases used (N_2 He, and CO_2, all > 99.99%,) were supplied by BOC.

2.2 Synthesis and characterisations for SBA-15 and MCF mesoporous silicas

The procedure for preparing SBA-15 was selected due to its high reproducibility [24]. In a typical synthesis, Pluronic P123 surfactant (4 g) was first dissolved in an acidic solution containing concentrated hydrochloric acid (10 mL) and deionised water (139 mL) at 30°C. Once the surfactant was fully dissolved, TEOS (8.3 g) was added dropwisely and the reaction mixture was allowed to stir for 24 h at 30°C. The solution was then transferred to a PTFE bottle and heated in an oven to 100°C for 72 h. The white precipitates were then filtered using a Büchner flask and funnel and allowed to dry overnight. The white solid was then calcined in air at 550°C for 6 hours to remove the surfactant template.

For MCF support materials, same procedure as the SBA-15 synthesis was carried out but the pore expanding agent TMB (1.2 g, 2.4 g and 4.0 g) was added to the surfactant solution and allowed to completely dissolve, prior to the addition of TEOS [25]. The samples were also calcined at 550°C for 6 h. These materials were denoted as MCF-n where n indicates the TMB/P123 w/w ratio, hence MCF-3 has a TMB/P123 ratio of 0.3 (i.e. 1.2 g TMB and 4.0 g P123).

2.3 Coating Chitosan on Silica Supports

In order to determine the optimum chitosan/silica ratio, a series of samples were prepared using fumed silica as a model support material. In a typical experiment, 1.0 g of fumed silica support was mixed with a chitosan solution (0.08 g, 0.16 g, 0.24 g, 0.32 g, 0.40 g and 0.48 g of chitosan to give 7.4%, 14%, 19%, 24%, 29%, and 32% w/w samples) in acetic acid (20 mL, 0.2 M). Once mixed the fumed silica/chitosan solutions were sonicated for 1 h to degas the samples in an ultrasonic bath in order to encourage pore filling with chitosan solution. After degassing, the sample suspensions were transferred to petri dishes to dry at room temperature in a fume cupboard. Petri dishes were used to increase the evaporation rate of acetic acid. After drying for 48 h the

samples were then dried in a vacuum oven at 50°C and a reduced pressure of *ca.* 20 mbar overnight to remove residual acetic acid. The dried samples were finally grinded using a set of mortar and pestle. The supported chitosan are notated as chitosan/support while the % in the notation indicates the designated chitosan content in % w/w. For example, chitosan/fumed silica (19%) refers to the 19% w/w chitosan on fumed silica, which was prepared with 0.24 g of chitosan with 1 g of support. Chitosan supported on other mesoporous silica samples (19% w/w) were similarly prepared using 1 g of silica support (SBA-15, MCF-3, MCF-6, or MCF-10) with a chitosan solution containing chitosan (0.24 g, based on the results from chitosan/fumed silica samples) and acetic acid (20mL, 0.2 M).

2.4 Sample Characterisations

The structural characters of SBA-15 and MCFs were studied using nitrogen adsorption-desorption isotherms and transmission electron microscopy (TEM). The N_2 adsorption-desorption isotherms were measured using a Micromeritics Gemini VII 2390p unit. All samples were outgassed at 80°C under flowing nitrogen for 2 h using a Flowprep unit (Micromeritics). Nitrogen adsorption/desorption isotherms were recorded at -196°C. The BET surface area, pore size distribution and BJH pore volume were calculated using Micromeritics software V1.03A. TEM analysis was carried out using a Tecnai T20 microscope (200keV).

The chitosan/mesoporous silica samples were characterised with nitrogen adsorption isotherms, thermogravimetric analysis (TGA), CHN elemental analysis, and vibration spectroscopies (FTIR and Raman). BET surface area and pore volume analysis was carried out using a Micromeritics Gemini VII 2390P unit with the same procedure described above. Thermal analysis (simultaneous TGA and DSC) was performed using a TA Instruments SDT Q600 thermobalance. TGA and DSC data were collected between 20°C and 800°C at a heating rate of 10°C min^{-1} with air as the carrier gas. Elemental analysis (CHN) was carried out using a CE 440 Elemental Analyser. Carbon, hydrogen and nitrogen content (as percentages) in samples were determined to an error of 0.15%. The FTIR spectra were recorded using a Perkin Elmer Spectrum 100 spectrophotometer. Spectra were collected at the wavenumber range between 650-4000 cm^{-1} with 16 scans at a resolution of 4 cm^{-1}. Raman spectroscopy was carried out on a

powdered sample on a Horriba LabRam-HR spectrometer operated in back-scattered geometry using a 532 nm laser at ambient temperature over a sample area of 100 μm^2. Calibration was performed by referencing the spectrometer to the 520.1 cm^{-1} silicon line. The typical acquisition times were 6 × 30 s. Several spectra recorded in different point for each probed samples indicated consistently that the peaks were associated with the spectra of chitosan. Raman imaging technique was also employed over a wider area of 50 × 60 mm on a selected sample to probe the bulk character of the coated materials and to test the distribution of the chitosan within the composite materials.

2.5 Volumetric and gravimetric CO_2 uptake and Regeneration study using adsorption isotherm and TGA

Volumetric adsorption study (p/p_0 = 0 – 760 mmHg) was carried out using the Micromeritics Gemini VII 2390p unit fitted with a chiller bath set at 25°C. The samples were outgassed at 80°C under flowing N_2 prior to CO_2 adsorption measurement. For the gravimetric adsorption measurements, the SDT Q600 unit was used with a cyclic custom programme. Samples were activated at 75°C overnight prior to adsorption studies. After activation, the samples were cooled down to 25°C and a 50:50 v/v gaseous mixture of CO_2:N_2 was purged through the sample for 90 min once the weight stabilised. After 90 min of exposure, the temperature was raised to 75°C at a rate of 5°C min^{-1} and held at 75°C for a further 30 min to allow CO_2 desorption and hence regeneration of samples to complete. The temperature was then decreased to 25°C for the second adsorption loop. This procedure was repeated for four cycles to test the regeneration of the chitosan/MCF-3 sample. CO_2 adsorption tests were also carried out at varying CO_2:N_2 volume ratios (100% CO_2, 13% CO_2 and 8% CO_2) using the chitosan/MCF-3 sample. This was carried out to mimic the flue gas environment of coal fired (13% CO_2) and gas fired (8% CO_2) power stations.

3. Results and discussion

3.1 Characterisation of Silica Supports

Fumed silica, a chosen support material for this study, is a commercial mesoporous silica (e.g. Cab-O-Sil) with a high surface area (200 $m^2 g^{-1}$) and widely used in industry, [26] implying that the chitosan/fume silica composites developed here would be suitable for large-scale applications including CO_2 capture. The structural parameters, including BET surface area, pore size distribution and pore volume, of all silica supports used in this work are summarised in **Table 1**. The fumed silica support was found to have a BET surface area of 186 $m^2 g^{-1}$ and a pore volume of 0.29 $cm^3 g^{-1}$. **Table 1** also shows the structural parameters for two types of synthetic mesoporous silicas (SBA-15 and MCF's), which were selected for the study on the effect of mesoporous structure of the support on the chitosan deposition. Nitrogen adsorption and desorption isotherms for all silica supports shown in **Figure 2b-e** exhibit Type IV isotherm character with a hysteresis loop, typical for mesoporous materials, while fumed silica (**Figure 2a**) showed a transitional Type II to Type IV isotherm due to its large mesopores. The pore size distribution of SBA-15 (calculated from the adsorption data, **Figure S1**) peaks at 8 nm in diameter, which is typical for an SBA-15 sample.

MCF's are essentially pore-expanded SBA-15 using trimethyl benzene (TMB) as the swelling agent. Control of pore size was achieved by varying the TMB:P123 ratio; the higher the ratio, the larger the pores were found. However, the meso-scaled structure becomes less ordered when the TMB:P123 ratio increases. In contrast to the 2-D hexagonal pore array structure of SBA-15, MCF silicas have a "foam-like" (or bubble-like) structure with interconnected cages. In **Table 1**, the pore volume data was presented as "small" mesopores (< 4 nm in diameter), "medium" mesopores (4 – 10 nm) and "large" mesopores (> 10 nm). Due to the long range order of tubular pores, the porous structure of SBA-15 was dominated by the "medium" mesopores (0.7 $cm^3 g^{-1}$). Regarding MCF supports, although the BET surface area was decreasing due to the loss of long range order, the pore volume of "large" mesopores gradually increases from 0.04 $cm^3 g^{-1}$ for SBA-15 to 0.7 $cm^3 g^{-1}$ for MCF-10. Among all MCF samples, the "medium" mesoporous volume remains roughly unchanged. Such difference in pore volume provides us a "structural tool" to study the effect of pore size on chitosan deposition and consequently CO_2 adsorption capacity.

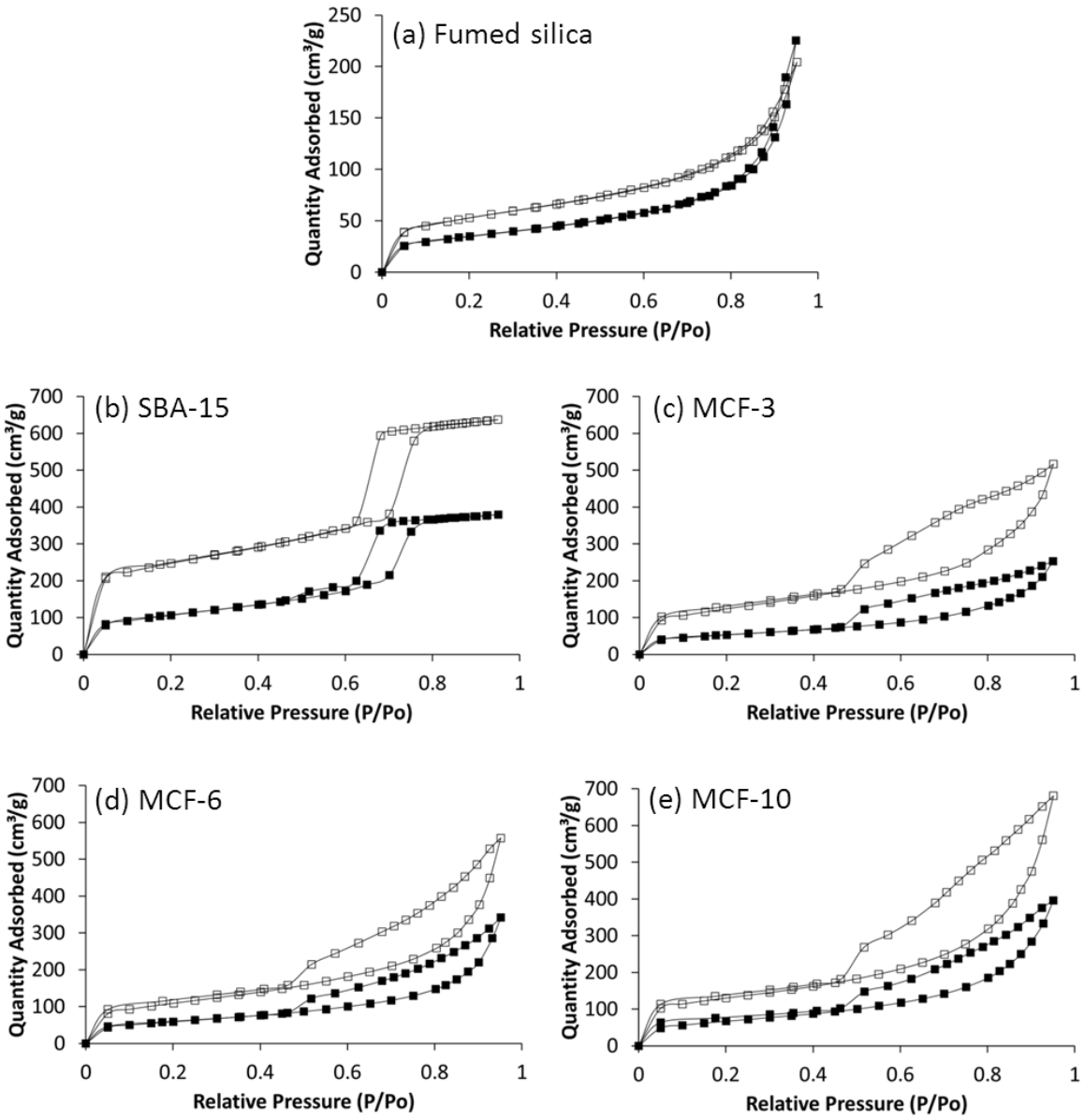

Figure 2. Structural analysis using N_2 adsorption isotherms for (a) fumed silica, (b) SBA-15, (c) MCF-3, (d) MCF-6 and (e) MCF-10 with (■) and without (□) chitosan. All isotherms show a decrease in overall N_2 adsorption with incorporation of chitosan. Pore volume decreases with chitosan incorporation as pores are now lined with chitosan or blocked completely.

	Unmodified Silica	Unmodified Silica Pore Volume [$cm^3\ g^{-1}$]				Chitosan on mesoporous silicas	Supported chitosan Pore Volume [$cm^3\ g^{-1}$]			
Mesoporous silica support	BET Surface Area [$m^2\ g^{-1}$]	Total	pore diameter range			BET Surface Area [$m^2\ g^{-1}$]	Total	pore diameter range		
			≤4 nm	4-10 nm	≥10 nm			≤4 nm	4-10 nm	≥10 nm
Fumed silica	186	0.29	0.04	0.07	0.18	123	0.33	0.02	0.05	0.26
SBA-15	530	0.81	0.09	0.70	0.04	376	0.56	0.05	0.49	0.03
MCF-3	439	0.75	0.10	0.20	0.45	187	0.38	0.04	0.11	0.23
MCF-6	387	0.83	0.08	0.18	0.57	210	0.53	0.05	0.11	0.37
MCF-10	375	1.01	0.06	0.25	0.70	241	0.60	0.04	0.16	0.41

*error in samples ±4 $m^2\ g^{-1}$

Table 1. Surface area and pore volume data for all chitosan/mesoporous silicas as well as fumed silica.

TEM analysis (**Figure 3a**) illustrates the 2-D hexagonal mesoporous structure of SBA-15, with a mean pore size around 7 – 9 nm, this is consistent with the pore size distribution data obtained from N_2 adsorption isotherms. In **Figure 3b**, the MCF-3 sample shows the effect on the structure of these materials due to pore expander. The hexagonal mesoporous structure of SBA-15 has been completely transformed to a foam-like porous structure. Both MCF-6 and MCF-10 (**c** and **3d**) showed a similar structure to MCF-3 but the increase in pore size was difficult to be depicted. The N_2 adsorption isotherm data shown in **Table 1** is therefore used to confirm the increase in total pore volume of large mesopores.

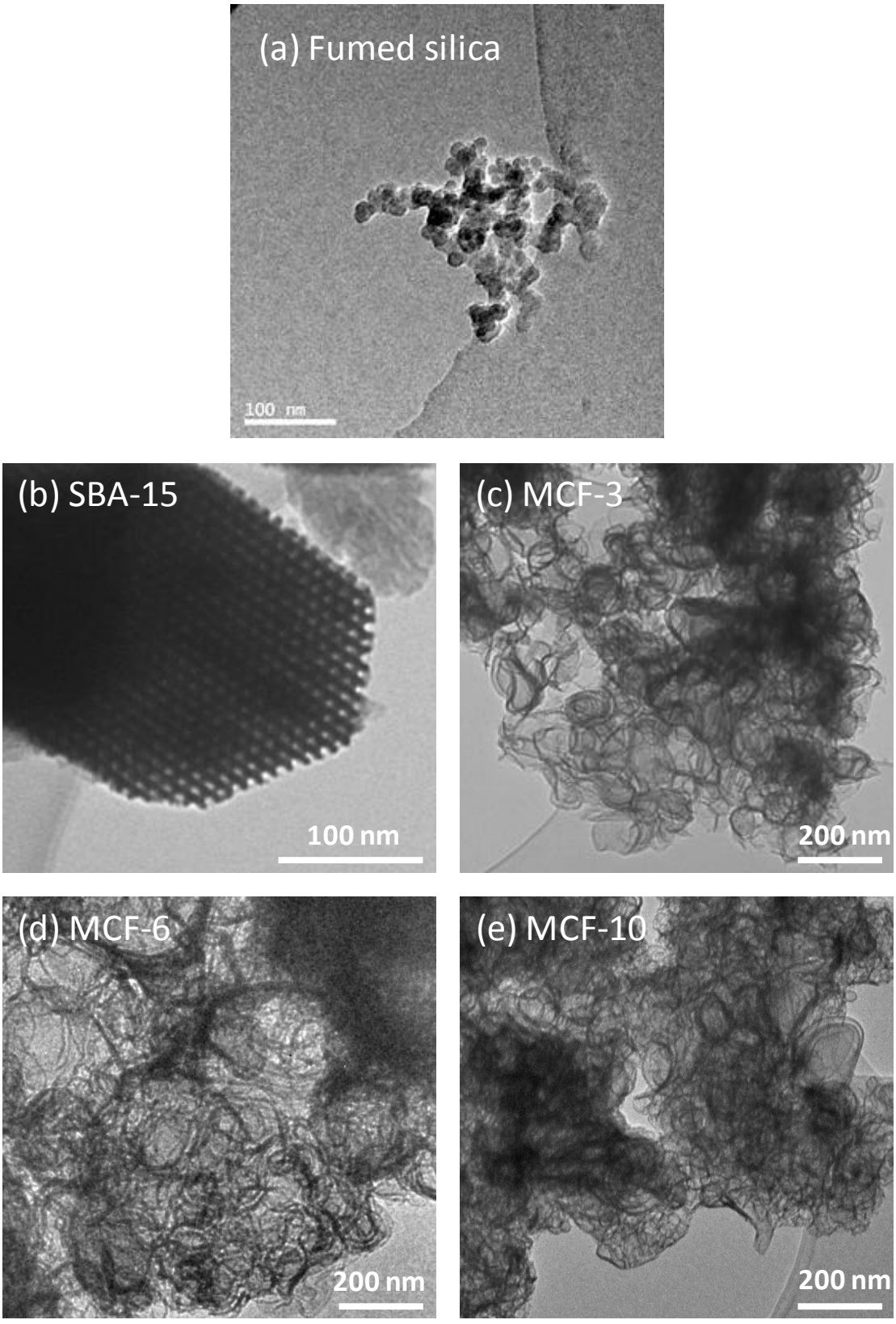

Figure 3. TEM micrographs of (a) fumed silica, (b) SBA-15, (c) MCF-3, (d) MCF-6, and (e) MCF-10. SBA-15 shows a highly ordered hexagonal porous array with a *p6mm* symmetry while all MCF samples show a foam-like structure.

3.2 Characterisation of Chitosan on Fumed Silica

Initially, chitosan was supported on fumed silica in a range of compositions (7.4%, 14%, 19%, 24%, 29% and 32% w/w) to determine the optimal chitosan-to-support ratio. Vibrational spectroscopic analyses (FTIR and Raman) were carried out on chitosan and used as a tool to identify the chitosan component on all chitosan/silica samples. The FTIR spectrum for chitosan and the assignment for peaks are shown in **Figure S2**. The twin peaks at 3355 cm^{-1} and 3290 cm^{-1} correspond to the R–NH_2 and R–OH groups. The C–H stretches of the chitosan backbone are shown at 2915 cm^{-1} and 2870 cm^{-1}. The C=O stretch of the residual N-acetyl-β-D-glucosamine units of chitin appears at 1645 cm^{-1}, while the NH_2 bending vibration appears at 1590 cm^{-1}. The C-H bending vibrations are shown at 1415 cm^{-1}, 1375 cm^{-1} and 1320 cm^{-1}. The C-O stretches of the alcohol and ether groups can be seen at 1060 cm^{-1}, 1025 cm^{-1} and 990 cm^{-1}. FTIR studies were also performed on all of the chitosan deposited on fumed silica samples, **Figure 4a** where the intensity of peaks corresponding to chitosan increases with increasing chitosan content. There was no peak observed within the range of 1690 – 1760 cm^{-1}, which corresponds to carboxylic acid or carboxylate species. Hence, it suggests that most of the acidic acid solvent had been removed during drying under vacuum. Also, it indicates that most –NH_2 groups on chitosan were not bound to carboxylate ions. TGA and CHN data verified the composition of each of the samples as being accurate (see **Table S1**).

Raman spectroscopy was used to probe on a microscopic scale the distribution of the chitosan within the sample. It is, therefore, a complementary technique to the FTIR-spectroscopy, which is a bulk technique and probes the presence of chitosan in the sample without giving a distinct answer about the distribution of the chitosan in the silica matrix. While the control sample of pristine fumed silica did not show any significant Raman activity even small amount of chitosan (7.4% w/w sample) was sufficient for observing the characteristic signals of the chitosan molecule as indicated in the **Figure 4b**. In contrast, the same sample showed very low peak intensity on its FTIR spectrum in **Figure 4a**. Furthermore, the intensity of the Raman signal also increases with the amount of the chitosan present in the sample. The most distinct peaks in the spectra are at 2900/2933 and 3311 cm^{-1} and associated with the R_2–CH_2 and R–NH_2 groups stretching frequency [27]. The clear split of the R_2–CH_2 group signal is due to out-of-phase and in-phase bond stretching vibrations. Indeed,

characterisation using Raman spectroscopy instead of FTIR avoids the interference from the silica support, a distinctive advantage for characterising samples with a low organic content. **Figure 4c** shows the Raman map of a 19% chitosan/fumed silica particle and chitosan is shown to be evenly distributed at a μm scale. Since chitosan has a large amount of hydroxyl groups (–OH), it is likely that chitosan interacts with the silica support via strong hydrogen bonds between these –OH groups and the Si–OH groups on the silica surface.

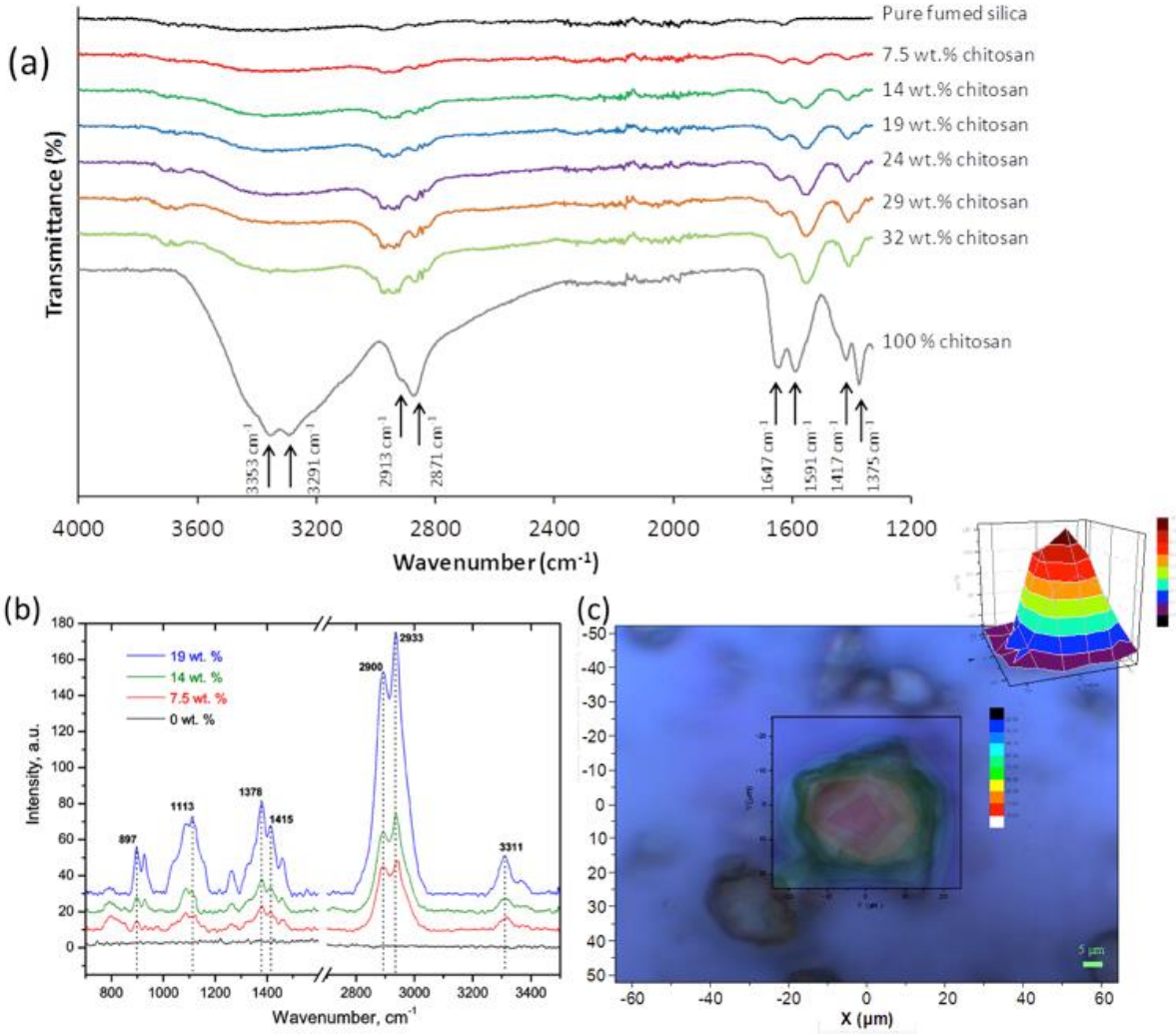

Figure 4. (a) FTIR spectra of chitosan and fumed silica composites with increasing chitosan content, (b) Raman spectra of pure fumed silica 0% and chitosan containing composites, illustrating the increasing chitosan content, (c) Raman mapping of chitosan fumed silica composite, showing even distribution of chitosan throughout the pores of the fumed silica.

From the analysis using N_2 adsorption isotherms, pure chitosan has shown a very low BET surface area (0.31 $m^2 g^{-1}$) and a pore volume of 0.0016 $cm^3 g^{-1}$, which suggests that it is virtually non-porous, leading to a negligible CO_2 adsorption capacity, consistent with Yoshida's finding.[21] This illustrates the need for deposition of chitosan on a suitable support and maximising the CO_2 adsorption capacity of a natural amine material. The thermal stability of chitosan was studied by simultaneous TGA/DSC analysis as shown in **Figure 5a.** There is an initial endothermic weight loss at approximately 100°C, corresponding to the removal of water from sample. Thermal decomposition, associated with a large exothermic peak, starts at about 230°C, indicating that chitosan can be used at an elevated temperature range. There is no recordable change (e.g. glass transition) for chitosan between 100 – 200°C.

Chitosan content (% w/w) on fumed silica (1g)	Mass of chitosan added in synthesis [g]	Measured BET Surface Area [$m^2 g^{-1}$]*
0	0	186
0 (control)**	0	188
7.4	0.08	153
14	0.16	136
19	0.24	123
24	0.32	109
29	0.40	80
32	0.48	65

*error in BET surface area ±3 $m^2 g^{-1}$

** fumed silica sample treated with acetic acid.

Table 2. Surface area values for chitosan deposited on a fumed silica support

From the N_2 adsorption isotherms analysis, there was a gradual decrease in BET surface area as the chitosan content of composite samples increased (**Table 2**). Since the chitosan can fill up the mesopores of fume silica supports, available surface area decreases. When the pore volume data of chitosan/silica composites was examined in details according to "small" (< 4 nm), "medium" (4-10 nm) and "large" (> 10 nm) mesopore classification (see **Table 1**), the chitosan/fumed silica samples showed a decrease in both small (from 0.04 to 0.02 $cm^3 g^{-1}$) and medium (from 0.07 to 0.05 $cm^3 g^{-1}$) mesopores regions due to pore blockage. Interestingly, the pore volume of the large mesopore range (> 10 nm) increased from 0.18 $cm^3 g^{-1}$ to 0.26 $cm^3 g^{-1}$ after coating with chitosan. This can be caused by large pores created from interconnecting the fumed silica particles with chitosan. Overall this leads to an increase in total pore volume upon deposition of chitosan from 0.29 to 0.33 $cm^3 g^{-1}$. Such phenomenon became more transparent in **Figure S3**, where the pore size distribution of samples with various chitosan content was presented. Upon incorporation of 7.4% chitosan into the pore network of fumed silica, there was a decrease in pore volume with a pore size below 8 nm when compared with the fumed silica support. However, an increase in pore volume was observed at pore size > 10 nm. It is worth noting that pure, unsupported chitosan is non-porous with a low BET surface area and pore volume (0.13 $m^2 g^{-1}$ and 0.0016 $m^3 g^{-1}$ respectively) and the coating process is unlikely to break up the porous structure of fume silica to form new larger pores > 10 nm. Hence, the assumption of large pores created by interconnecting fumed silica particles offers a reasonable explanation for this observation. For samples with a higher percentage of chitosan (>24%), the surface area and pore volume of samples decrease significantly, likely to reduce the CO_2 adsorption capacity. The 19% chitosan sample still retains a high surface area (123 $m^2 g^{-1}$) and pore volume (0.33 $cm^3 g^{-1}$), while having a significant chitosan loading. Therefore 19% chitosan was chosen as a benchmark loading for this work.

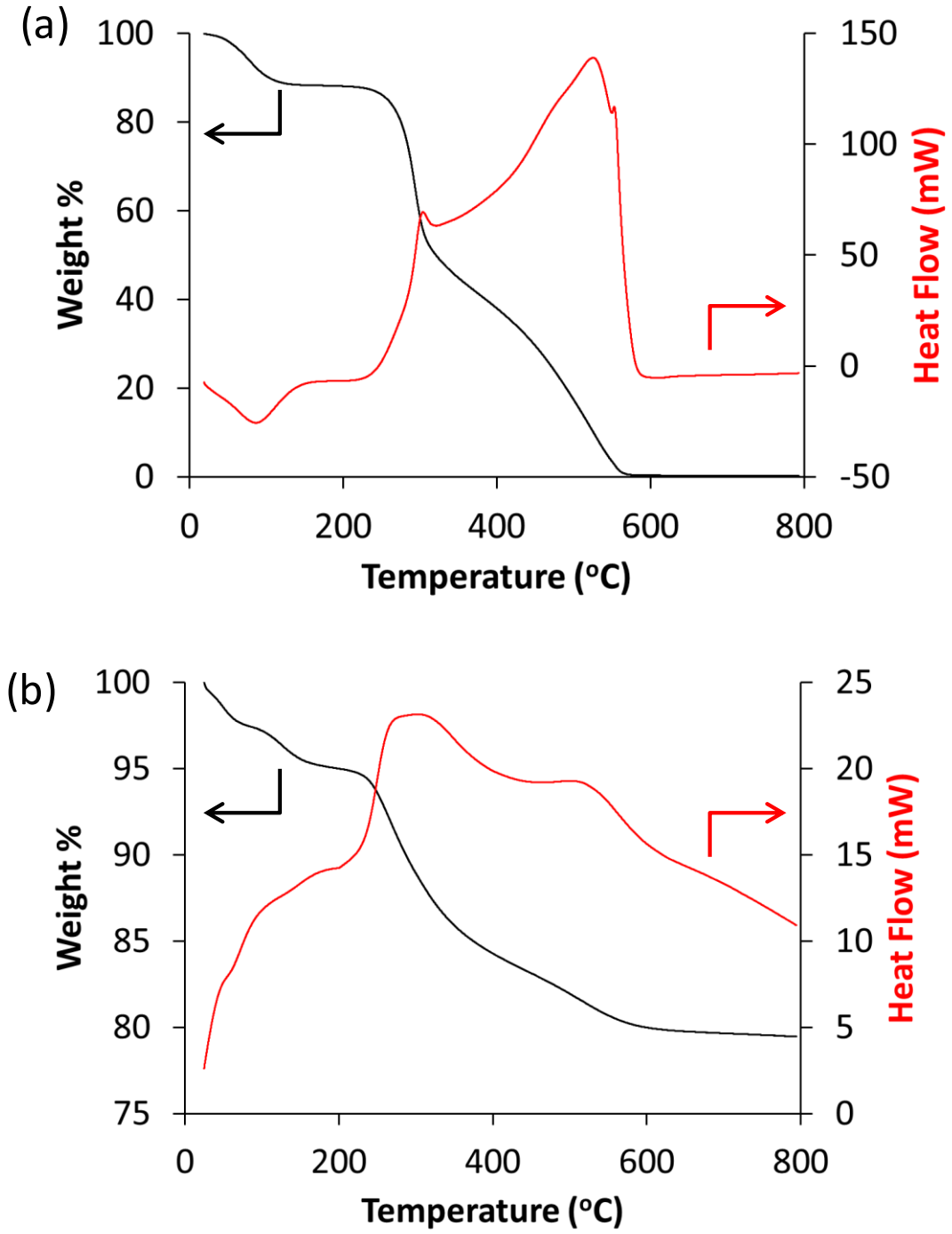

Figure 5. (a) TGA/DSC traces of pure chitosan from 20°C to 400°C using air as the carrier gas, showing thermal decomposition of the chitosan. Thermal decomposition begins at approximately 200°C. (b) TGA/DSC traces for 19% chitosan/fumed silica sample using air as the carrier gas. Thermal decomposition starts at ca. 200°C, similar to the pure chitosan sample in (a).

3.3 Characterisation of Chitosan on Mesoporous Silicas

Chitosan (19%) was coated on SBA15 (chitosan/SBA15), MCF-3 (chitosan/MCF-3), MCF-6 (chitosan/MCF-6) and MCF-10 (chitosan/MCF-10) in order to study the effect of porosity of support on the chitosan deposition and on CO_2 adsorption capacity. These composite materials showed no significant difference in the FTIR analysis when compared to pure chitosan, with all samples showing peaks associated with both chitosan and silica (**Figure S2b**). Organic content from TGA analysis for the composite materials was found to be consistent across all chitosan/mesoporous silica samples (see TGA data in **Figure S4** and **Table S1**). The surface area and pore size distribution data in **Table 1** showed a decrease of 30 – 50% in pore volume in both medium (4-10 nm) and large mesopore ranges (>10 nm), suggesting that chitosan has been coated evenly across all pore ranges. Hence, there was no apparent preference for deposition/blockage to one particular pore range, leading to an overall decrease in total pore volume as well as the BET surface area. If the chitosan was only deposited on the exterior of the support without entering the mesopores, such a high amount (19% w/w) would have led to a large decrease in both pore volume and BET surface area. Our results suggested that chitosan entered the pores, aided by sonication during deposition. These samples retained a high BET surface area (187 – 376 m^2g^{-1}), which is adequate for use as gas adsorbents.

3.4 Volumetric and Gravimetric CO_2 Adsorption Analysis

The CO_2 capacity of chitosan/silica composites was measured using two different methods; volumetric and gravimetric adsorptions. The volumetric CO_2 adsorption capacity of the 19% chitosan/fumed silica sample was found to be 0.29 mmol g^{-1} and that measured gravimetrically was 0.09 mmol g^{-1}, as shown in **Table 3**. No uptake of CO_2 was recorded from the gravimetric measurement for a pure fumed silica sample, (see **Figure S5)**, indicating that the CO_2 uptake from these samples is attributed to the coated chitosan. Considering that pure chitosan has a CO_2 adsorption capacity of ca. 0.02 mmol g^{-1},[21] our results have shown a remarkable 23-fold increase in capacity per unit mass of chitosan (0.47 mmol $g_{chitosan}^{-1}$), a unique property of these chitosan/silica composites. A higher capacity measured from the volumetric analysis than that from the gravimetric measurement is consistent with other works in the literature [28]. The difference between these two measuring systems is that the gravimetric analysis was

carried out in a dynamic flow system while a static closed system was used for the volumetric measurement. Moreover, a 50% CO_2 in N_2 purge stream was used for the gravimetric measurements instead of 100% CO_2 for the latter. In the next section, we will discuss the effect of CO_2 concentration in gas adsorbate to the CO_2 adsorption capacity.

CO_2 adsorbent	volumetric CO_2 capacity (100% CO_2) [mmol g^{-1}]	gravimetric CO_2 capacity (50% CO_2 in N_2) [mmol g^{-1}]
Chitosan/fumed silica (19%)	0.29	0.09
Chitosan/SBA-15	0.80	0.32
Chitosan/MCF-3	0.98	0.34
Chitosan/MCF-6	0.75	0.29
Chitosan/MCF-10	0.79	0.26

Table 3. Volumetric and gravimetric CO_2 adsorption capacity measured for chitosan/mesoporous silica adsorbents.

The results of the volumetric CO_2 adsorption analysis of the chitosan on mesoporous silica supports (SBA-15 and MCF's) are shown in **Figure 6** and **Table 3**. The chitosan/MCF-3 sample has shown the highest adsorption capacity at 0.98 mmol g^{-1}, while other samples vary from 0.75 – 0.80 mmol g^{-1}. These recorded capacities are comparable with other high-surface-area nanomaterials designed for CO_2 adsorption such as MOFs (e.g. MOF-5 at ca. 2 mmol g^{-1}, measured with a volumetric method).[29] Indeed, we can compare this result in terms of adsorption efficiency (i.e. CO_2:NH_2 ratio) with an adsorbent of similar structure NH_2-MCM-41, which gives a CO_2 adsorption capacity of 1.0 mmol g^{-1} at 1 atm and 20°C.[15] NH_2-MCM-41 has 2.48 mmol g^{-1} of NH_2 groups, resulting in a CO_2:NH_2 ratio of 0.4. The chitosan/MCF-3 sample has ca.

0.76 mmol g^{-1} NH_2 group (based on the CHN analysis) and a CO_2:NH_2 ratio of 1.3, which can be viewed as a 3-fold increase in efficiency compared with NH_2-MCM-41. In theory, the adsorbent with the highest BET surface area should adsorb the highest amount of CO_2 due to physisorption. However, this was not observed here as chitosan/MCF-3 had the lowest BET surface area among all samples except chitosan/fumed silica. In Table 3, there is also no obvious correlation between pore volume of adsorbents and their CO_2 adsorption capacity, suggesting a complex relationship between adsorption and structural parameters (surface area and pore volume). We should note that these structural parameters were measured for the whole composite, with no distinction between the gas adsorption (N_2 or CO_2) from the silica surface or from the chitosan coating. It would be difficult to pin point the critical structural factor influencing the overall CO_2 adsorption capacity.

Similar to that from chitosan/fumed silica, adsorption results from the gravimetric analysis, (**Table 3**) show a lower capacity for all chitosan on mesoporous silica samples when compared the adsorption capacity from the volumetric method. Nonetheless, the CO_2 adsorption capacity of all chitosan/silica composite samples follows the same trend, with the gravimetric adsorption being approximately one third of the volumetric adsorption capacity. On comparison between these two techniques, CO_2 adsorption capacity measured with gravimetric method is more representative to the real adsorption from flowing flue gas, in contrast to the volumetric measurement from a closed system. Therefore, many recent research works in the literature have adapted the gravimetric method for measuring the CO_2 adsorption capacity for adsorbents [30-32].

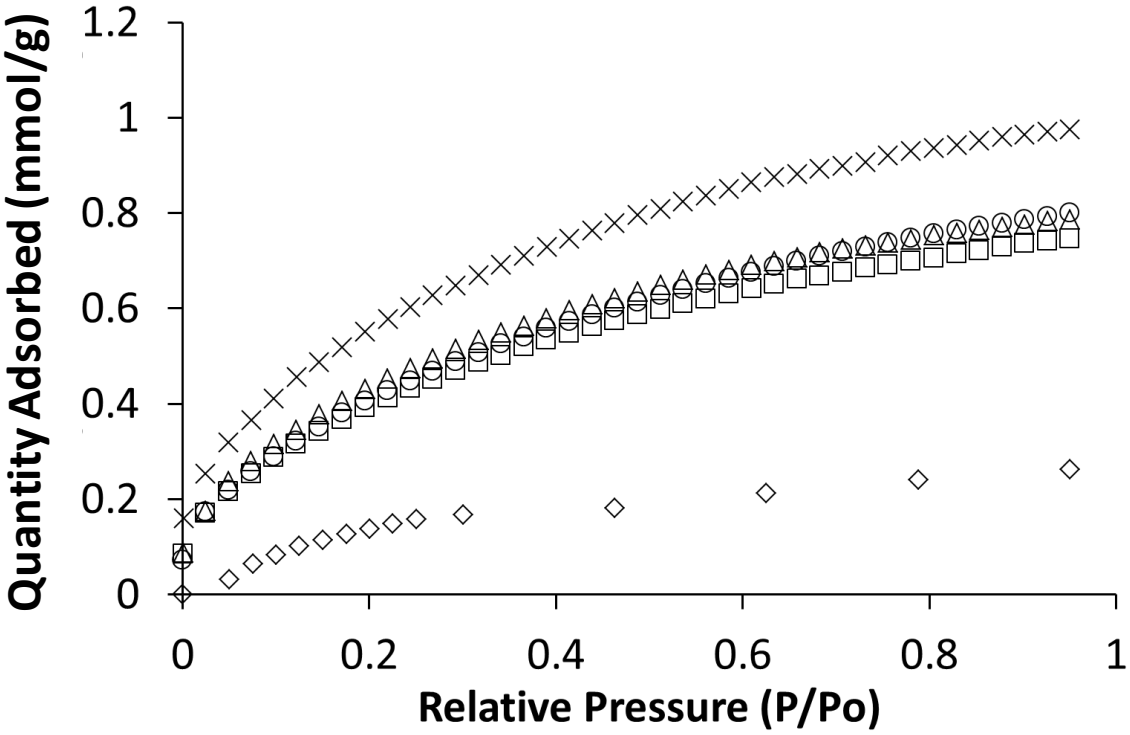

Figure 6. Volumetric CO_2 adsorption isotherms of chitosan/fumed silica (◇), chitosan/SBA-15 (○), chitosan/MCF-3 (×), chitosan/MCF-6 (□), and chitosan/MCF-10 (△). The CO_2 adsorption capacity recorded is an order of Chitosan/MCF-3 > Chitosan/SBA15 > Chitosan/MCF-10 > Chitosan/MCF-6 > Chitosan/fumed.

3.5 Gas composition analysis

In order to examine the effect of CO_2 content in gas stream on adsorption capacity, gravimetric analysis using four CO_2 in N_2 gas compositions (100%, 50%, 13% and 8% v/v) was also carried out with chitosan/MCF-3, which had shown the highest capacity, as the adsorbent (**Figure S6**). With a 100% CO_2 stream, a maximum adsorption capacity of 0.42 mmol g^{-1} was achieved quickly, within 30 minutes, faster than that with a 50% stream (90 min). Gas streams containing 13% and 8% CO_2 were used to simulate the CO_2 content in the flue gas from coal fired and gas fired power stations respectively. In both cases, the same adsorption capacity (0.10 mmol g^{-1}) was recorded after 90 minutes. This suggested that chitosan/MCF-3 has the potential to be used as a CO_2 adsorbent for power stations, with a reasonable capacity achieved by utilising a waste polymer material as the major component for adsorption.

Water is another flue gas component (around 6 – 15% v/v) to influence the efficiency of the CO_2 adsorbents during carbon capture. Many solid-state adsorbents, such as zeolites and MOF's, can be deactivated by high moisture content. On the other hand, aminated silicas have not shown deactivation and, in some instance (e.g. SBA-15 grafted with ethylenediamine $–NH–CH_2CH_2–NH_2$ groups), shown an improved CO_2 adsorption capacity as well as adsorption efficiency in presence of water [16]. The chitosan/silica composites also utilise surface amine groups for interaction with CO_2, hence deactivation by water is unlikely. Indeed, these composites were prepared in an aqueous medium and so water should have little negative effect on their adsorption behaviour.

3.6 Regeneration Study

In addition to adsorption capacities, study on regeneration of materials at a low temperature is also important. A high energy requirement for regenerating the liquid amine absorbent (e.g. 10% - 30% MEA in water regenerated at 140°C) in conventional carbon capture systems presents a major obstacle for a wider application. During the regeneration of these liquid phase systems, much of the energy was spent on the evaporation of water, which is the "non-adsorptive" component of the adsorbent. To

circumvent this obstacle, water-free solid state adsorbents with a low regeneration temperature (<100°C) are preferred.

In our regeneration study four adsorption-regeneration cycles were carried out using the chitosan/MCF-3 sample as shown in **Figure 7**. The overall adsorption for each cycle retained a minimum of 88% of the capacity from the previous cycle, while the overall drop in capacity is less than 15% over four cycles. Therefore, this adsorbent can be regenerated at a low temperature (75°C) with little loss in adsorption capacity. A higher retention of capacity, up to 98%, can be achieved by regenerating at 100°C but this would lead to higher energy consumption. When compared with solid state CaO adsorbent, which has been suggested for large scale carbon capture but requires a high temperature regeneration at 700°C,[33] our chitosan/MCF-3 adsorbent represents significant advancement in terms of reducing the energy consumption for regeneration, saving operational cost, and more importantly, reducing overall carbon footprint. One interesting feature in this study was that there was a "step-wise" weight loss after every regeneration cycle but without effect on the adsorption. This may be due to the strongly bound water or acetic acid from the adsorbent being displaced by the adsorbed CO_2. During regeneration, these molecules (water and acetic acid) left the system when the CO_2 was desorbed at 75°C. Nonetheless, this feature has no impact on the overall performance of the adsorbent.

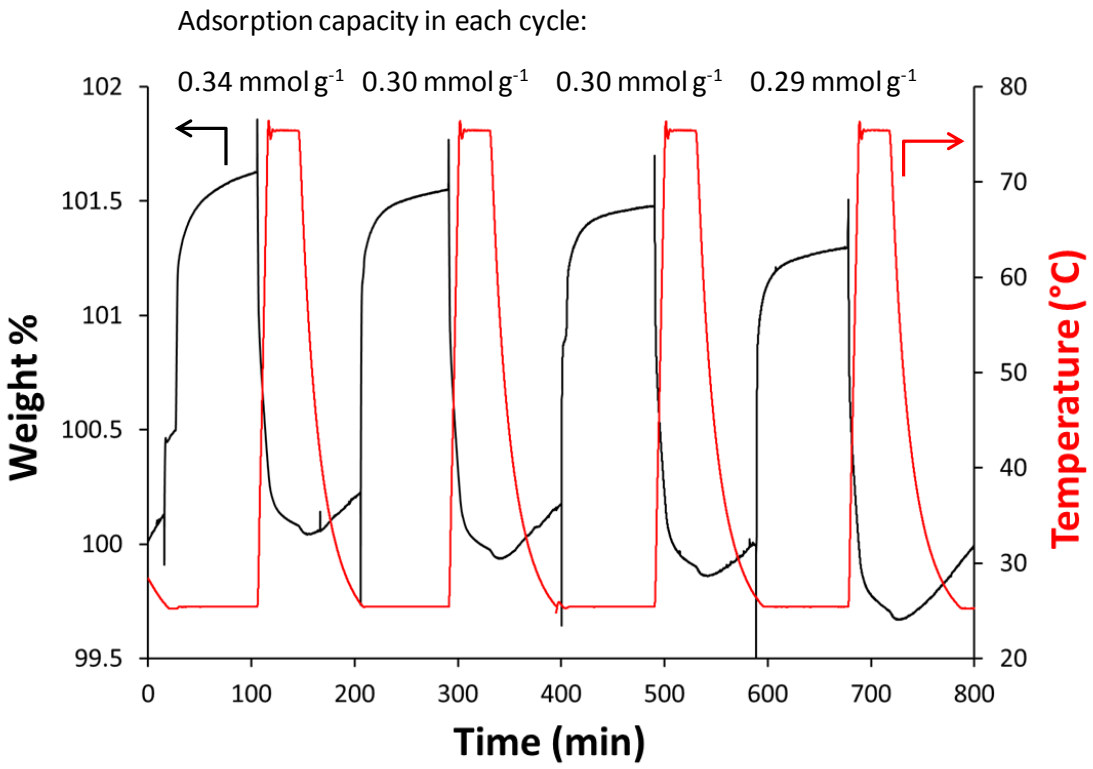

Figure 7. Gravimetric adsorption of CO_2 by Chitosan/MCF-3. Four regeneration cycles are shown with a 90 minutes adsorption at 25°C and a 30 minute desorption at 75°C. The adsorption capacity measured for each cycle is shown about the corresponding adsorption peak.

4. Conclusion

A family of chitosan/mesoporous silica composite materials were prepared with a simple deposition method. Unlike many other solid state adsorbents, including aminated mesoporous silicas, MOF's and carbon nanotubes, the procedure for preparing these materials follows closely to the green chemistry principles (room temperature and pressure conditions, avoiding use of toxic solvents, with 0.2 M acetic acid as the only solvent, and a minimum waste emission). These adsorbents, with a maximum volumetric CO_2 adsorption capacity of 0.98 mmol g^{-1} at 25°C, are also chemically and thermally stable (up to 200°C). More importantly, they can be regenerated at a low temperature 75°C and retained 85% capacity after 4 cycles. Such low energy consumption is advantageous for industrial applications, particularly compared to liquid phase monoethanolamine (MEA) solutions, which requires an energy intensive regeneration regime.

Indeed, chitosan is one major food waste and making use of it for tackling another environmental problem is an attractive approach. Large-scale use of chitosan/fumed silica composite can be easily adapted as both chitosan and fumed silica are already commonly used in industries. To further enhance the CO_2 adsorption capacity, mesoporous silicas of high surface areas (e.g. SBA-15 and MCF-3) can be used as the support material. These mesoporous silicas synthesised from surfactant templates have yet been widely used in industry but room temperature synthesis methods and continuous preparation processes have already been reported [34]. Surfactant-free preparation routes were also reported in the literature [35]. Therefore, large-scale use of these high surface area silicas could be available in the near future. Alternatively, if there is a new non-silica material with a high surface area and a similar porous structure to MCF-3, coating chitosan on it could have similar adsorptive property to chitosan/MCF-3.

Currently, the high running cost associated with carbon capture technology is one major obstacle for CCS to become popular and the energy required for adsorbent regeneration contributes significantly to such cost. To fully realise the potential of carbon capture technologies, lowering the running cost is fundamental. The low-cost sustainable preparation for adsorbents in a large quantity, together with their low-

temperature regeneration, presented here can reduce the overall operational cost for CCS. Furthermore, green CO_2 adsorbents, such as chitosan/mesoporous silica composites from this work, will have to be considered in order to achieve a net reduction on carbon footprint.

Acknowledgement

The authors acknowledge financial support from the EPSRC S&I Award (EP/ F034482/1), EPSRC AMPGas constortium (EP/J02077X/1) and the Scottish Carbon Capture and Storage (SCCS) programme. We also acknowledge the Kelvin Nanocharacterisation Centre, University of Glasgow for their assistance in TEM imaging.

References

[1] L. Li, N. Zhao, W. Wei, Y. Sun, *Fuel* 2012, **108**, 112.

[2] Annual Energy Outlook 2014 (AEO2014) Early Release Overview published by the U.S. Energy Information Administration (EIA), 2013, http://www.eia.gov/forecasts/aeo/er/pdf/0383er(2014).pdf

[3] R. Trage, *Chem. World*, 2014, **11**, 8

[4] B. A. Oyenekan, G. T. Rochelle, GT, *AIChE J.* 2007, **53**, 3144.

[5] A. Yamasaki, *J. Chem. Eng. Japan.* 2003, **36**, 361.

[6] M. S. Ojala, N. F. Serrano, P. Uusi-Kyyny, V. Alopaeus, *Fluid Phase Equilibr.* 2014, **376**, 85.

[7] D. J. Fauth, E. A. Frommell, J. S. Hoffman, R. P. Reasbeck, H. W. Pennline, *Fuel Process. Technol.* 2005, **86**, 1503.

[8] K. P. Resnik, J. T. Yeh, H. W. Pennline, *Int. J. Environ. Technol. and Manag.* 2004, **4**, 89.

[9] J. T. Yeh, K. P. Resnik, K.Rygle, H. W. Pennline, *Fuel Process. Technol.* 2005, **86**, 1533.

[10] L. Espinal, D. L. Poster, W. Wong-Ng, A. J. Allen, M. L. Green, *Environ. Sci. Technol.* 2013, **47**, 11960.

[11] G. Sneddon, A. Greenaway, H. H. P. Yiu, *Adv. Energy Mater*. 2014, **4**, 1301873

[12] D. M. D'Alessandro, B. Smit, J. R. Long, *Angew. Chem. Int. Ed.* 2010, **49**, 6058.

[13] S. Choi, J. H. Drese, C. W. Jones, *ChemSusChem* 2009, **2**, 796.

[14] H. Y. Huang, R. T. Yang, D.Chinn, C. L. Munson, *Ind. Eng. Chem. Res.* 2002, **42**, 2427.

[15] M. R. Mello, D. Phanon, G. Q. Silveira, P. L. Llewellyn, C. M. Ronconi, *Microporous Mesoporous Mater*. 2011, **143**,174.

[16] F. Y. Chang, K. J .Chao, H. H. Cheng, C. S. Tan, *Sep. Purif. Technol.* 2009, **70**, 87.

[17] L. X. Zhang, C. C. Yu, W. R. Zhao, Z. L. Hua, H. R. Chen, L. Li, J. L. Shi, *J. Non-Cryst. Solid*, 2007, **353**, 4055

[18] J. Berger, M. Reist, J. M. Mayer, O. Felt, N. A. Peppas, R. Gurny, *Eur. J. Pharm. Biopharm.* 2004, **57**, 19.

[19] A. Danon , P. C. Stair, E. Weitz, *J. Phys. Chem. C* 2011, **115**, 11540.

[20] M. Rinaudo, *Prog. Polym. Sci.* 2006, **31**, 603.

[21] H. Yoshida, S. Oehlenschlaeger, Y. Minami, M.Terashima, *J. Chem. Eng. Japan.* 2002, **35**, 32.

[22] H. Yoshida, S. Oehlenschlaeger, Y. Minami, M. Terashima in *Adsorption Science and Technology* (Ed. D.D. Do), World Scientific Publishing, Singapore, **2000**, pp. 693-697.

[23] X. Li, B. H. Li, J. J. Deng, T. T. Lu, S. Wang, J. B. Li, D. S. Chen, Y. Q. Liu, S. H. Wang, *Ind. Eng. Chem. Res.* 2014, **53**, 11137.

[24] H. H. P. Yiu, M. A. Keane, Z. A. D. Lethbridge, M. R. Lees, A. J. El Haj, J. Dobson, *Nanotechnology* 2008, **19**, 255606.

[25] P. Schmidt-Winkel, C. J. Glinka, G. D. Stucky, *Langmuir* 2000, **16**, 356.

[26] O. W. Flörke, H. A. Graetsch, F. Brunk, L. Benda, S. Paschen, H. E. Bergna, W. O. Roberts, W. A. Welsh, C. Libanati, M. Ettlinger, D. Kerner, M. Maier, W. Meon, R. Schmoll, H. Gies, D. Schiffmann in *Silica. Ullmann's Encyclopedia of Industrial Chemistry*, Vol. 32, Wiley-VCH, Weinheim, **2008**, 421.

[27] N. B. Colthup, L. H. Daly, S. E. Wiberley in *Introduction to Infrared and Raman Spectroscopy* (3rd Edition), Academic Press, Waltham, **1990**, 387.

[28] R. Babarao, J. Jiang, *Langmuir* 2008, **24**, 6270.

[29] Z. Zhao, X. Ma, A. Kasik, Z. Li, Y. S. Lin, *Ind. Eng. Chem. Res.* 2013, **52**, 1102.

[30] X. Wang, C. Song, A. M. Gaffney, R. Song, *Catal. Today* 2014, **238**, 95.

[31] Y. Labreche, Y. Fan, F. Rezaei, R. P. Lively, C. W. Jones, W. J. Koros, *ACS Appl. Mater. Interfaces* 2014, **6**, 19336.

[32] Y. Han, G. Hwang, H. Kim, B. Z. Haznedaroglu, B. Lee, *Chem. Eng. J.* 2015, **259**, 653.

[33] S. P. Wang, L. J. Fan, C. Li, Y. J. Zhao, X. B. Ma, *ACS Appl. Mater. Interfaces* 2014, **6**, 18072.

[34] J. Jammaer, T. S. van Erp, A. Aerts, C. E. A. Kirschhock, J. A. Martens, *J. Am. Chem. Soc.* 2011, **133**, 13737.

[35] S. C. Kung, C. C. Chang, W. Fan, M. A. Snyder, *Langmuir*, 2014, **30**, 11802.

Supporting Information

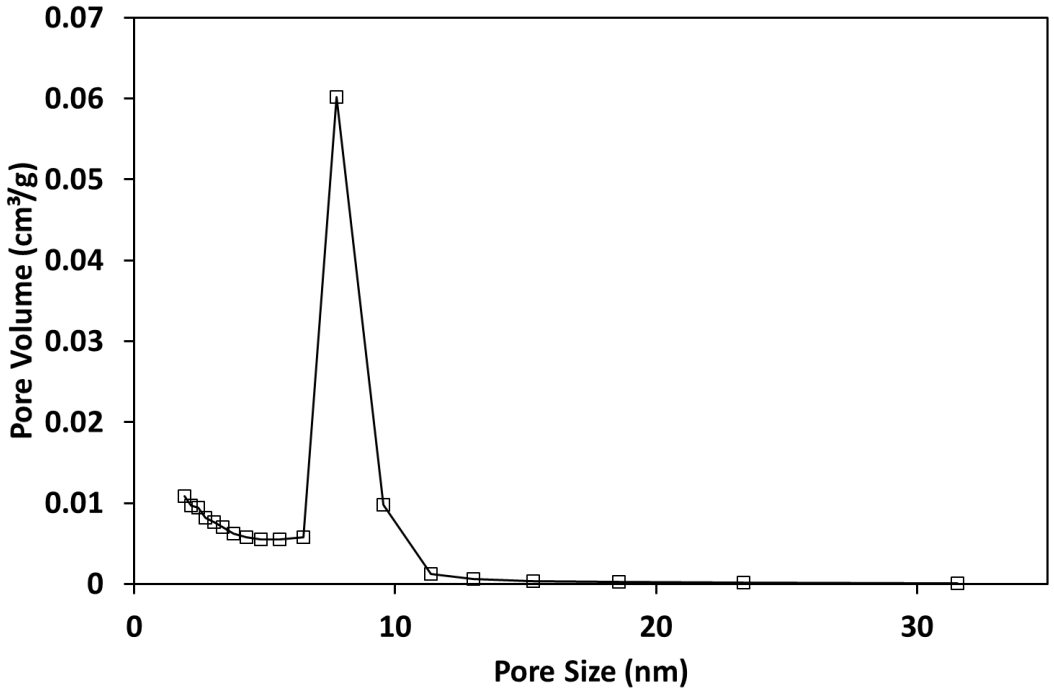

Figure S1. Pore size distribution of SBA-15 showing majority of pores with the pore diameter of the SBA-15 = ca. 8 nm.

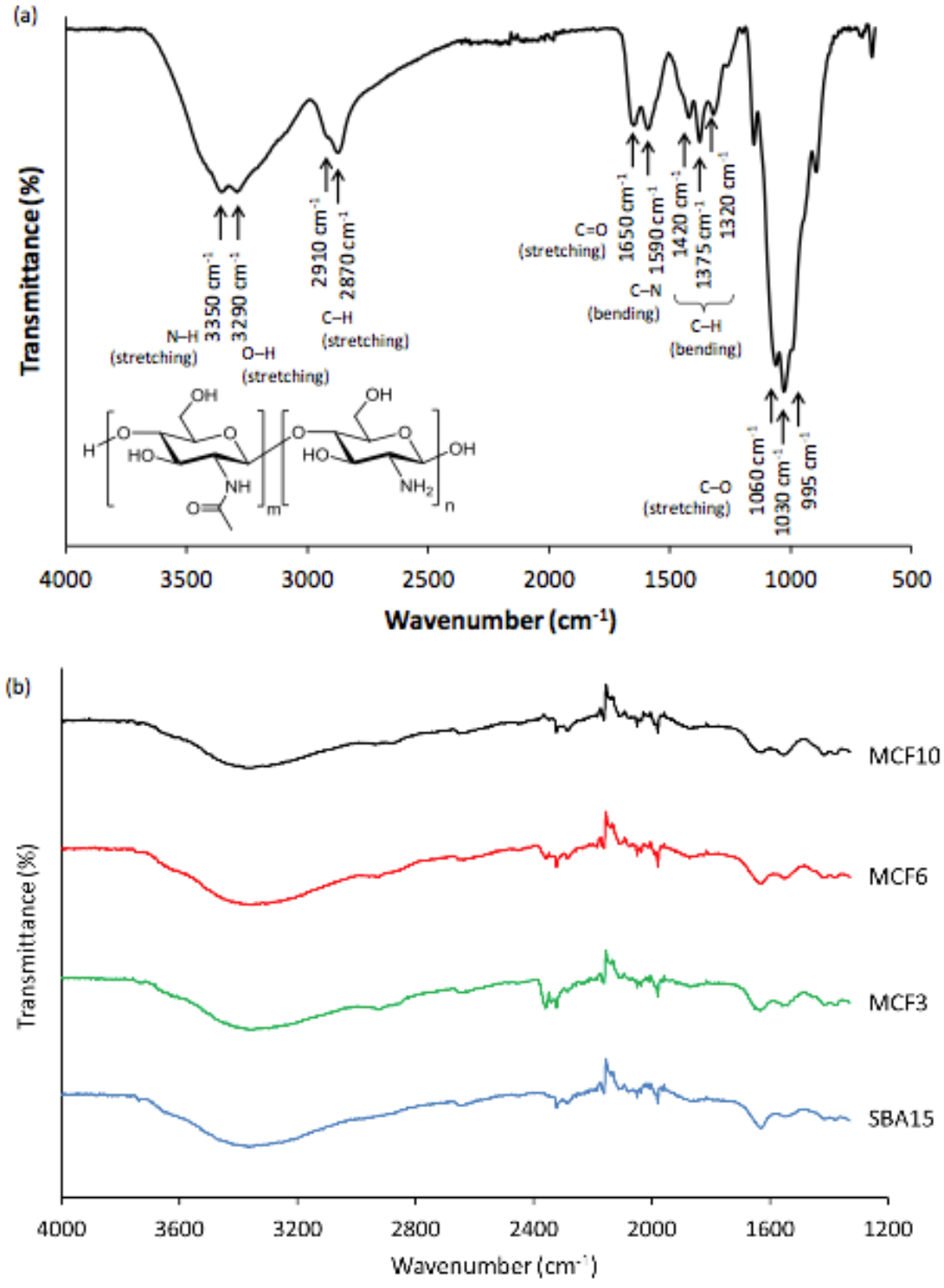

Figure S2. (a) Full FTIR spectrum of chitosan showing assignment of all main peaks. (b) FTIR spectrum of chitosan/mesoporous silicas showing chitosan peaks are present.

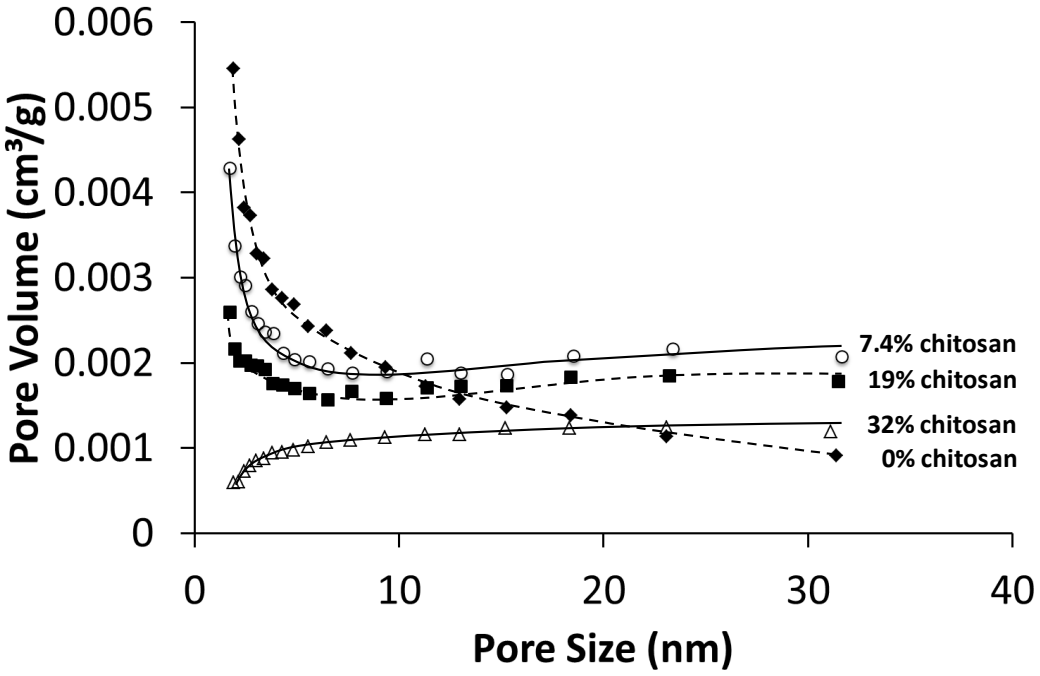

Figure S3. Pore size distribution chitosan/fumed silica samples. Increasing chitosan content shows a corresponding loss in micropore and mesopore volume but an increase in macropore volume.

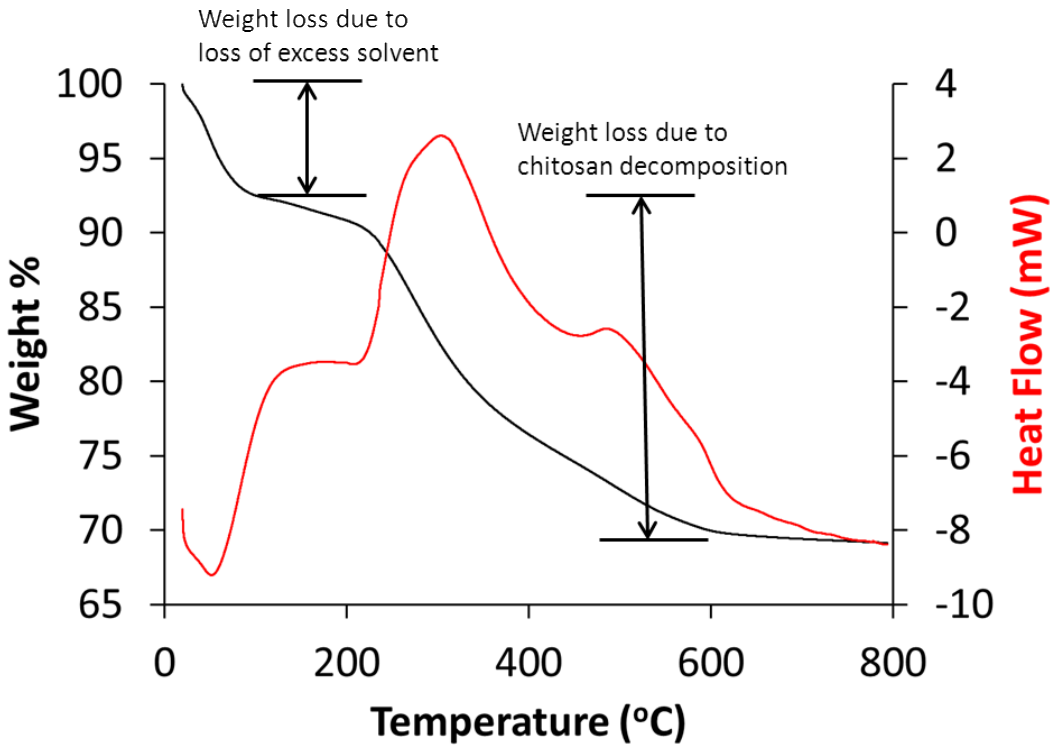

Figure S4. TGA thermal decomposition of chitosan/SBA-15 in air. Initial loss of weight from residual solvent, with thermal decomposition of the chitosan starting at approximately 230 °C.

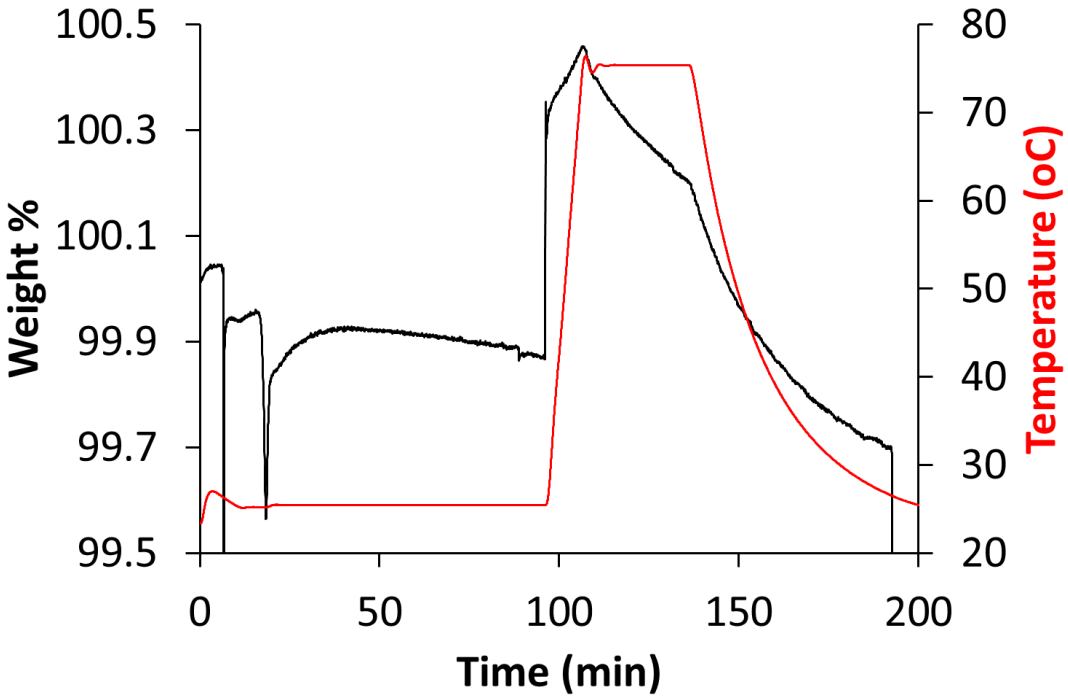

Figure S5. Gravimetric CO_2 adsorption for pure fumed silica support. A gas flow of 50:50 CO_2:N2 was started at 15 minutes as indicated by a jump in weight %. Adsorption continues until 105 minutes, as indicated by another jump in the weight %. Resulting adsorption is less than 0.1% and below the starting weight of the sample. A second step in the weight percentage is seen at 105 minutes when gas flow is switched back to 100% N_2 flow.

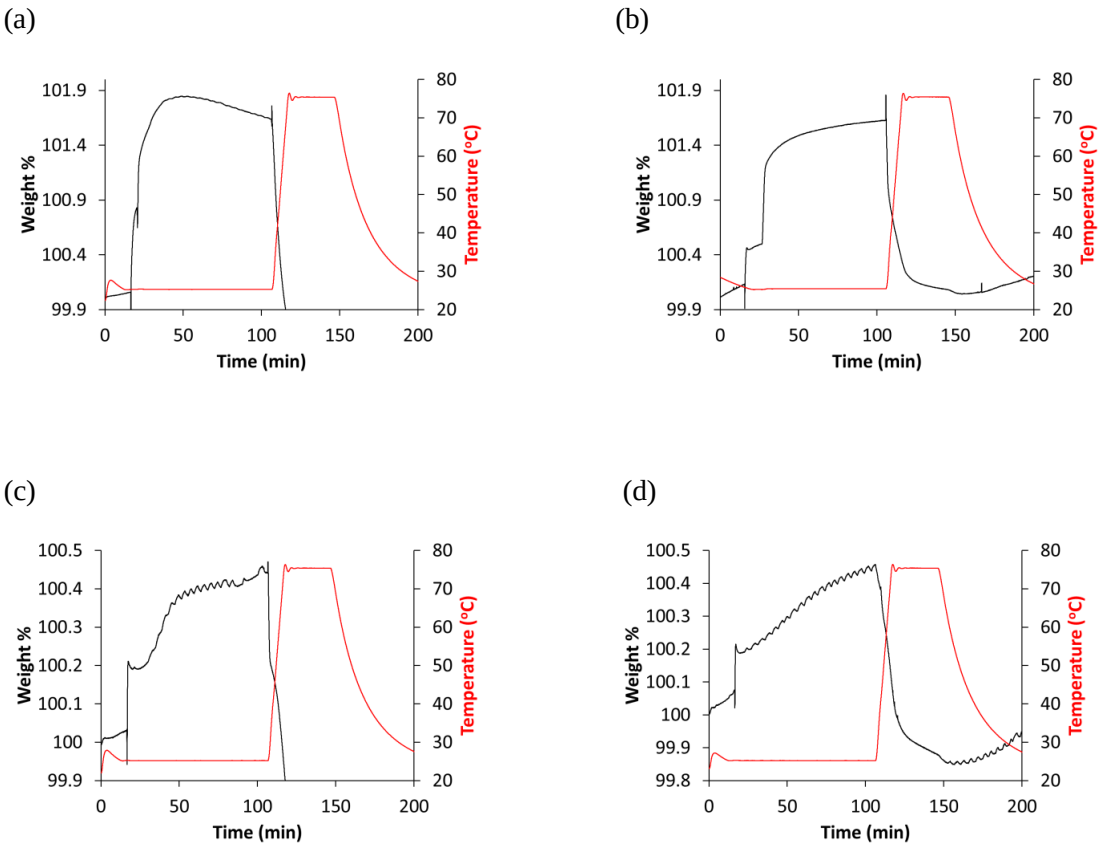

Figure S6. CO_2 adsorption on chitosan/MCF-3 using different gas compositions. (a) CO_2 adsorption in a 100% CO_2 stream. Quick maximum adsorption of CO_2 seen after 30 minutes of 0.42 mmolg^{-1}. (b) CO_2 adsorption in a 50:50 CO_2:N_2 stream. Maximum adsorption of 0.34 mmol g^{-1} seen after 105 minutes of adsorption. (c) CO_2 adsorption in a 13:87 CO_2:N_2 stream. A maximum adsorption of 0.1 mmol g^{-1} is seen after the full 105 minute cycle. (d) CO_2 adsorption in an 8:92 CO_2:N_2 stream. A maximum adsorption of 0.1 mmol g^{-1} is also seen after the full 105 minute cycle.

CO_2 adsorbent	Expected organic content	Organic content from TGA thermal decomposition (%)	Organic content from CHN analysis
Chitosan/fumed silica	19	16	17
Chitosan/SBA-15	19	20	19
Chitosan/MCF-3	19	17	20
Chitosan/MCF-6	19	19	16
Chitosan/MCF-10	19	18	20

Table S1. Organic content of composite samples from TGA and CHN analysis

CHAPTER 3

Aminated Poly(Vinyl Chloride) Solid Sorbents with Hydrophobic Function for Post-Combustion CO_2 Capture

3.1 Background

The importance of carbon capture has already been stressed in previous chapters, with the development of sustainable and efficient solid-state CO_2 adsorbents of critical importance to combat ever-increasing CO_2 levels. In this work program a family of amine modified poly(vinyl chloride) (PVC) composite materials were synthesised and characterised with the aim of adsorbing CO_2 selectively from flue gas streams. Since water is a major component of the flue gas stream, and the deactivation of some solid-state adsorbents in the presence of water can be problematic, as discussed. Use of these naturally hydrophobic PVC composites could help to reduce the negative effect of water in the CO_2 adsorption process from the flue gas stream. PVC has many household applications but is not widely recycled, with the majority of PVC waste ending up in landfill sites. Modification of PVC with a suitable amine is required before adsorption of CO_2 is undertaken, as the PVC backbone does not possess functional groups with the ability to naturally chemisorb CO_2. Once aminated (APVC), the PVC material can be used for CO_2 adsorption, however as with chitosan materials, a suitable solid support is required in order to increase the available surface amine groups available for interaction with CO_2. In this paper, a variety of amines, supports, and APVC loading were investigated in order to determine the optimum conditions for CO_2 adsorption with these composite materials.

3.2 Methodology/Synthesis of Materials

APVC/mesoporous silica composites were prepared and tested as the CO_2 adsorbents in this chapter. The preparation procedure in general consists of 3 steps; preparation of support materials, preparation of APVC and APVC deposition. The composite adsorbents were then characterised using FTIR spectroscopy, CHN elemental analysis, thermogravimetric analysis/differential scanning calorimetry (TGA/DSC), BET surface area measurement, and hydrophobicity testing. Synthesis of SBA-15 and MCF-3 mesoporous silica supports was identical to that performed in Chapter 2.

3.2.1 Synthesis of Amine Modified APVC Polymers

Amination of PVC material was required in order to incorporate some capacity for CO_2 adsorption to the polymer backbone in the form of amine nitrogen. Modification of PVC through substitution of the secondary chloro-groups is already an established process within the literature [3.1], with substitutions using ethylenediamine (EDA), diethylenetriamine (DETA) and ethanolamine (MEA) already reported [3.2-3.4]. Initial experiments involved the incorporation of ethylenediamine (EDA) to introduce amine functionality on PVC backbone. Firstly, PVC (5%) was dissolved in refluxing methyl ethyl ketone (MEK) at 80°C to form a 5% w/v solution. To the PVC solution EDA (8mL) was added and the resulting reaction mixture allowed to reflux with stirring at 80°C for 24 hours. The resulting EDA-PVC solution was used as a stock solution for supporting onto silica supports. A small amount of aminated polymer sample from this stock solution was precipitated for analysis by slowly adding dropwise to a swirling vortex of excess ethanol. The polymer solid was then washed in ethanol using a soxhlet extractor to remove any unreacted amine and ketone solvent from the polymer surface. The same procedure was used as above with all other amination agents including, diethylenetriamine (DETA), monoethanolamine (MEA) and diethanolamine (DEA). All materials were named using the aminating agent for the process as the suffix of the material. Therefore, material that had been modified using EDA as the aminating agent was denoted as EDA-PVC.

3.2.2 Coating APVC on Silica Supports

Due to some amines used having two or more reactive functional groups, the APVC materials may contain a high degree of cross-linking throughout the polymer network. Hence, once precipitated from solution, re-dissolution of the polymer material can be extremely difficult and will result in swelling of the polymer rather than dissolution. This would make impregnation of the silica pore network impossible. To circumvent this the reaction mixture was kept in solution after 24 hours and used as a stock solution for deposition into the pore network of mesoporous silicas. Deposition of APVC on mesoporous silica supports was carried out using a similar procedure to that used for chitosan deposition experiments. The volume of stock solution for deposition was determined based on the input PVC material to the reaction, with approximately 50 mL of the stock solution containing 2g of PVC. The total volume of solution used for each

dissolution experiment was adjusted to 20mL with MEK. For example, to deposit 0.2g of APVC onto 1.0g of silica support, 5mL of stock solution was diluted with 15mL of MEK to give a total volume of 20mL. Initially, EDA-PVC was deposited on fumed silica, SBA-15 and MCF-3 at percentages of 4%, 7%, 14% and 19% (0.04g, 0.08g, 0.16g and 0.24g of PVC to 1.0g of silica support). Degassing and drying was carried out as per chitosan deposition experiments. Additional experiments were carried out depositing DETA-PVC, TEPA-PVC, MEA-PVC and DEA-PVC (at 4% organic content) on SBA-15 and MCF-3 silica supports. Naming of supported PVC materials followed the same nomenclature as that used for chitosan experiments.

3.2.3 Adsorbent Samples Characterisations and CO_2 Adsorption Capacity Determination

The same techniques were used as per Chapter 2 for the determination of the composite materials physical properties and CO_2 adsorption capacity. BET analysis was carried out by Jessica McGlynn, University of Glasgow chemistry department. Additionally contact angle experiments were carried out using an Attension Theta unit in order to probe the hydrophobic nature of the APVC/mesoporous silica supports in comparison to the unsupported APVC and the unmodified support material. Contact angle experiments were carried out by Dr Cem Bayram, Hacettepe University, Ankara, Turkey.

3.3 Aim/Objectives

The main aim of this study was to demonstrate that APVC/mesoporous silica composite materials can be used for the selective adsorption of CO_2 as a new direction for adsorbent development. The effect of the chosen support on the CO_2 adsorption capacity will also be explored with fumed silica, SBA-15 and MCF-3 mesoporous silica supports investigated. The role of the amine used to functionalise the PVC polymer will also be discussed and a best candidate identified by their CO_2 adsorption capacity. It will also be demonstrated that the hydrophobic nature of the APVC material is maintained within the APVC/mesoporous silica composite materials, in an attempt to reduce the role of water in the CO_2 adsorption process.

3.4 Findings

3.4.1 Initial Characterisation of EDA-PVC and EDA-PVC/Silica Composites

Etylenediamine (EDA) was chosen as the initial aminating agent for this study as the modification of PVC with EDA was already well established within the literature. Initial analysis of unmodified PVC and EDA-PVC by TGA/DSC in an air atmosphere indicated significant differences within the polymer materials. Pristine PVC did not show any significant thermal events until the endothermic decomposition at 260°C, whereas the EDA-PVC indicated a small exothermic event at *ca.* 170°C, likely due to a solid phase transition. Decomposition of the EDA-PVC polymer starts after this transition, earlier than that of the pristine PVC material, likely due to the initial loss of amine crosslinkers before depolymerization. These results indicate the APVC materials to be stable up to temperatures of 140°C, suggesting them to be stable for regeneration without decomposition and thus deactivation.

Analysis of the EDA-PVC/mesoporous silica composite materials by TGA and CHN elemental analysis indicated a higher than expected organic content when compared to the unsupported EDA-PVC material. This suggested that the soxhlet extraction of the composites as with the unsupported EDA-PVC, cannot remove all trapped solvent and unreacted amines. Nevertheless, high surface areas were maintained for the supported EDA-PVC composites, 314 m^2g^{-1} for EDA-PVC/SBA-15 (4%) and 122 m^2g^{-1} for EDA-PVC/MCF-3 (4%). Generally, the BET surface area of samples was observed to decrease with increasing EDA-PVC content as expected due to some blockage of pores within the structure. Although some pore blockage is inevitable, the pore size distributions for the composite materials indicated that large pore volumes were maintained, 0.66 cm^3g^{-1} for EDA-PVC/SBA-15 (4%) and 0.34 cm^3g^{-1} for EDA-PVC/MCF-3 (4%). Interestingly, surface area and pore volume measurements for fumed silica samples remained largely unchanged after deposition of EDA-PVC. Except when fumed silica was loaded with 19 wt% EDA-PVC, an increase in the pore volume > 5.0 nm was observed. This is similar to the phenomenon observed with chitosan/fumed silica composite materials in Chapter 2, where the deposition of the adsorbent on the mesoporous silica surface lead to interconnection of the larger pores within the structure.

The presence of the APVC materials within the composite materials was further determined through the use of FTIR. EDA-PVC/SBA-15 (4%) was compared to equivalent DETA-PVC, MEA-PVC and DEA-PVC/SBA-15 composite materials. All samples exhibit a similar FTIR spectrum due to the presence of common components, most significantly the PVC backbone itself, but also NH_2 and CH_2 groups associated with the amination agents. Interestingly, all samples indicated a strong adsorption band associated with the stretching mode of C=O, due to residual ketones present within the structure. Although there is some residual solvent present in these samples it has already been demonstrated to have minimal effect on the surface area and pore volume.

3.4.2 CO_2 Adsorption Capacity Measurements of EDA-PVC and EDA-PVC/Silica Composites

A gravimetric method of CO_2 adsorption was undertaken for this study due to the similarities when compared to a real carbon capture environment. The gravimetric approach better represents the dynamic adsorption process observed in industry, when compared to the closed system that is needed in a volumetric CO_2 adsorption measurement. CO_2 adsorption was carried out using a 1:1 v/v CO_2:N_2 mix at 25°C for each of the composite materials studied. As a benchmark, the CO_2 adsorption capacity of the unsupported EDA-PVC was determined by TGA and found to be a low value of 0.73 cm^3g^{-1}. This is not surprising for this material as it exhibits a very low surface area, too low for the instrument to measure in fact. The highest CO_2 adsorption capacity was measured when using EDA-PVC/SBA-15 (4%) of 12 cm^3g^{-1}. A maximum adsorption capacity of 11 cm^3g^{-1} was observed for the equivalent EDA-PVC/MCF-3 (4%) sample. Generally, for both the SBA-15 and MCF-3 composite series a decrease in CO_2 adsorption capacity in line with surface area measurements was observed with increasing polymer content, likely attributed to pore blockage. CO_2 adsorption measurements on fumed silica materials indicated low adsorption capacities, with values of < 1 cm^3g^{-1} measured.

A second parameter was considered during CO_2 adsorption measurements, the CO_2:N ratio. This parameter was used as a way to relate the nitrogen content (determined from CHN elemental analysis) to the CO_2 adsorption capacity, as a measure of the efficiency of the composite material. As the increase in polymer content

within the composite material lead to a decrease in the CO_2 adsorption capacity, he adsorption efficiency (CO_2:N_2 ratio) decreases as the polymer content increases. There was only one exception to this, when using EDA-PVC/SBA-15 (19%). This sample saw an increase in adsorption efficiency when compared to the EDA-PVC/SBA-15 (7%) sample. This was attributed to the high carbon content (35%) determined from elemental analysis, this data suggested an abnormally high solvent content within the composite. This observation highlights one of the major problems when dealing with a 2D non-connected pore system like that of SBA-15.

3.4.3 CO_2 Adsorption Capacity Measurements of Other APVC/Silica Composites

The CO_2 adsorption capacity of APVC/SBA-15 (4%) was determined using diethylenetriamine (DETA), monoethanolamine (MEA) and diethanolamine (DEA) as the amination agent. All of these composite materials recorded CO_2 adsorption capacities lower than that of EDA-PVC/SBS-15 (4%) when using a gravimetric method, despite all of the composites displaying higher surface areas and pore volumes when compared to EDA-PVC/SBA-15 (4%). This phenomenon can be explained by examining the available space for CO_2 adsorption at the adsorption sites. Of the amines used for CO_2 adsorption, ethylenediamine (EDA) appears to have the most ideal geometry for carbamate formation under anhydrous conditions. The introduction of an extra amine chain in diethylenetriamine (DETA) leads to a reduction in the effectiveness of carbamate formation. The use of monoethanolamine (MEA) and diethanolamine (DEA) is even less effective, with DEA the least effective of the amines studied due to additional steric hinderance introduced from the extra ethyl hydroxyl group.

3.4.4 Determination of Hydrophobicity of EDA-PVC/SBA-15 (4 %) Composite Material

The hydrophobicity of the experimentally determined ideal adsorbent EDA-PVC/SBA-15 (4%) was determined through contact angle experiments. These experiments were carried out on the SBA-15 support alone, the EDA-PVC/SBA-15 (4%) composite material and the unsupported EDA-PVC. The unsupported polymer indicated a high contact angle of 76.7°, suggesting a hydrophobic surface, as expected for a PVC

material. The unmodified SBA-15 support resulted in a low contact angle of 15.4°, indicating the support itself to be hydrophilic in nature. After deposition of only 4% EDA-PVC onto the silica surface, a contact angle of 35.6° was measured. This is a significant increase in hydrophobicity when using only a small amount of EDA-PVC.

3.5 Conclusion

A series of APVC/mesoporous silica composite materials were successfully generated with the ultimate goal of being used for selective CO_2 adsorption. Of the fumed silica, SBA-15 and MCF-3 mesoporous silicas studied, SBA-15 supports were observed to give the highest surface area, pore volume and CO_2 adsorption capacities. The highest CO_2 adsorption capacity measured in this study was attributed to EDA-PVC/SBA-15 (4%) composite material of 12 cm^3g^{-1}. Of the additional aminating reagents studied for modification of PVC, none were able to surpass the ability of EDA-PVC when loaded on SBA-15 at 4%.

The presence of water in the flue gas stream is inevitable as it is a major combustion product. As previously discussed, the deactivation of the solid-state adsorbents by water is a common problem when using zeolites, amine-grafted mesoporous silicas and MOFs, due to the hydrophilic nature of the adsorbent materials. The use of hydrophobic adsorbents derived from PVC thus present a unique advantage of these hydrophilic supports by helping to eliminate the role of water in the CO_2 adsorption process.

3.6 Impact On Literature and Research

This research provides an application of PVC materials destined for landfill, for post combustion CO_2 adsorption. The benefits of using PVC in this way are two-fold, not only that a waste material which would not degrade in a short time period is saved from landfill, but it is also used to combat rising CO_2 levels through adsorption from the flue gas stream. The chemistry used for amination was already established in the literature, with this work providing evidence that amination of the PVC backbone is possible with a wide range of amines. It has also been proven that the use of these APVC materials

can introduce a level of hydrophobicity to the CO_2 adsorption process. Furthermore, the hydrophobicity of the support material can be enhanced by deposition of as little of 4 % EDA-PVC onto the surface. This may have interesting scope for increasing the hydrophobicity of solid state adsorbents that suffer from deactivation due to the presence of water.

3.7 References

[3.1] S. C. Ma, N. A. Chaniotakis, M. E. Meyerhoff, *Response properties of ion-selective polymeric membrane electrodes prepared with aminated and carboxylated poly (vinyl chloride),* Anal. Chem. **60**, 2293-2299 (1988)

[3.2] M. S. Mohy Eldin, M. R. Elaassar, A. A. Elzatahry, M. M. B. Al-Sabah and E. A. Hassan, *Covalent immobilization of β-galactosidase onto amino-functionalized PVC microspheres*, J. Appl. Polym. Sci., **125**, 1724-1735 (2012)

[3.3] M. S. Mohy Eldin, H. A. El Enshasy, M. E. Hassan, B. Haroun and E. A. Hassan, *Covalent immobilization of penicillin G acylase onto amine-functionalized PVC membranes for 6-APA production from penicillin hydrolysis process. II. Enzyme immobilization and characterization*, J. Appl. Polym. Sci., **125**, 3820-3828 (2012)

[3.4] A. Singh, M. S. M. Rawat and C. S. Pande, *Chemical modification and characterization of poly(vinyl chloride) by crosslinking of multifunctional amines*, J. Appl. Polym. Sci., **118**, 876-880 (2010)

DECLARATION

As primary author of this publication, I can confirm the majority of the work to be my own, with BET, CHN and contact angle sample analysis carried out by other parties as outlined in Section 3.2.3.

Signature: _____

PUBLICATION 3

Aminated Poly(Vinyl Chloride) Solid Sorbents with Hydrophobic Function for Post-Combustion CO_2 Capture

Gregor Sneddon, Jessica C. McGlynn, Marie S. Neumann, Halil M. Aydin, Humphrey H. P. Yiu and Alexey Y. Ganin

Accepted for publication in Journal of Materials Chemistry A on 31 March 2017

Abstract

In this paper, we show a novel sustainable route for the production of sorption materials for carbon capture technologies by utilizing a general plastic waste. By supporting aminated poly(vinyl chloride) on mesoporous silicas, a family of polymer / silica composites was synthesized, characterised and tested gravimetrically for adsorption of CO_2 from the 1:1 v/v CO_2-N_2 mixture. The composites show good adsorption capacity for CO_2 peaking at 12 $cm^3\ g^{-1}$ for ethylenediamine-treated PVC products on SBA-15 support. The adsorption efficiency (CO_2:N ratio) is comparable to those observed for other nanoporous materials, such as amine-grafted mesoporous silicas. Ethylenediamine was found to be the best aminating reagent for PVC as the composite prepared from EDA-PVC gave the highest CO_2 adsorption efficiency. Moreover, contact angle measurements suggested a significant improvement in hydrophobicity of the selected composites when they were compared with the unfuctionalized silica supports. This very useful development could make the composites suitable for applications in elevated moisture content environments found in flue vapours of gas-fired power plants.

Introduction

Carbon capture and storage (CCS) technologies offer viable solutions for tackling problems linked to greenhouse gas emission.[1] Among these post-combustion capture (PCC) of CO_2 has seen progressive development with major scientific efforts focused on the separation of CO_2 from industrial gas sources.[2, 3] To enable compression, transport and storage, any advanced adsorbent for post-PCC processes is required to have an appreciable ability to capture CO_2 selectively from mixtures of gases.[4] Generally, such adsorbents possess basic sites on their surfaces, *e.g.* hydroxyl or amine groups, to facilitate chemical interaction with acidic CO_2 molecules. Inorganic bases such as calcium oxide (CaO), magnesium oxide (MgO), and sodium hydroxide (NaOH) are an obvious choice due to their natural abundance and relatively low cost, and they have been widely investigated as adsorbents for CO_2 capture before.[5-7] However, the high decomposition temperature of the corresponding carbonates presents a challenge, thereby preventing traditional inorganic bases from being integrated in a close cycle process often required within an industrial PCC operation.[8] Aqueous solutions of organic bases such as monoethanolamine (MEA) are therefore preferred for PCC as they require a relatively lower amount of energy for the regeneration (172 kJ/mol_{CO2} for MEA *vs*. 225 kJ/mol_{CO2} for CaO).[2, 3, 9] The processes for isolating CO_2 from 10 – 20% MEA aqueous solution for later re-utilization or storage with CCS systems have been tested on a large scale.[10] However, substantial operational expenditure costs are required for solvent regeneration, for example, to mitigate for the loss of the solvent. Aqueous solutions of amines are also prone to degradation by NO_x and SO_x, which are present in a typical gas-flue mixture, with up to 2 kg of solvent depleting per one ton of CO_2 stored. Moreover, operating and integrating the relatively corrosive and toxic amine solution as part of a commercial CCS system presents additional environmental and safety constrains as well as national security concerns.[11] Solid-state adsorbents can overcome these issues as regeneration can be carried out by the reduction of pressure rather than heat. It is also relatively simple to integrate them at a full-scale CCS system either as retrofits or as new builds.

Several classes of solid materials such as cation-exchanged zeolites,[12] metal organic frameworks (MOFs),[13] amine-functionalized mesoporous silicas,[14] porous polymeric networks,[15] and organic framework materials[16] have demonstrated high sorption capacity and good selectivity for CO_2 from a N_2 / CO_2 mixture which is

routinely used in laboratory settings. Typically, CO_2 adsorption capacities of 10 – 120 $cm^3\ g^{-1}$ have been reported depending on the tested conditions (Table S1). Since amine groups can be integrated into polymers there is an exciting opportunity to utilize the existing non-biodegradable plastics as future solid-state adsorbents.[17] As such their application in CCS presents a viable alternative to pyrolysis which is a current end-of-life solution for some of these non-recyclable polymers.[18] Pyrolysis of poly(vinyl chloride), PVC, is particularly problematic as it leads to the generation of toxic chloro-organic compounds.[19, 20] Moreover, re-use of waste PVC presents an additional challenge due to cross-contamination with polyethylene terephthalates (PET).[21] A large amount of CO (13 wt% of PET) has been shown to be released upon pyrolysis due to the presence of PET. There are few incentives for recycling and the majority of PVC ends up as landfill waste. A sustainable route for reutilization of waste PVC will be of particular interest to environmental and scientific communities and a facile route for coupling amines and alkyl chloride groups via a nucleophilic substitution reaction through the secondary chloro-groups on the PVC backbone is already developed.[22] Furthermore, the solid-liquid heterogeneous interface reactions between a PVC polymer (solid phase) and an ethylenediamine solution (liquid phase) have been also applied for functionalisation of PVC microspheres and membranes.[23] It has also been shown that PVC could be aminated by ethylenediamine (EDA), diethylenetriamine (DETA) and ethanolamine (MEA).[24] The authors were also able to generate crosslinked PVC with enhanced thermal stability and ion exchange capacity. However, no gas sorption measurements have been carried out on amine functionalized PVCs so far as one would expect the pristine unsupported materials to possess low surface areas. Supporting low surface material on robust and high surface area mesoporous substrates such as silicas could help to produce composites with high number of basic sites and to achieve improved gas sorption characteristics.[25]

In this work, we report for the first time the synthesis of a family of high surface area composite materials that contain amine-functionalized PVC as the source of basic sites for CO_2 adsorption. The proposed synthesis is based on a relatively simple one-step reaction making the protocol potentially scalable for the development of advanced adsorbents suitable for industrial CCS units. Furthermore, the aminated-PVC adsorbents show superior hydrophobic characteristics when compared with the

unfuctionalized mesoporous substrates. This is a potentially useful utility for the design of future CO_2 adsorbents operating in elevated moisture content flue gases.

EXPERIMENTAL SECTION

Chemicals

Ethylenediamine (99.5%), PVC powder (M_w = 43,000), methyl ethyl ketone (MEK, or butan-2-one, 99 %), trimethylbenzene (TMB, 98%), fumed silica (denoted as *f*-SiO_2) were all purchased from Sigma Aldrich. Aminating agents, diethylenetriamine (DETA, 98%), monoethanolamine (MEA,99%), ethylenediamine (EDA, 99%), diethanolamine (DEA, 99%) and tetraethylorthosilicate (TEOS, 98%) were supplied by Acros Chemicals. Concentrated hydrochloric acid HCl (35% w/w) was supplied by Fisher Scientific. Pluronic P123 surfactant ($EO_{20}PO_{70}EO_{20}$, M_w = 5800) was a gift from BASF. Deionised water was used in all synthesis. High purity CO_2 and N_2 gases were supplied by BOC. All chemicals were used as received without further purification.

Synthesis of mesoporous SBA-15 and MCF silicas

Mesoporous silica SBA-15 was prepared following a well-developed literature procedure.[26] Briefly surfactant Pluronic P123 (4 g) was dissolved in 138 cm^3 of deionized water and the solution was acidified by adding of 12 cm^3 of concentrated HCl. After being fully dissolved, the silica precursor TEOS (8.3 g, 0.04 mol) was added into the solution. After 24 h of stirring at 40°C a white precipitate was formed. It was then transferred to a PTFE bottle, which was heated in an oven at 100°C for 3 days. The white precipitate was filtered, washed, dried and calcined at 550°C in air. Mesocellular foam (MCF) silica was prepared with the same procedure as SBA-15 except that a swelling agent trimethylbenzene (TMB, 1.2 g) was added to the surfactant solution prior to the addition of TEOS.[25] The mass ratio of surfactant : MB = 1 : 0.3. The same calcination regime was applied to the as-prepared MCF silica.

Synthesis of aminated PVC (APVC) / mesoporous silica composites

For consistency, all composites were prepared from stock solutions of relevant APVC using a homogeneous liquid-phase reaction. To make a stock solution, 1 g of PVC was

dissolved in 50 cm^3 of MEK giving a clear solution. After adding an excess of an aminating agent (1 g) into the resulting solution it was refluxed at 80°C for 24 h. After cooling to ambient temperature, the resulting APVC stock solution with a nominal concentration of the polymer of *ca.* 2 wt. % was used for functionalization of the mesoporous silicas. It should be noted that to achieve the maximum functionalization of the surface of the polymer by amine groups an excess of amine and reflux times in excess of 18 hours were required.

In a typical coating procedure, 100 mg of a related mesoporous silica support (fumed silica, SBA-15 or MCF) were suspended in 10 ml of MEK solvent. A corresponding volume of the stock solution was then added to the suspension. Depending on the amount of the stock solution added, the composites with three different ratios of 4%, 7% and 19% w/w between the APVC and silica substrate were prepared as exemplified in Table 1 for composites between SBA-15 or MCF and the EDA-PVC stock solution.

Adsorbent	Stock solution, ml	Amount of APVC, mg	Amount of silica, mg
EDA-PVC/SBA-15 (4%)	0.2	4	100
EDA-PVC/SBA-15 (7%)	0.35	8	100
EDA-PVC/SBA-15 (19%)	0.95	24	100
EDA-PVC/MCF (4%)	0.2	4	100
EDA-PVC/MCF (7%)	0.35	8	100
EDA-PVC/MCF (19%)	0.95	24	100

Table 1. Exemplified ratios required for synthesis composites using the SBA-15or MCF silicas and the ethylenediamine (EDA) / PVC stock solution.

After adding the stock solution the suspension was sonicated in a degas mode for 60 min and transferred on a glass Petri dish in a fume cupboard to allow the solvent to evaporate at ambient temperature. Finally, the samples were washed in ethanol using Soxhlet extraction for at least 6 h to remove any unreacted amine. The resulting solid was heated to 80°C at a reduced pressure in a vacuum oven for 8 hours to remove any residual solvent.

Control experiments were carried out to isolate pristine APVC solids (*e.g.*, without a silica matrix). The solids were precipitated by adding ethanol to aliquots of the corresponding stock solutions. Similar to the composite materials the solids were washed with ethanol using a Soxhlet extraction setup to remove any unreacted amine from the surface of the polymer and were finally dried in a vacuum oven at 80°C overnight.

Characterization of materials

Pristine APVC products and their composites with mesoporous silicas were characterized using Fourier-transform infrared (FTIR) spectroscopy. FTIR spectroscopic analysis was carried out using a Perkin Elmer Spectrum 100 spectrometer fitted with an ATR sampling unit. For the sample measurement, 32 scans in the region from 650 to 4000 cm^{-1} were accumulated with a resolution of 4 cm^{-1}. CHN elemental analysis was performed with an Exeter CE-440 Elemental Analyzer. Simultaneous thermogravimetric analysis with differential scanning calorimetry (TGA/DSC) was carried out using a TA instruments SDT Q600 unit. In a typical analysis, a sample of *ca.* 5 mg was heated up to 800°C at a heating rate of 5°C min^{-1} under flowing air (100 cm^3 min^{-1}). Experimental datasets were analysed using Advantage Software v5.5.22 (TA Instruments).

Surface area was studied using N_2 adsorption-desorption isotherms and transmission electron microscopy (TEM). Nitrogen adsorption-desorption isotherms were measured at –196°C using a Quantachrom Autosorb Evo unit. The samples were degassed at 80°C overnight under vacuum before the measurements. The pore size distribution (PSD) of samples was calculated using a DFT method with the Quandrawin software (Quantachrom). A FEI Tecnai TF20 microscope fitted with a field emission gun and operated at 200 keV was used for the TEM analysis. The samples were suspended in ethanol before being dispersed on holey carbon sample grids (Agar Scientific).

Gravimetric CO_2 adsorption capacity of the samples was measured using a SDT Q600 unit (TA Instrument) fitted with a CO_2 dosing valve. The sample was first

activated at 75°C under flowing N_2 overnight and cooled down to 25°C. After that, the adsorption was carried out in a purge gas consisting of a 1:1 v/v CO_2-N_2 mixture for 90 min, the sample was then heated to 75°C for 2 h for regeneration. The CO_2 capacity was calculated by the weight gain during the adsorption period.

The hydrophobicity of the composites was examined with contact angle measurements using an Attension Theta unit and data analysis was carried out using OneAttension v2.4 software. Generally, a powder sample, 20 mg, was pressed into a disc using a standard hydraulic press. A water droplet was placed on the disk surface and the image of the drop was recorded. The value of contact angle was taken at t = 1 s after the water droplet was loaded onto the sample disk surface and the data reported was an average of three measurements.

For mechanical stability tests *ca.* 100 mg of sample were ground thoroughly with pestle and mortar for at least 5 minutes and then the resulting powder was investigated by gas sorption measurements. Additional tests involved pressing EDA-PVC/SBA-15(4%) under pressure of *ca.* 1 ton to a 5 mm pellet which was probed by gas sorption as well. It should be mentioned that the resulting pellet was very robust and could be easily handled with tweezers without crashing the pellet. To test the hydrothermal stability, EDA-PVC/SBA-15(4%) sample was boiled in water for 1 h and then dried at 80°C in vacuum in line with the drying protocol for all samples used in gas sorption measurements. The sample was then analyzed with TGA (heating rate at 5°C min^{-1} to 800°C under flowing air) / surface area measurements. The results were compared with the sample before hydrothermal treatment.

RESULTS AND DISCUSSION

Pristine APVC materials

Before discussion of the composite materials, it is important to highlight the properties of pristine APVC materials. Figure 1a illustrates the possible reaction routes depending on the aminating agent used for the reaction with PVC.[24] A certain amount of crosslinking between polymer strands is possible and the proposed reaction mechanism is shown in Figure 1b.

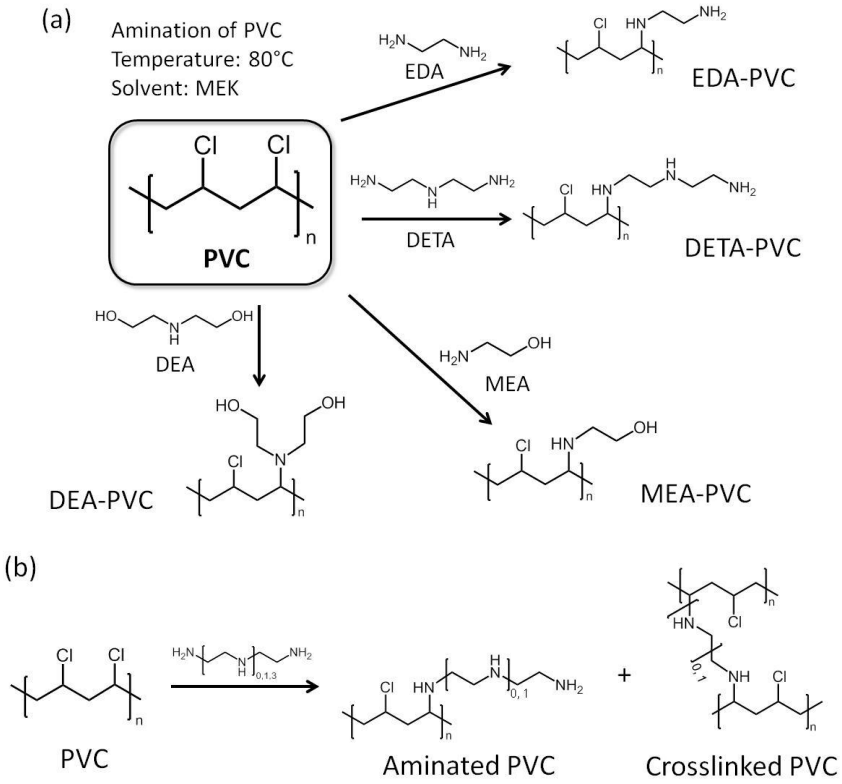

Figure 1. (a) Possible amination route of PVC with the selected amines; EDA = ethylenediamine, DETA = diethylenetriamine, MEA = monoethanolamine, DEA = diethanolamine and MEK = methyl ethyl ketone, and (b) A possible crosslinking mechanism for two products functionalized by diamine precursors.

Ethylenediamine (EDA) was chosen as a model aminating agent for optimising the process as other groups have tested a coupling reaction between EDA and PVC before.[22-24] Analysis of several samples by elemental analysis consistently showed *ca.* 2.9 *wt.* % of nitrogen indicating that the washing in a Soxhlet setup have led to a reproducible results. The level of functionalization is also higher than reported previously due to the modified synthetic procedure.[23, 24] Figure 2 shows the results of TGA / DSC measurements for unmodified PVC in airflow. An endothermic weight loss at 260°C is attributed to the loss of monomers after the depolymerization.

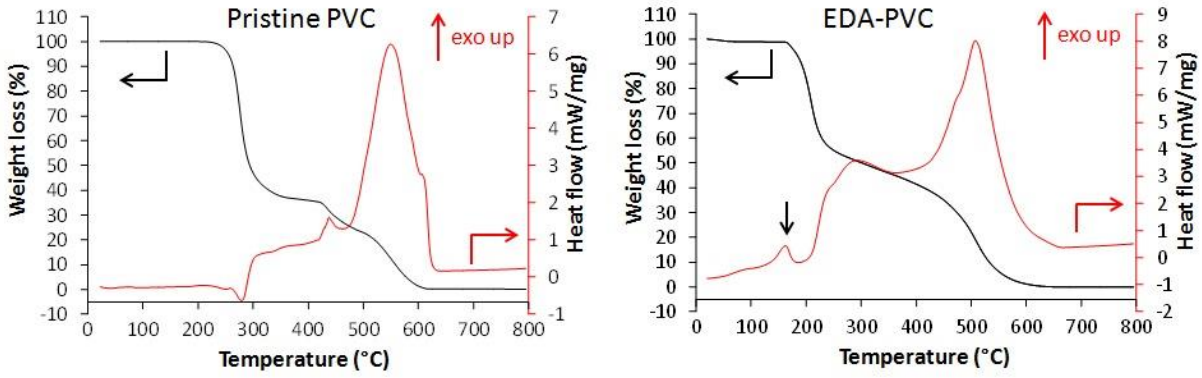

Figure 2. TGA (black, left scale) and DSC (red, right scale) for unmodified PVC and EDA-PVC. The exothermic transition at around 160°C (indicated with a black arrow) appeared only with cross-linkable aminated PVC samples.

Two following exothermic steps are due to combustion of the polymer. EDA-PVC sample (Figure 2) showed a small weight loss from 70°C to ca. 160°C due to the loss of the solvent. A minor exothermic peak appeared at around 170°C which is likely due to a solid-phase transition (*e.g.* non-isothermal crystallization or polymorphic conversion)[23,24] which is absent in the PVC polymer.[27] A significant weight loss between 170 and 210°C is accompanied by a corresponding exothermic peak on the DSC curve. This weight loss could be attributed to the possible loss of amine crosslinkers followed by a gradual depolymerization of PVC at higher temperatures. When compared with other aminated PVC samples prepared in this work (Figure S1), this is a common feature to the aminating reagents with potential for crosslinking / self-polymerizing, e.g. DETA-PVC (Figure S1c). MEA-PVC and DEA-PVC, which are unlikely to be crosslinked due to amination, showed no exothermic peak in this region (Figure S1d and S1e). Overall, the thermal analysis results indicate that aminated PVC materials are stable up to 140°C without decomposition. The thermal stability is sufficient for thermal regeneration of the composites to be carried out sustainably in the associated carbon capture process.[1]

EDA-PVC/silica composites

Two mesoporous silica materials (SBA-15 and MCF) were chosen as the support for APVC due to their high surface area and mesoporous characteristic. The latter is important as high surface area materials with microporous structure (pore

diameter < 2nm) could suffer from pore blockage upon polymer deposition, hence reducing the gas adsorption capacity.[1] The organic content of the APVC/silica composite samples was analyzed with TGA and elemental analysis with the results presented in Table 2.

The observed nitrogen content is almost double when compared with the pristine EDA-PVC samples. For example, 4.4, 4.5 and 4.2 % for 4%, 7% and 19 % EDA loaded on MCF silica respectively *versus* 2.9 *wt.*% observed for the pristine EDA-PVC products. This is consistent with the TGA results for products with different loadings of the EDA-PVC on SBA-15 and MCF supports (Figure 3). In comparison with a pristine EDA-PVC sample (*c.f.* Figure 2) the TGA results suggested the remains of the solvent and unreacted amines were still present within the samples.

Adsorbent	Organic content (% w/w)	BET surface area (m^2g^{-1})	Pore Volume (cm^3g^{-1})	Pore radius (nm)
Unsupported EDA-PVC	100	0	0	0
SBA-15	0	481	0.98	4.4
EDA-PVC/SBA-15 (4%)	20	314	0.66	3.0
EDA-PVC/SBA-15 (7%)	22	295	0.58	2.8
EDA-PVC/SBA-15 (19%)	53	116	0.25	3.1
MCF	0	559	0.87	5.3*
EDA-PVC/MCF (4%)	10	122	0.34	5.4*
EDA-PVC/MCF (7%)	17	98	0.34	4.8*
EDA-PVC/MCF (19%)	44	81	0.20	4.3*

Table 2. The organic content, BET surface area, pore volume and mean pore size for aminated PVC-silica composites and the silica supports. The PSD data of MCF samples were calculated from the adsorption branch due to their interconnected porous structure.[28]

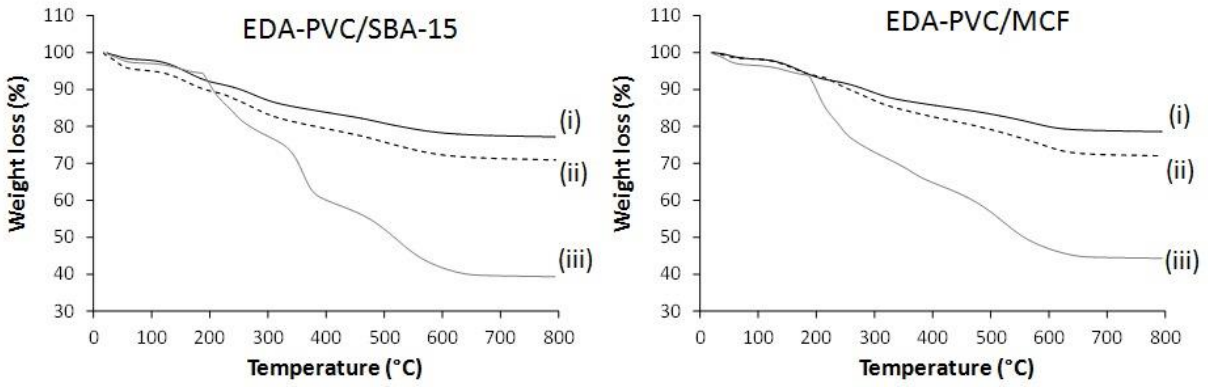

Figure 3. TGA curves for EDA-PVC/SBA-15 and EDA-PVC/MCF samples with (i) 4%, (ii) 7% and (ii) 19% loadings.

Representative FTIR spectrum of EDA-PVC/SBA-15 in comparison with three other APVC composites is shown in Figure 4. The highlighted broad absorbance bands at 3200-3500 cm^{-1} are assigned to NH stretching as well as OH stretching in cases of MEA-PVC and DEA-PVC coated samples. This indicates the similarity of the composite materials depending on the nature of the amination agent. Composite samples appear similar due to the similarity in the functional groups on the aminated PVC coatings.

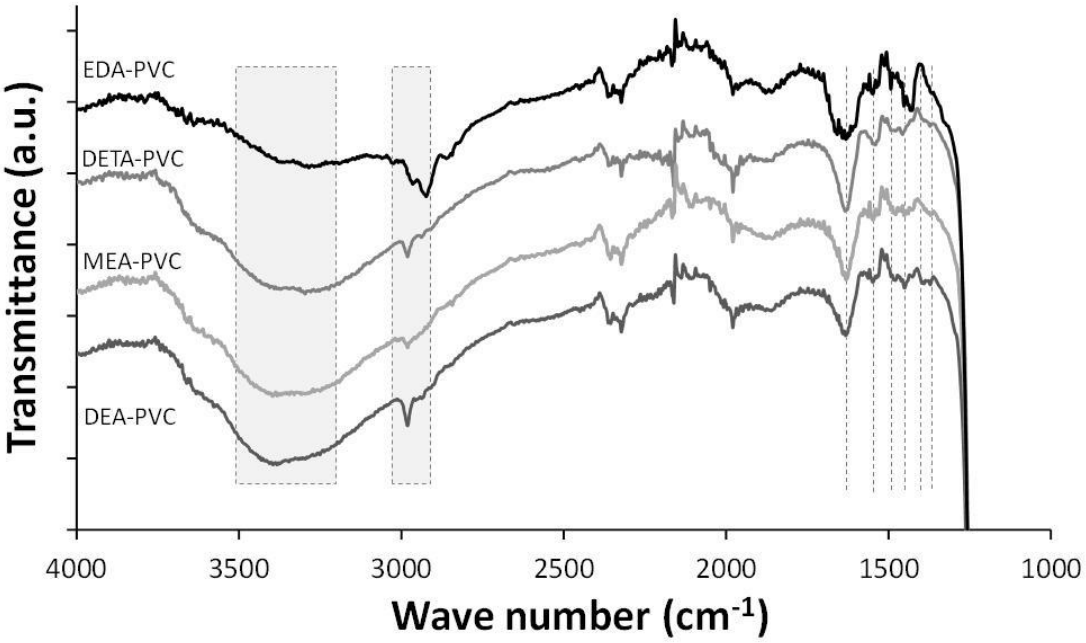

Figure 4. FTIR spectroscopy of EDA-PVC/SBA-15 (4%), DETA-PVC/SBA-15 (4%), MEA-PVC/SBA-15 (4%) and DEA-PVC/SBA-15 (4%).

Absorption band at 2800–3000 cm^{-1} are due to the CH_2 stretching modes, both on the PVC backbone and the amines. NH_2 bending modes appear in ~1540 cm^{-1} while bands at 1450–1480 cm^{-1} and ~1350 cm^{-1} are assigned to CH_2 bending modes. The strong absorbance band shown at 1750 cm^{-1} is due to the C=O stretching from the residual ketone groups from the solvents. Below 1200 cm^{-1}, all spectra were dominated by the strong silica absorbance and therefore this data range was omitted. The retention of the solvent as indicated by FTIR data is expected considering the highly porous nature of the silica. However, the observed increase of the amount of the remains has very limited effect as a significant porosity and high surface area were retained, especially for products with 4 % loading of APVC according to the surface area measurements.

The adsorption / desorption measurement results of EDA-PVC composites with SBA-15 and MCF are shown in Figure 5 with the results summarized in Table 2. In addition to surface area measurements all three supports (MCF, SBA-15 and fumed silica) were investigated by HRTEM (Figure S2). For all tested EDA-PVC composites there is a gradual decrease in the surface area and pore volume depending on the amount of amine-functionalised PVC used. In the case of SBA-15, which showed very well defined pores (Figure S2), the PSD data suggested that the pore radius was reduced from 4.4 nm to *ca.* 3 nm depending on the amount of the loaded EDA-PVC. The pore sizes of the MCF substrate were generally unaffected. The adsorption properties of fumed silica (*f*-SiO_2) were also tested due its importance as a commercial standard. It showed a broad size distribution of mesopores with radius > 1 nm. Interestingly, an increased polymer content (at 19%) for the fumed silica sample seemed to lead to larger pores at a radius > 5.0 nm the phenomenon observed before for chitosan/fumed silica composites (Figure S3).[25] It was also suggested that the pore structure of the adsorption sites plays a significant role on the total CO_2 adsorption capacity, in addition to the available amine sites.[29, 30] Therefore, the pore structures of the composites were also mapped with the CO_2 adsorption data as discussed in the next section. This allowed us to extrapolate the critical parameters for optimizing CO_2 adsorption capacity. In contrast to SBA-15 and MCF control experiments carried out on EDA-PVC / fumed silica samples showed both the surface area and pore volume were hardly affected upon polymer deposition (Figure S3).

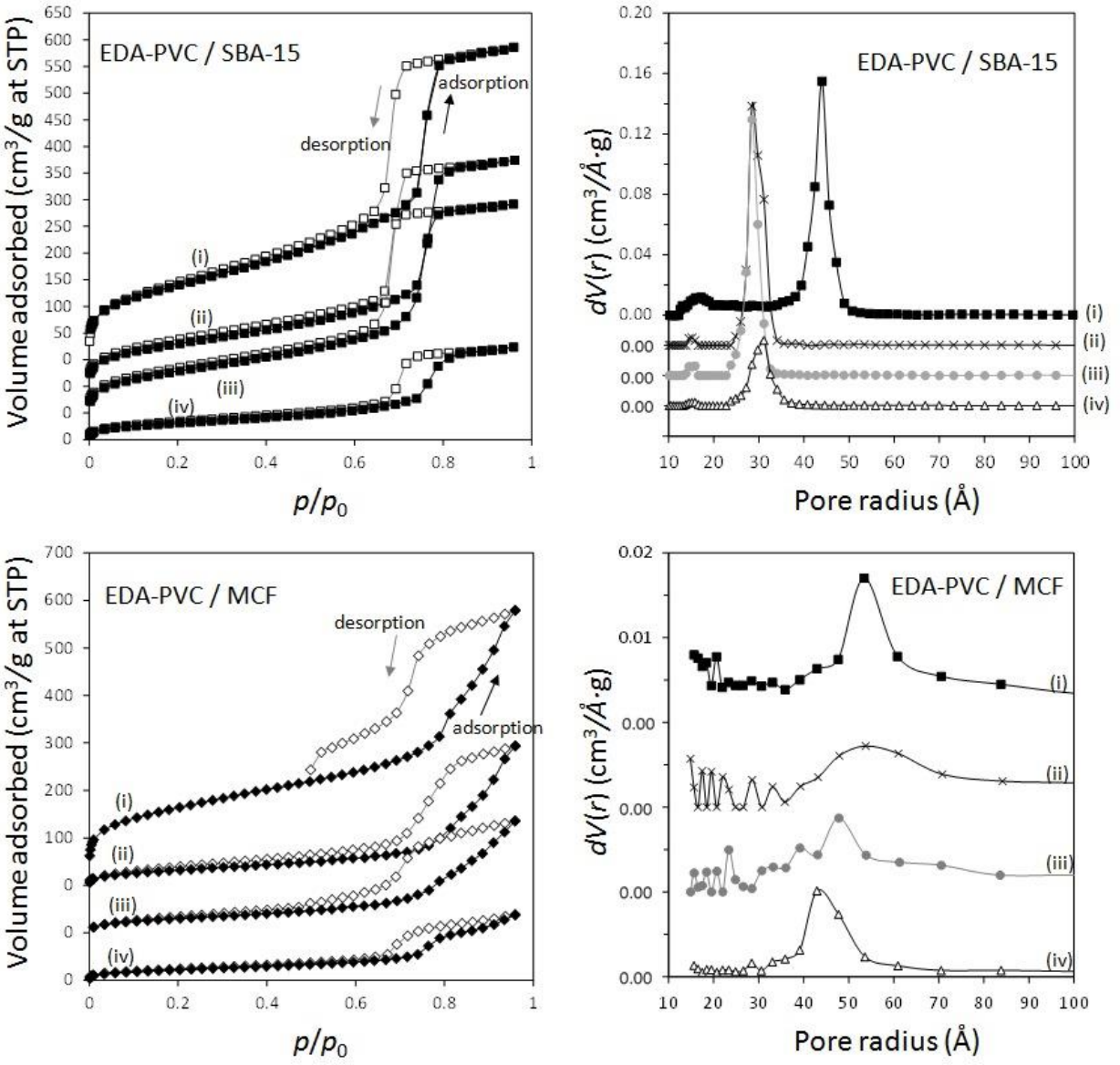

Figure 5. Nitrogen adsorption-desorption isotherms and pore size distribution (PSD) of MCF and SBA-15 composites with (i) 0%, (ii) 4%, (iii) 7%, (iv) 19% loading of EDA-PVC. Both the isotherms and PSD graphs were off-set along the y-axis for clarity.

Gravimetric CO_2 adsorption capacity of APVC composites

Carbon dioxide adsorption capacity of EDA-PVC on mesoporous silica composites was measured gravimetrically, *e.g.* by purging CO_2/N_2 mix (1:1 v/v, 50%) over the adsorbent samples at 25°C and the results are shown in Figure 6.

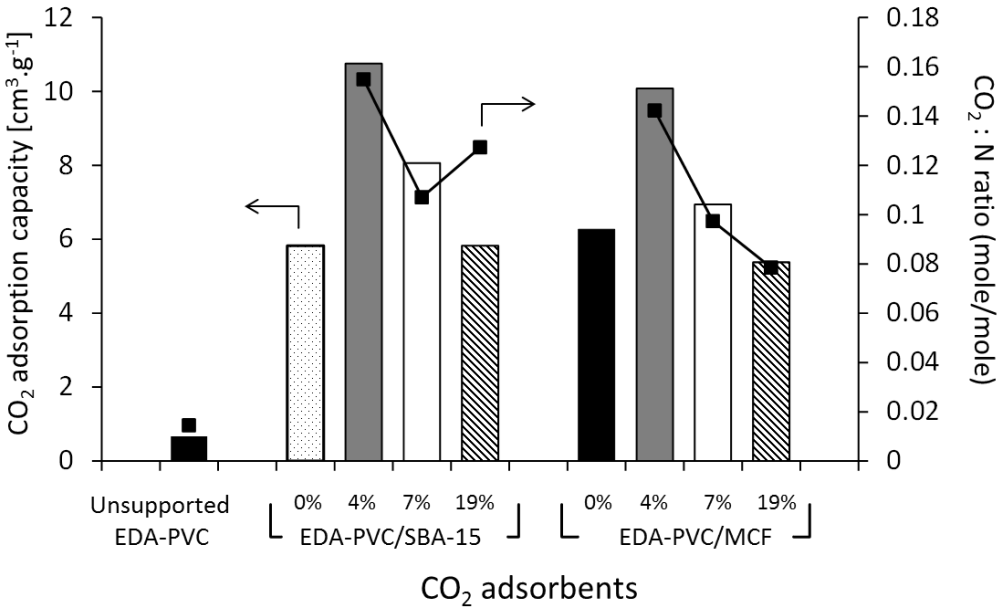

Figure 6. CO_2 adsorption capacity at 25°C measured by gravimetric method (left scale) and CO_2 : N ratio (right scale) for EDA-PVC / mesoporous silica samples depending on the amount of APVC. The CO_2 : N ratio is calculated from the CO_2 adsorption capacity while the nitrogen content was calculated from CHN analysis.

The gravimetric method for measuring the CO_2 adsorption capacity was chosen here because it models the real carbon capture environment more closely than the volumetric method. As expected the unsupported EDA-PVC sample has shown a very low capacity below a measureable limit of our instrument of 0.73 $cm^3\ g^{-1}$. On examining the CO_2 adsorption capacity of EDA-PVC/SBA-15(4%) composite has shown the highest adsorption capacity of 12 $cm^3\ g^{-1}$. In line with the surface area measurements results the capacity to store CO_2 gradually decreases as the polymer content increases. A similar trend was also observed for MCF series that showed maximum CO_2 storage capacity peaking at 11 $cm^3\ g^{-1}$. A comparable study on related amine-grafted mesoporous silicas MCM-41 with a capacity of 14 $cm^3\ g^{-1}$ has also shown that an increase in pore size can enhance

CO_2 adsorption capacity while connectivity speed up the adsorption process.[30] In context of this study, EDA-PVC/MCF (4%) composites, which possess larger pores (between 4.0 to 8.0 nm in radius) and interconnecting porous structure, may be advantageous for carbon capture over 2D SBA-15 adsorbents.

The ratio was used as an indicator of the efficiency of the amount of CO_2 adsorbed. Since the increase in polymer content did not yield higher CO_2 adsorption capacity, the adsorption efficiency (or CO_2:N) ratio decreases as the polymer content increases. One exception was EDA-PVC/SBA-15 (19%), which showed a higher CO_2:N ratio than that of the sample with 7% loading. This was due to high organic residues content (53 %) observed in this product (Table 2) which suggested an excessive amount of trapped solvent MEK in pores. This case also illustrated the disadvantage of 2D non-connected pore networks. EDA-PVC on commercial fumed silica was also tested for CO_2 adsorption but the capacity shown was rather low (<1 cm^3 g^{-1}). Supporting the aminated PVC polymer on SBA-15 and MCF mesoporous silica with 4% polymer content showed the highest CO_2 adsorption capacity among tested candidates. They, therefore, meet three important criteria for an effective solid state adsorbent (1) being readily available on operational scale due to simple synthetic protocol, (2) possessing good adsorption capacity and (3) easy to handle with low environmental impact due to utilization of abundant waste material. However, the final criteria and ultimate challenge for any solid state adsorbent is its economic viability, *e.g.* an ability to regenerate with low energy duty. This was tested by analysis of kinetic of adsorption / desorption on selected samples.

The representative CO_2 adsorption kinetic profiles are shown in Figure S5. All samples reach saturation at 90 min and 90% of the adsorption capacity in 20 min. In all profiles, we observed an "initial step" following by an increase in weight to saturation due to CO_2 adsorption. One possible explanation for this observation is that the adsorption on the readily accessible sites on the outer surface or near the entrance of pores. Once these sites are occupied the pores become partially blocked and further adsorption is slowed down. When the CO_2 molecules migrate towards the inner sites, pores open again and allow further adsorption. Such assumption is also supported by the assessment of the porosity of the adsorbents, *e.g.* with narrower pores on adsorbent showing a wider step. In

particular, the EDA-PVC/MCF (4%) sample showed the smallest step due to its wider pores and interconnected porosity. Initial blockage became a less significant issue. The observed "non-linear" adsorption behaviour in Figure S5 could also be attributed to change in nature of polymer coating around the exterior pores of the support due to interaction between CO_2 molecules and amine sites during initial adsorption of carbon dioxide. This may be accompanied by heat release leading to a reduction of diffusional resistance and as such, CO_2 molecules could enter more facile into the interior pores of the support as manifested by a subsequent region of fast CO_2 uptake. All adsorbents also recorded ~100% desorption at 75°C, which leads to an thermal energy duty at *ca.* 60 kJ/mol_{CO2}, a considerable improvement from CaO and MEA solution. It should be noted that the TGA results suggested that the EDA-PVC products were stable up to 140°C. Therefore, higher regeneration temperatures can be employed to speed up the regeneration process. However, regeneration at a lower temperature of 75°C can reduce the energy consumption, which is critical for a competitive CCS system.

The role of the aminating agent on the CO_2 storage capacity

In addition to EDA, three other aminating reagents, diethylenetriamine (DETA), monoethanolamine (MEA) and diethanolamine (DEA) were tested and composites of aminated PVC on SBA-15 (all 4%) prepared from these reagents were analyzed. The structural data and CO_2 adsorption capacity for these composite samples are summarized in Figure 7 and Table S2. N_2 adsorption isotherms are given in Figure S4.

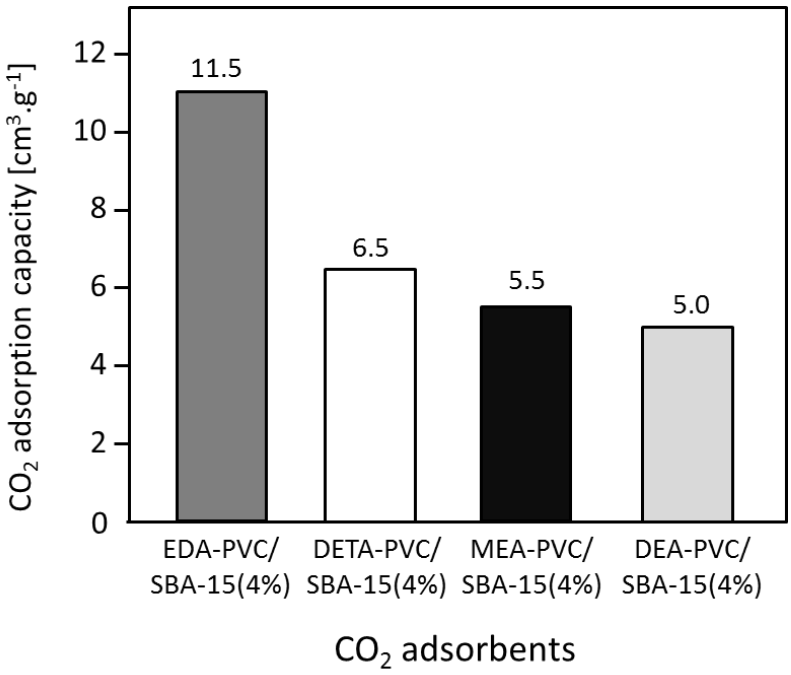

Figure 7. CO_2 adsorption capacity of APVC / SBA-15 (4%) composites depending on the nature of the aminating reagent.

A decrease in adsorption capacity was observed for all samples compared with EDA-PVC/SBA-15. Generally, CO_2 adsorption on amine groups under dry conditions leads to a formation of a carbamate following the chemical equation shown in Figure 8a. Such adsorption may become less effective if the two amine groups are further apart.[31] Among the aminating reagents that we used, ethylenediamine (EDA) appear to possess the best geometry for forming carbamate as illustrated in Figure 8b. With an extra amine on the chain, diethylenetriamine (DETA) becomes less effective. Although widely used in liquid phase adsorption, mono- and diethanolamine (MEA and DEA) seem to be the least effective reagents for this task with DEA further hampered by steric hinderance due to the extra ethyl hydroxyl group. Compared with EDA-PVC/SBA-15, all three samples showed a higher surface area, higher pore volume and larger pore sizes. All of these structural parameters seem to be essential for a high CO_2 adsorption capacity, but none of the samples outperformed EDA-PVC/SBA-15. This highlights that the distribution of amine sites on the adsorbents is critical to high CO_2 adsorption performance.

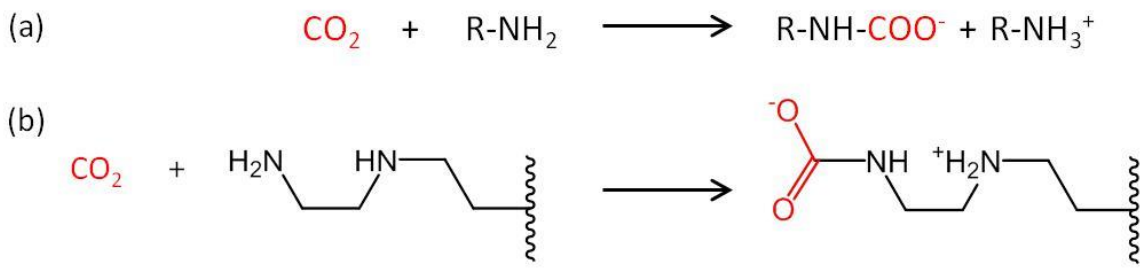

Figure 8. Proposed reaction schematic for CO_2 chemisorption on a generic amine (a) and supported ethylenediamine (EDA) with carbamate formation in anhydrous condition (b).[31]

There are examples of composite materials prepared by coating polymers and mesoporous silicas that have been tested as adsorbents for CCS,[1, 13] with the research primarily dedicated to polyethyleneimine (PEI) functionalized silicas.[31] PEI physically coated on MCF has achieved impressive CO_2 adsorption characteristics with similar amine efficiency (CO_2:N ratio) to results in this work. Further enhancement was also shown from the adsorption under humid condition (1% water in flue gases).[31] We also tested mechanical stability of EDA-PVC/SBA-15 (4%) sample, which showed the highest CO_2 adsorption capacity among all samples tested in this work. The outcome of these experiments is summarized in Table S3. Within the measurement error, there is a negligible difference between surface area, pore sizes and pore volume of the pristine and reground samples. There is a *ca.* 10 % reduction in surface area accompanied by a similar reduction in pore volume for the pelletized sample while the pore sizes are the same. The resulting pellet is very robust and could be manipulated with the tweezers without breakage. This could be a useful property in industrial settings, *e.g.* for retrospective addition to existing CCS facilities.

There was a marginal difference between the TGA profiles of the untreated sample and the sample subject to hydrothermal treatment in boiling water for 1 hour (Figure S6). The resulting sorption characteristic of the hydrothermally treated sample after degassing at 100°C is less than 5% lower when compared with the untreated composite indicating the good hydrothermal stability.

Hydrophobicity of the absorbents measured by contact angle tests

When compared with other amine-based adsorbents such as aminated mesoporous silicas,[32] one distinctive property of PVC-based materials is their

hydrophobicity. Hydrophobic adsorbents can be of particular use when the flue gas has excessive moisture content and the adsorbing system needs to avoid moisture. To study the hydrophobilicity of the adsorbents, the contact angle of a water droplet on the adsorbent surface was measured. Figure 9 shows the water droplet on the surface of fumed silica, EDA-PVC / SBA-15 (4%) composite. The pristine EDA-PVC product showed a high hydrophobicity as evident by a contact angle of 76.7°. SBA-15 is a highly hydrophilic support as apparent by the recorded contact angle of 15.4°. However, the minor 4% loading of EDA-PVC was sufficient to more than double the contact angle to 35.6°.

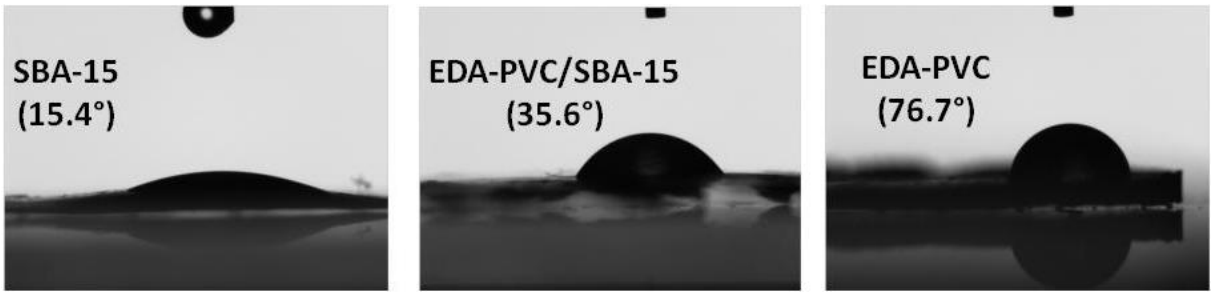

Figure 9. Images from the contact angle measurement experiment on SBA-15, EDA-PVC/SBA-15(4%) and unsupported EDA-PVC polymer.

The ability to control the hydrophobic – hydrophilic function is important as it could present an efficient way for stabilising compounds with high adsorption characteristics for CO_2 sorption. For example, inducing hydrophobicity has been highlighted as a very efficient method in rendering compounds with limited stability (such as many MOFs) in elevated water content flues.[33] Using PVC as a raw material for the preparation of adsorbent aiming at CO_2 adsorption from flue gas could therefore present a unique advantage. Most solid state adsorbents such as zeolites, amine-grafted mesoporous silicas (MCM-41 and SBA-15) and many MOF systems are hydrophilic. High moisture content in flue gas is a natural by-product of combustion. For example, gas-fired power plants, preferred by developed countries, could generate a clean flue gas but with a much higher moisture content of up to 14%. As such, the moisture content could pose a negative effect on the efficiency of the adsorbents in a carbon capture system. This effect is particularly noticeable using zeolites as adsorbent as they are known to be deactivated in presence of moisture.[34, 35]

Therefore, hydrophobic CO_2 adsorbents which can be operated under high moisture content is a step in the right direction towards finding the ultimate CO_2 adsorbent. Moreover, as most current amine-based solids selectively adsorb acidic gases such as CO_2 on surface basic sites this adsorption can be interfered by other acidic gases such as SO_2 and NO_x. Modified PVC has already shown its potential in the separation of CO_2 from SO_2,[36] making promising solid adsorbents for flues from coal power stations, *e.g.* with a high sulphur content which is particularly common in developing countries.

Conclusions

This work demonstrates a novel recycling / reusable pathway for waste PVC. Using a simple, robust route a range of hydrophobic aminated PVC were coated on silica support materials to form composites with high surface areas. Among these composites, EDA-PVC/SBA-15 with 4% w/w loading gave the highest CO_2 adsorption capacity of 12 $cm^3\ g^{-1}$ which also showed good mechanical and hydrothermal stability manifested by the marginal loss in surface area upon pressing to a compact pellet and after boiling in water. Higher polymer content seemed to cause pore blockage, which is a commonly observed feature in composites with mesoporous materials. The assessment of the adsorption / desorption kinetics for selected composites suggested an energy consumption of regeneration value of at 60 kJ/mol_{CO2}. When compared with pristine supports the enhanced hydrophobicity of the composites suggests an interesting development opportunity for novel adsorbents capable of operating in the flue gas emitted from a gas-fired power plant with higher water content. Future research directions in this area should focus on optimising the aminated PVC-silica composites towards cost-efficiency, enhanced CO_2 adsorption capacity, and CO_2 selectivity under realistic simulated flue gas streams.

ACKNOWLEDGEMENTS

AG and JCM acknowledge the University of Glasgow for funding. GS, MSN and HHPY thank Scottish Carbon Capture and Storage (SCCS) program and the EPSRC, UK (EP/F034482/1 and EP/J02077X/1) for funding. We also thank Dr. Cem Bayram (Hacettepe University, Ankara, Turkey) for his assistance in contact angle measurements.

REFERENCES

[1] G. Sneddon, A. Greenaway and H. H. P. Yiu, *Adv. Energy Mater*., 2014, **4**, 1301873; S. Choi, J. H. Drese and C. W. Jones, *ChemSusChem*, 2009, **2**, 796.

[2] N. MacDowell, N. Florin, A. Buchard, J. Hallett, A. Galindo, G. Jackson, C. S. Adjiman, C. K. Williams, N. Shah and P. Fennell, *Energy Environ. Sci*., 2010, **3**, 1645; F. Zeman, *Energy Environ. Sci*., 2007, **41**, 7558.

[3] M. Wang, A. Lawal, P. Stephenson, J. Sidders and C. Ramshaw, *Chem. Eng. Res. Design*, 2011, **89**, 1609.

[4] Y. S. Bae and R. Q. Snurr, *Angew. Chem. Int. Ed*., 2011, **50**, 11586.

[5] H. C. Chen, P. P. Zhang, Y. F. Duan and C. S. Zhao, *Chem. Eng. J*., 2016, **295**, 218.

[6] A. T. Vu, K. Ho, Keon, S. Jin and C. H. Lee, *Chem. Eng. J*., 2016, **291**, 161.

[7] J. K. Stolaroff, D. W. Keith and G. V. Lowry, *Environ. Sci. Technol.*, 2008, **42**, 2728.

[8] A. Iizuka , K. Hashimoto , H. Nagasawa , K. Kumagai , Y. Yanagisawa, A. Yamasaki, *Sep. Purif. Technol.* 2012, **101** , 49.

[9] F. Barzagli, F. Mani and M. Peruzzini, *Environ. Sci. Technol.*, 2016, **50**, 7239.

[10] M. Sharifzadeh, P. Bumb and N. Shah, *Appl. Energy*, 2016, **163**, 423.

[11] L. M. Romeo, I. Bolea and J. M. Escosa, *Appl. Therm. Eng.*, 2008, **28**, 1039.

[12] F. S. Su, C. Y. Lu, S. C. Kuo and W. T. Zeng, *Energy Fuel*, 2010, **24**, 1441.

[13] J. Wang, L. Huang, R. Yang, Z. Zhang, J. W. Wu, Y. S. Gao, Q. Wang, D. O'Hare and Z. Y. Zhong, *Energy Environ. Sci*., 2014, **7**, 3478.

[14] M. B. Yue, Y. Chun, Y. Cao, X. Dong and J. H. Zhu, *Adv. Funct. Mater*., 2006, **16**, 1717.

[15] T. C. Drage, C. E. Snape, L. A. Stevens, J. Wood, J. Wang, A. I. Cooper, R. Dawson, X. Guo, C. Satterley and R. Irons *J. Mat. Chem.*, 2012 **22**, 2815.

[16] T. Tozawa, J. T. A. Jones, S. I. Swamy, S. Jiang, D. J. Adams, S. Shakespeare, R. Clowes, D. Bradshaw, T. Hasell, S. Y. Chong, C. Tang, S. Thompson, J. Parker, A. Trewin, J. Bacsa, A. M. Z. Slawin, A. Steiner and A. I. Cooper, *Nat. Mater*., 2009, **8**, 973.

[17] J. Hopewell, R. Dvorak and E. Kosior, *Phil. Trans. R. Soc. B*, 2009, **364**, 2115.

[18] C. B Zhou, W. J. Fang, W. Y. Xu, A. X. Cao and R. S. Wang, *J. Clean. Prod.*, 2014, **80**, 80.

[19] L. Sorum, M. G. Gronli and J. E. Hustad, *Fuel*, 2001, **80**, 1217.

[20] M. A. Keane, *ChemSusChem*, 2009, **2**, 207.

[21] P. T. Williams and E. A. Williams, *Energy Fuel*, 1999, **13**, 188.

[22] S. C. Ma, N. A. Chaniotakis, M. E. Meyerhoff, *Anal. Chem.* 1988, **60**, 2293.

[23] M. S. Mohy Eldin, M. R. Elaassar, A. A. Elzatahry, M. M. B. Al-Sabah and E. A. Hassan, *J. Appl. Polym. Sci*., 2012, **125**, 1724.; M. S. Mohy Eldin, H. A. El Enshasy, M. E. Hassan, B. Haroun and E. A. Hassan, *J. Appl. Polym. Sci.*, 2012, **125**, 3820.

[24] A. Singh, M. S. M. Rawat and C. S. Pande, *J. Appl. Polym. Sci*., 2010, **118**, 876.

[25] G. Sneddon, A. Y. Ganin and H. H. P. Yiu, *Energy Technol*., 2015, **3**, 249.

[26] H. H. P. Yiu, M. A. Keane, Z. A. D. Lethbridge, M. R. Lees, A. J. El Haj and J. Dobson, *Nanotechnology*, 2008, **19**, 255606.

[27] J. Choi, S. W. Chun and S. Y. Kwak, *J. Polym. Sci. Pt. B-Polym. Phys.*, 2007, **45**, 577.

[28] P. I. Ravikovitch and A. V. Neimark, *J. Phys. Chem. B*, 2001, **105**, 6817; J. C. Groen, L. A. A. Peffer and J. Pérez-Ramírez, *Microporous Mesoporous Mater*., 2003, **60**, 1.

[29] R. Ryoo, C. H. Ko, M. Kruk, V. Antochshuk and M. Jaroniec, *J. Phys. Chem. B*, 2000, **104**, 11465.

[30] V. Zelenak, M. Badanicova, D. Halamova, J. Cejka, A. Zukal, N. Murafa and G. Goerigk, *Chem. Eng. J.*, 2008, **144**, 336.

[31] W. J. Son, J. S. Choi and W. S. Ahn, *Microporous Mesoporous Mater*., 2008, **113**, 31; J. J. Ma, Q. M. Liu, D. D. Chen, S. Wen and T. H. Wang, *J. Porous Mater*., 2014, **21**, 859; D. J. N. Subagyono, M. Marshall, G. P. Knowles and A. L. Chaffee, *Microporous Mesoporous Mater*., 2014, **186**, 84.

[32] N. Hiyoshi, K. Yogo and T. Yashima, *Chem. Lett*., 2004, **33**, 510.

[33] N. Ding, H. W. Li, X. Feng, Q. Y. Wang, S. Wang, L. Ma, J. W. Zhou and B. Wang, *J. Am. Chem. Soc.*, 2016, **138**, 10100; Z. J. Zhang, H. T. H. Nguyen, S. A. Miller, A. M. Ploskonka, J. B. DeCoste and S. M. Cohen, *J. Am. Chem. Soc.*, 2016, **138**, 920.

[34] J. C. Fisher, R. V. Siriwardane, and R. W. Stevens, Robert, *Ind. Eng. Chem. Res*., 2011, **50**, 13962.

[35] F. Brandani and D. M. Ruthven, *Ind. Eng. Chem. Res*., 2004, **43**, 8339.

[36] K. Kim, S. Hong, J. Kim and H. Lee, *AIChE J*., 2014, **60**, 2298.

Supporting Information

Absorbent type	P_{CO2} [bar]	Temperature [°C]	CO_2 adsorption capacity [$cm^3\ g^{-1}$]	Reference
Zeolites	1.0	25 – 30	34 – 134	[1]
MOFs	0.15	25 – 40	22 – 134	[2]
NH_2-grafted mesoporous silica	0.1 – 0.15	25 – 60	11 – 45	[1]
PEI-impregnated mesoporous silica	0.15	75	31 – 67	[1]
PEI-impregnated mesoporous silica (humid condition)	0.15	75 - 115	0.26 - 2.2	[3]
Nanoporous carbon materials	1.0	25	34 – 67	[1]

Table S1. CO_2 adsorption characteristic of the current state-of-the-art materials

[1] A. Samanta, A. Zhao, G. K. H. Shimizu, P. Sarkar and R. Gupta, Ind. Eng. Chem. Res. 2012, 51, 1438.
[2] Q. Wang, J. F. Bai, Z. Y. Lu, Y. Pan and X. Z. You, Chem. Commun., 2016, 52, 443.
[3] D. J. N. Subagyono, M. Marshall, G. P. Knowles, A. L. Chaffee, Microporous Mesoporous Mater., 2014, 186, 84.

Figure S1

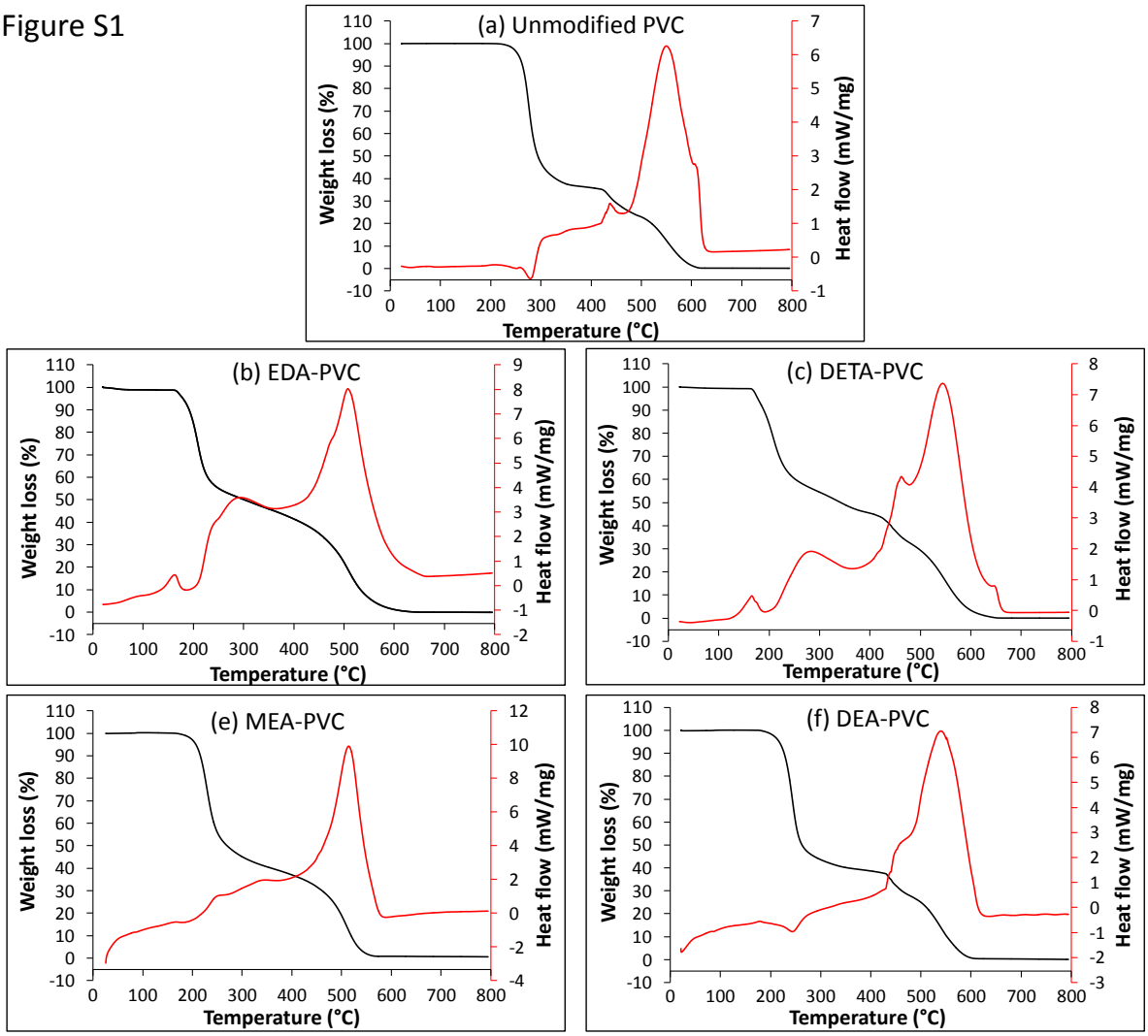

Figure S1. TGA (black, left scale) and DSC (red, right scale) for aminated PVC composites and untreated PVC prepared in this work showing high stability up to 140°C.

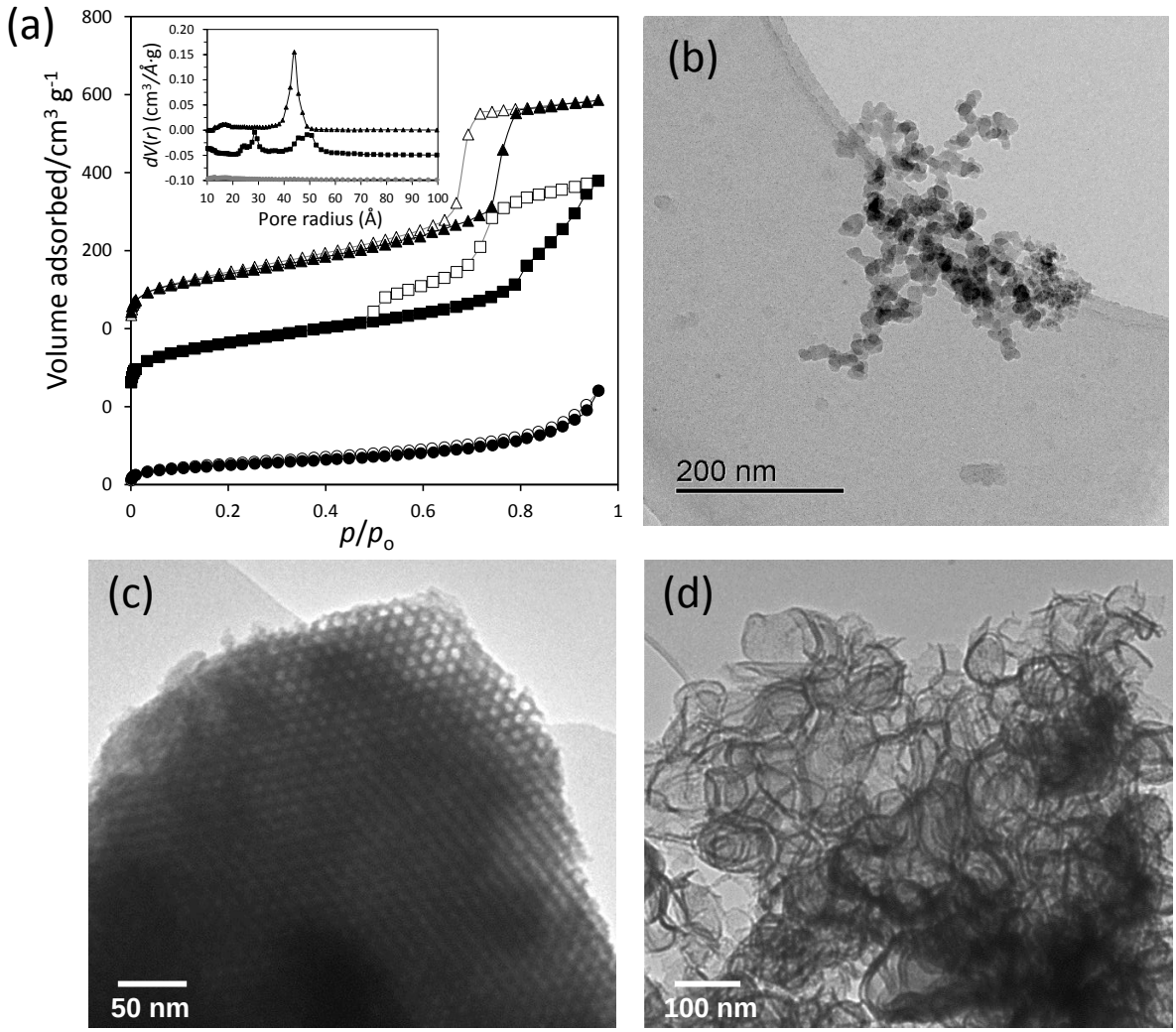

Figure S2. Surface characterisation of supports used in this work. (a) N_2 adsorption and desorption isotherms for fumed silica (circles, ●/○), SBA-15 (triangles, ▲/△) and MCF (squares, ■/□). Filled markers indicate the adsorption points while open markers are for desorption. Pore size distribution of all three samples is shown in inset. SBA-15 and MCF show distinct hysteresis loops that are consistent with results in the literature. (P. I. Ravikovitch and A. V. Neimark, *J. Phys. Chem. B*, 2001, **105**, 6817). TEM images for fumed silica (b), SBA-15 (c) and MCF (d). Fumed silica has a random structure of microsized particles while SBA-15 has a highly ordered 2D hexagonal array of pores of around 4 – 5 nm in diameter. MCF silica support has a "foam-like" structure.

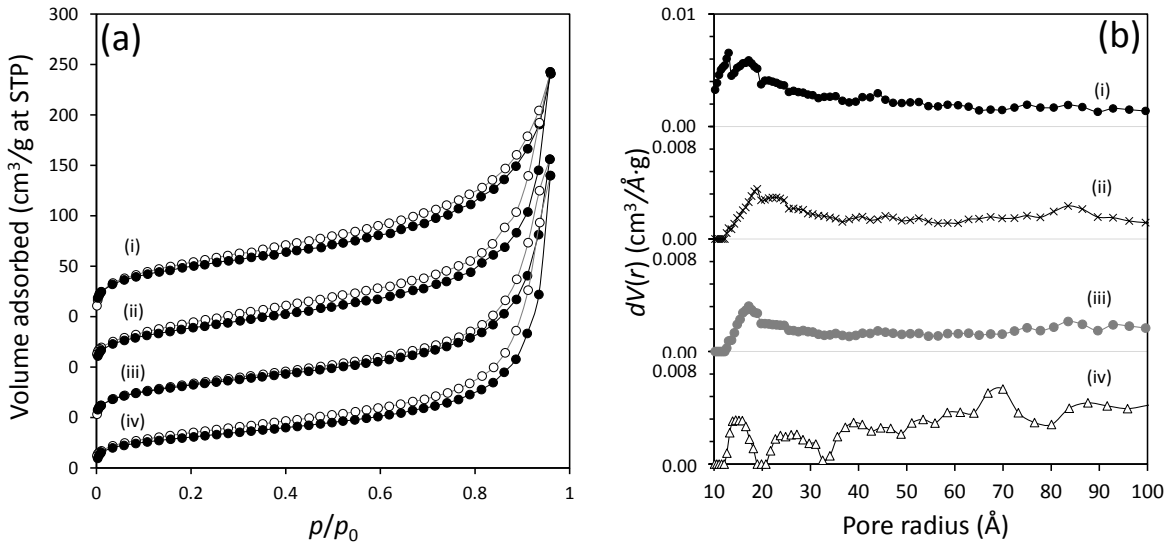

Figure S3. Control experiments for N_2 adsorption and desorption isotherms and PSD for EDA-PVC/ fumed silica composites. (i) for 0%, pure fumed silica, (ii) for 4%, (iii) 7% and (iv) for 19%. Both the isotherms and PSD graphs were off-set along the y-axis for clarity.

Adsorbent	BET surface area (m^2g^{-1})	Pore Volume (cm^3g^{-1})	Pore radius (nm)	CO_2 adsorption capacity (cm^3g^{-1})
Unsupported EDA-PVC	0	0	0	0.7
EDA-PVC/SBA-15(4%)	314	0.66	3.0	11.7
DETA-PVC/SBA-15(4%)	441	0.88	4.4	6.6
MEA-PVC/SBA-15(4%)	404	0.81	4.4	5.6
DEA-PVC/SBA-15(4%)	463	0.79	3.8	5.1

Table S2. Correlation between BET surface area, pore volume and mean pore size and CO_2 adsorption capacity for APVC-mesoporous silica composites.

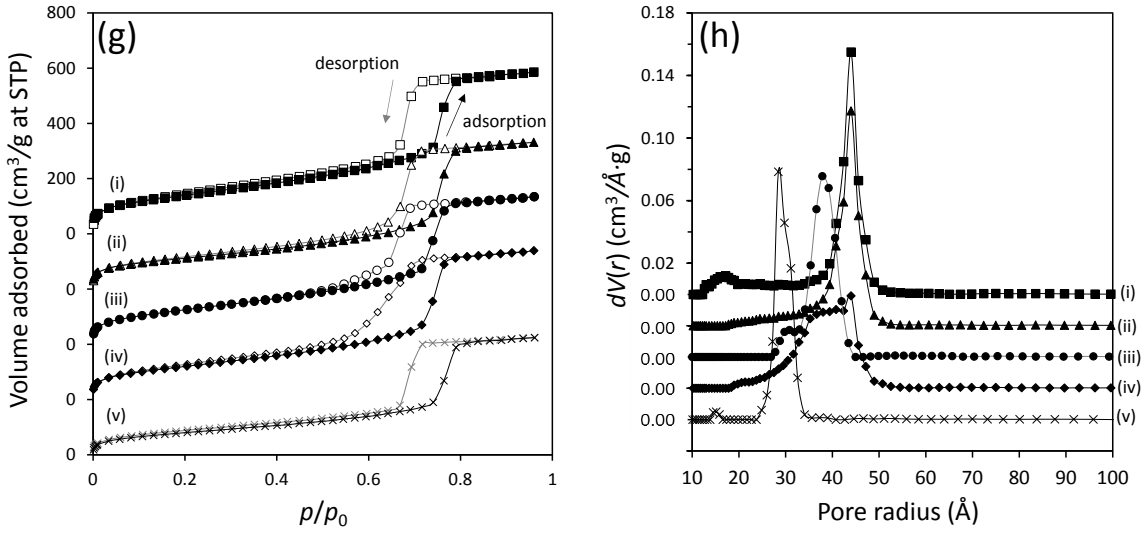

Figure S4. N_2 adsorption and desorption isotherms and PSD for EDA-PVC/ fumed silica composites. (i) for pure SBA-15 support, (ii) for 4% EDA-PVC, (iii) 4% MEA-PVC, (iv) for 4% DEA-PVC and (v) for 4% DETA-PVC. Both the isotherms and PSD curves were off-set along the y-axis for clarity.

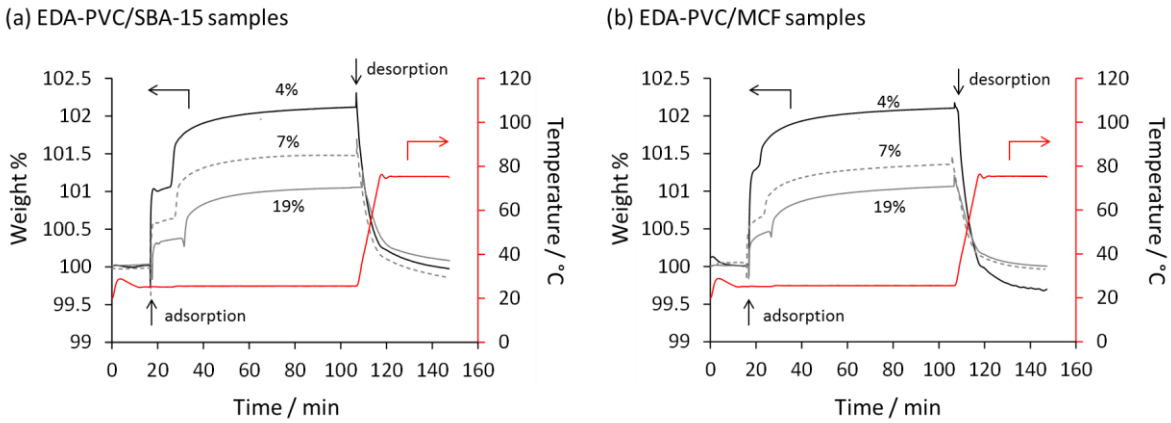

Figure S5. Kinetic profiles of CO_2 adsorption by (a) EDA-PVC/SBA-15 and (b) EDA-PVC/MCF samples. The red curves refer to the temperature profile (right scale).

Adsorbent	BET surface area (m^2g^{-1})	Pore Volume (cm^3g^{-1})	Pore radius (nm)
Pristine	333	0.71	3.0
Pestle / Mortar	335	0.72	3.0
Pellet	295	0.63	3.0
Hydrothermal	319	0.71	3.0

Table S3. Assessment of mechanical properties by gas sortion experiment for EDA-PVC/SBA-15(4%) composites subject to grinding with pestle and mortar for 5 minutes, pelletized to a 5 mm pellet under 1 ton and boiled for 1 hour in water. The slight difference from the pristine material characteristics quoted for analogue in the Table S2 is due to the fact that the experiments were carried out on different batches.

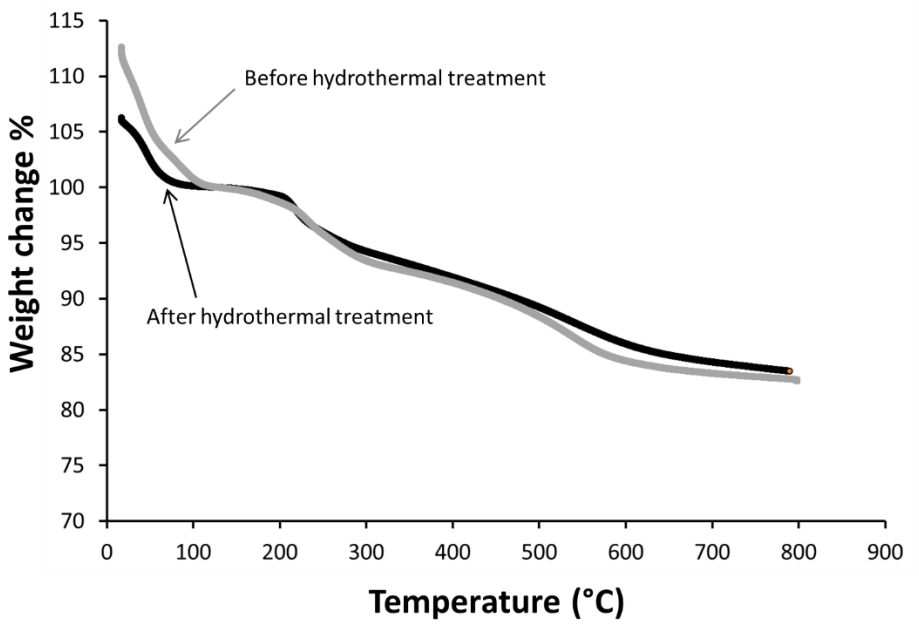

Figure S6. TGA curves for EDA-PVC/SBA-15 before and after hydrothermal treatment at 100°C.

CHAPTER 4

EDA-PVC on Hydrophobic Supports as New Adsorbents for CO_2

(Unpublished Results)

4.1 Background

The hydrophobic property of ethylenediamine (EDA) modified PVC has already been shown in Chapter 3. The potential importance of hydrophobocity within adsorbent materials was also discussed. As many conventional CO_2 adsorbents can be deactivated by water, an inevitable component of the flue gas stream, this study investigates the use of not only a hydrophobic polymer for deposition but also on hydrophobic supports. Carbon based materials have been examined in the literature for the process of CO_2 adsorption, including: activated carbons [4.1], carbon nanofibers [4.2], ordered mesoporous carbons [4.3] and carbon nanotubes [4.4]. Carbon nanotubes have been exstensively studied within the literature for the adsorption of CO_2 [4.4, 4.5] and can offer high adsorption capacities of up to 0.5 $mmolg^{-1}$. However, these materials are still expensive to produce on a large scale, although continuous production has been reported [4.6]. Ordered mesopoorus carbon, CMK-3, is synthesised by using an SBA-15 silica template, with the resulting material having an "inverse" porous structure to that of the SBA-15 template material (Figure 4.1). High CO_2 adsorption capacities of up to 2.4 $mmolg^{-1}$ have been reported for unmodified CMK-3 adsorbents [4.3]. Microporous activated carbon materials are the best candidates for CO_2 adsorption on an industrial scale. They can be produced on a large scale using various plant wastes at high temperature in the absence of oxygen, with high surface areas achieved [4.7]. A high CO_2 adsorption capacity of 2.92 $mmolg^{-1}$ can be achieved with activated carbon using a volumetric adsorption method. Amine groups were grafted to the activated carbon surface via microwave irradiation in a nitrogen atmosphere, this further increased the CO_2 adsorption capacity to 3.75 $mmolg^{-1}$ [4.8]. However, activation of the activated carbon surface prior to functionalisation requires the use of concentrated hydrofluoric acid, a highly corrosive and dangerous acid.

The use of a hydrophobic support with a hydrophobic polymer coating for adsorption should in theory further reduce the effect of water in the CO_2 adsorption process by limiting the presence of water at the adsorption sites. Several hydrophobic supports were chosen for comparison in this study, including activated carbons, carbon nanofibers, ordered mesopoorous carbon (CMK-3) and alkyl-modified SBA-15 silica. Activated carbons and carbon nanofibres are common materials actively in industry for water purification and decolorisation [4.9], their ready availability make them good candidates for testing as large scale CO_2 adsorbents. An increase in the hydrophobicity

of the SBA-15 support was attempted by grafting hydrophobic alkyl chains to the surface of the SBA-15 prior to deposition of EDA-PVC. Grafting of functional groups onto the surface of mesoporous silicas via silanisation is already a common method for introducing organic functionality to the silica surface [4.10]. Deposition of EDA-PVC into the mesopores of the hydrophobic SBA-15 support will allow for direct comparison to results shown in Chapter 3 for EDA-PVC/SBA-15 composite materials.

4.2 Methodology/Synthesis of Materials

Various EDA-PVC/hydrophobic support composites were prepared and tested as the CO_2 adsorbents in this chapter. The preparation procedure in general consists of 2 steps; preparation of support materials and EDA-PVC deposition. The adsorbent samples were characterised using thermogravimetric analysis/differential scanning calorimetry (TGA/DSC) and transmission electron microscopy (TEM), with some BET surface area measurements and hydrophobicity tests also performed.

4.2.1 Synthesis and Characterisation of Hydrophobic CMK-3 by Templation with SBA-15

SBA-15 was used as a template in the synthesis of CMK-3 mesoporous carbon support material [4.11, 4.12]. Synthesis of SBA-15 template material was carried out as previously outlined in Section 2.2.1. In general, the long mesopores of the SBA-15 were impregnated with carbon using sucrose as the carbon source, before removal of the silica template to leave a hexagonally ordered carbon mesostructure, as illustrated in Figure 4.1.

In a standard synthesis procedure, SBA-15 (0.25 g) was weighed into a glass crucible, and to this was added a solution containing sucrose (0.3 g), sulfuric acid (0.04 g) and water (1.25 g) then mixed thoroughly. The resulting slurry mixture was heated in a furnace set to 373K and the reaction allowed to proceed for 6 hours. After 6 hours the reaction mixture was heated to 433 K and kept at this temperature for a further 6 hours. A second impregnation step was performed, by mixing the now black slurry with a solution containing sucrose (0.2 g), sulfuric acid (0.02 g) and water (0.75 g). The

heating regime was then repeated with an initial 6 hours at 373K then a further 6 hours at 433 K. To complete carbonisation, the sample was heated from 273 K to 1073 K at a rate of 1 °C/min with a nitrogen flow rate of 60 mL/min. Once the final temperature of 1073 K was reached, the material was held isothermal for 12 hours.

Dissolution of the silica template was performed by sonicating the material in 1M NaOH (20 mL) at 60 °C overnight (ca. 16 hours). The carbon solid was then filtered using a Buchner flask and funnel and the residue washed with water (50 mL) three times. The final CMK-3 product was dried at 393 K overnight (ca. 16 hours) before use in deposition experiments.

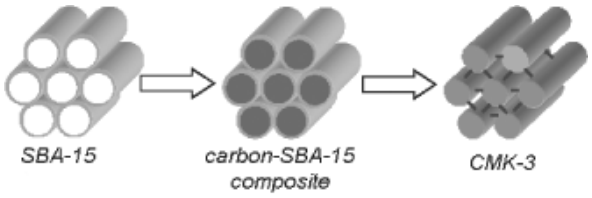

Figure 4.1 Schematic view of CMK-3 synthesis showing initial deposition of carbon into the long pores of SBA-15 followed by removal of the SBA-15 template [4.13].

4.2.2 Synthesis of Hydrophobic SBA-15 Through Silane Functionalisation

SBA-15 was functionalised using the hydrophobic silane material, n-propyltriethoxysilane. Introduction of hydrophobic moieties into the SBA-15 structure should increase selectivity of the NH_2 on PVC for CO_2 over water by excluding water from the structure. In a typical synthesis procedure, SBA-15 (1.0g) was suspended in toluene (100 mL) and allowed to stir at ambient temperature for *ca.* 16 hours. After 16 hours n-propyltriethoxysilane was then added dropwise to the suspension, the temperature raised to 112 °C to allow for reflux for 24 hours. The functionalised material was filtered using a Buchner flask and funnel and washed 4 times with acetone (150 mL). The washed material was dried in the vacuum oven at 100 °C for 24 hours before characterisation by TGA and surface area analysis. The final functionalised support was referred to as SBA-15-C3, where C3 indicates the propyl functional group.

4.2.3 Deposition of Aminated PVC (EDA-PVC) onto Hydrophobic Supports

EDA functionalised PVC was deposited onto activated carbon, carbon nanofibres, n-propyltriethoxysilane functionalised SBA-15 and CMK-3 hydrophobic supports. The same procedure was used as per that of Section 3.2.2 for deposition. EDA-PVC was deposited on each support using 1.0g of support and 0.04 g of EDA-PVC to give an EDA-PVC content of 4 %. EDA-PVC was additionally deposited onto CMK-3 and activated carbon supports at a 2 % loading to investigate the impact of lower loading on CO_2 adsorption capacity.

4.2.4 Adsorbent Samples Characterisations and Measuring of CO_2 Adsorption Capacities

Support materials were characterised by TEM using a Tecnai T20 microscope (200 keV), to study the porous structure at a nanoscale and ensure uniformity. TEM analysis was carried out by Colin How, University of Glasgow physics department. Samples were also analysed using contact angle experiments to determine hydrophobicity of support and composite materials. Contact angle experiments were carried out by Dr Cem Bayram, Hacettepe University, Ankara, Turkey. CMK-3 support material was additionally analysed by N_2 adsorption/desorption isotherms using a Quantachrome Quadrasorb surface area analyser to determine surface area and pore volume. BET analysis was carried out by Jessica McGlynn, University of Glasgow chemistry department. The activated carbon support material and the EDA-PVC/CMK-3 composite material was analysed by TGA/DSC using a TA Instruments SDT Q600 TGA/DSC to confirm the oxidative decomposition of the supported EDA-PVC and the support itself. A gravimetric method of CO_2 adsorption was carried out using the TGA/DSC with a cyclic customised programme as outlined in Section 2.2.4. A gas mixture with a CO_2:N_2 ratio of 50:50 v/v was utilised for all gravimetric CO_2 adsorption experiments in this chapter.

4.4 Results and Discussion

4.4.1 Physical Characterisation of Adsorbent Supports and Composites

The porous structure of hydrophobic support materials were initially examined using TEM and the resulting images are presented in Figure 4.1. The microporous structure of the activated carbon support is highlighted in Figure 4.1(a). This microporous material has already been shown to have a high CO_2 adsorption capacity [4.5], although not selective to CO_2 without modification. A single nanofibre of carbon is shown in Figure 4.1(b), this fibre has an ultralarge mesoporous tube structure with a pore width of *ca.* 40 nm. The mesoporous structure of CMK-3 is displayed in Figure 4.1(c). The inverse structure of SBA-15 is highlighted in this image with long pores of CMK-3 of radius *ca.* 8 nm based on pore volume data in Chapter 2, based on previous experiments with mesoporous silica materials, a mesoporous structure should provide a suitable support for EDA-PVC.

Analysis of CMK-3 support material using N_2 adsorption/desorption isotherm measurements yielded a type IV isotherm as shown in Figure 4.2, with a hysteresis loop upon desorption of N_2. Calculation of the BET surface area revealed a high surface area of 1250 m^2g^{-1} for the CMK-3 support material and a large pore volume of 1.04 cm^3g^{-1}.

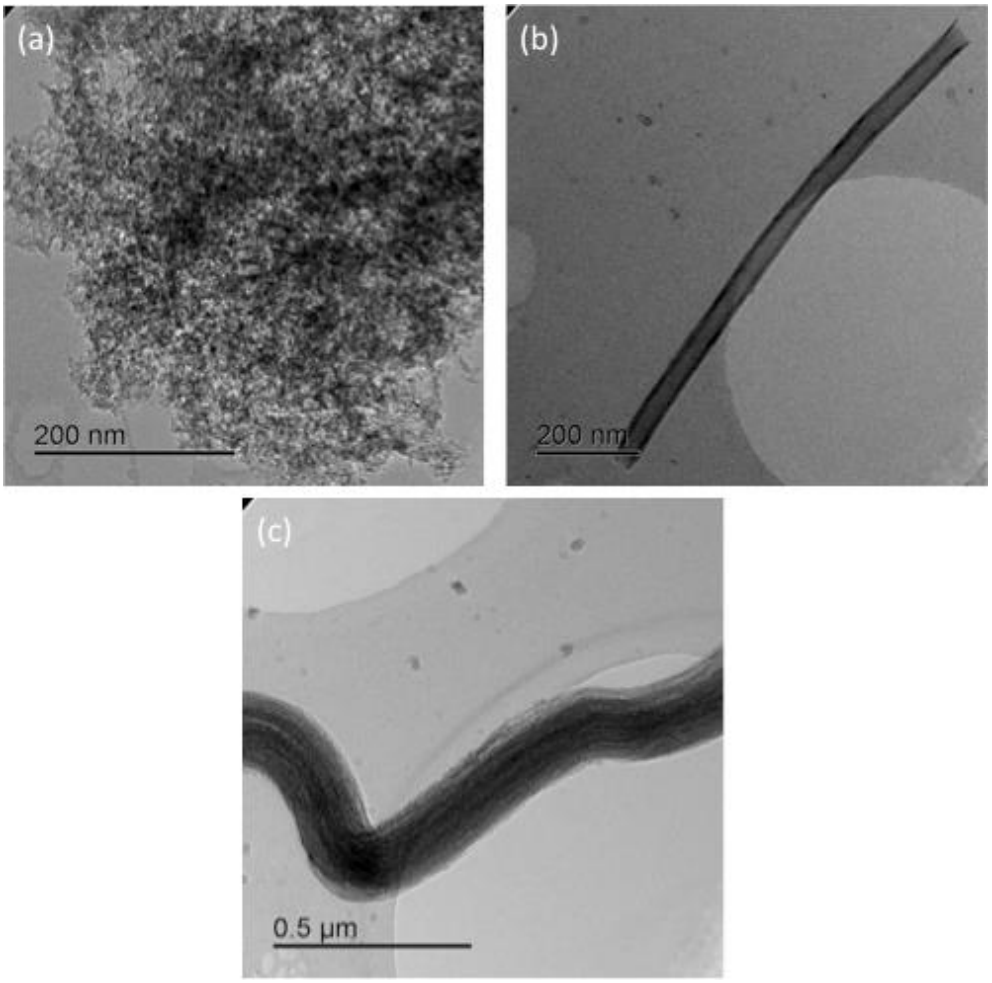

Figure 4.1 TEM images of hydrophobic support materials (a) microporous structure activated carbon (b) mesoporous structure of carbon nanofibre (c) CMK-3 carbon mesoporous structure.

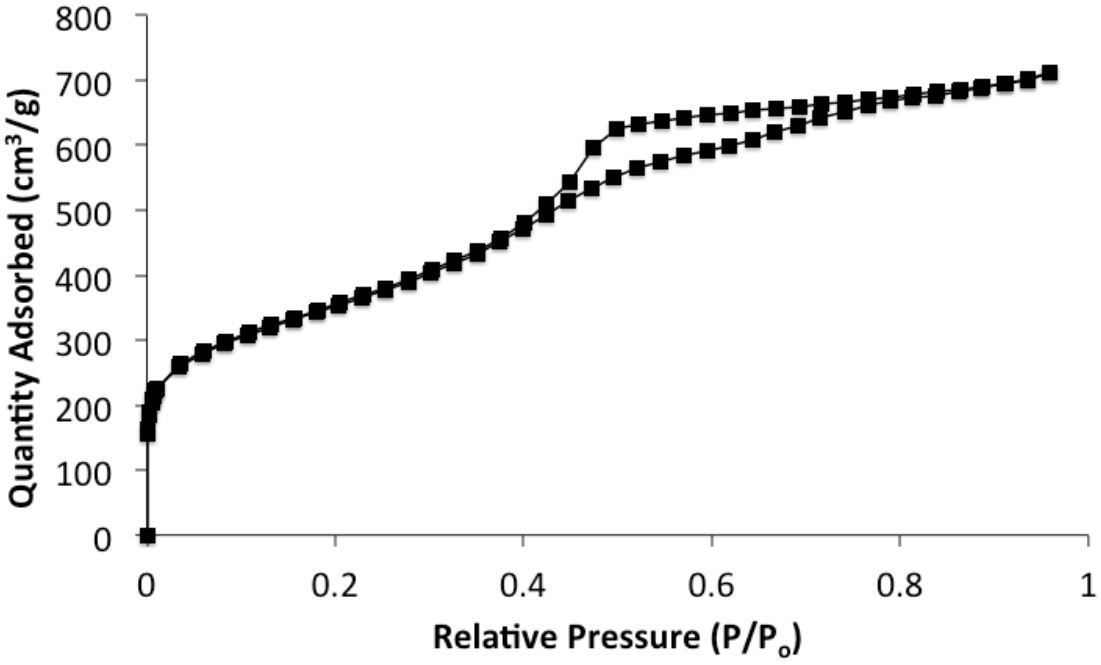

Figure 4.2 N_2 adsorption isotherm of CMK-3 hydrophobic support material. A hysteresis loop is observed between a relative pressure of 0.8 and 0.4 during the desorption isotherm.

Analysis of CMK-3 support material by TGA/DSC after removal of the SBA-15 template is shown in Figure 4.3. Complete oxidative decomposition is not observed with *ca.* 7.5 wt% remaining after heating to 800 °C in an air atmosphere. This is likely due to incomplete removal of the SBA-15 template material.

Thermogravimetric analysis of the EDA-PVC/activated carbon (4 %) composite material by TGA/DSC (Figure 4.4) indicated complete oxidative decomposition of the supported polymer and hydrophobic support. An initial mass loss was observed up to 200 °C due to loss of unbound solvent or organic residues, with oxidative decomposition starting after 200 °C. Complete decomposition of the composite material was observed by *ca.* 650 °C.

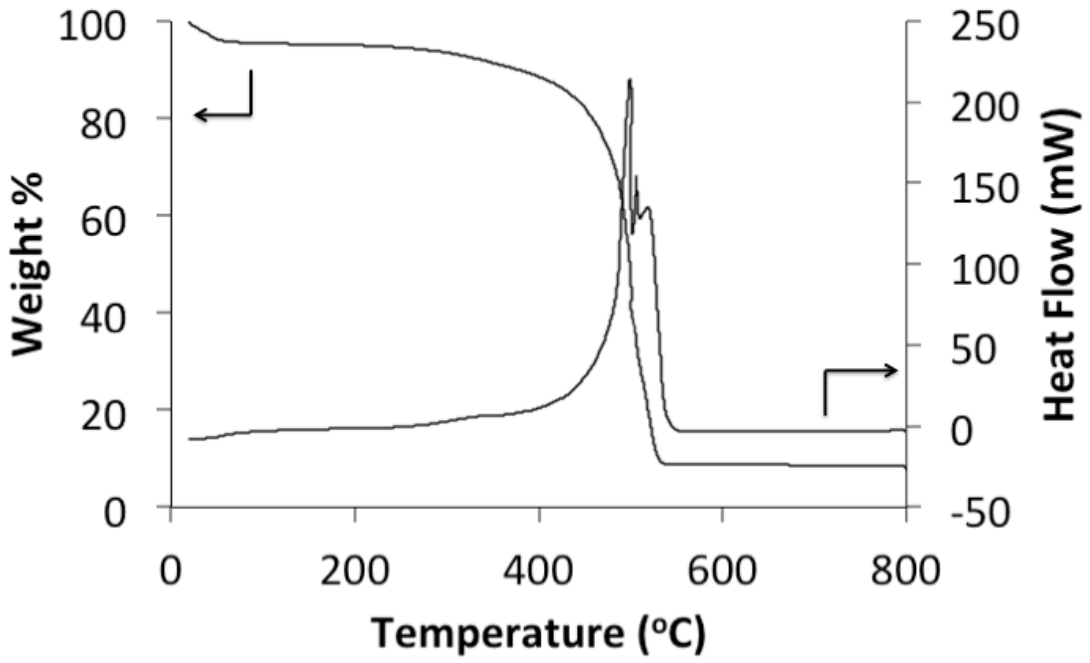

Figure 4.3 TGA/DSC analysis of CMK-3 support material after removal of the SBA-15 template, indicating the incomplete oxidative decomposition at 800 °C.

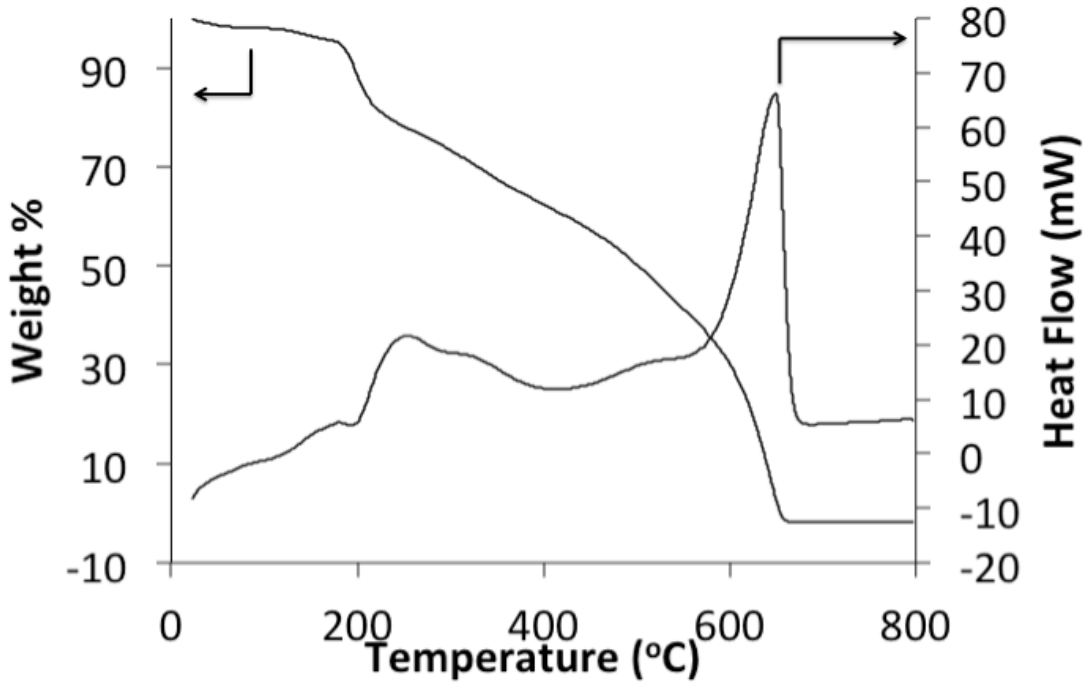

Figure 4.4 TGA/DSC analysis of EDA-PVC/activated carbon (4 %) composite material indicating the complete oxidative decomposition of the composite material

4.4.2 Hydrophobicity Measurements of Adsorbent Supports and Composites

The contact angle for selected support materials as well as the EDA-PVC deposited samples were measured, Figure 4.5. As previously reported in Chapter 3, EDA-PVC is hydrophobic with a contact angle of 76.7 ° measured, Figure 4.5(a). Unfortunately measurements could not be made on activated carbon, carbon nanofibre and CMK-3 support materials, as suitable disks could not be pressed to allow for measurements to be made. The SBA-15-C3 support material was observed to not be hydrophobic at all, with no contact angle observed. Deposition of 4 % EDA-PVC onto the SBA-15-C3 support resulted in an increase in hydrophobicity of the surface with a contact angle of 55.9 ° measured for the composite material, Figure 4.5 (b). For the EDA-PVC/activated carbon (4 %) composite material a contact angle of 44.2 ° was measured, Figure 4.5(c). This is an enhancement in hydrophobicity when compared to the EDA-PVC/SBA-15 (4%) composite from Chapter 3, with a measured contact angle of 35.6 °. These results highlight the ability of EDA-PVC to increase the hydrophobicity of a support material through deposition of only a small amount of EDA-PVC.

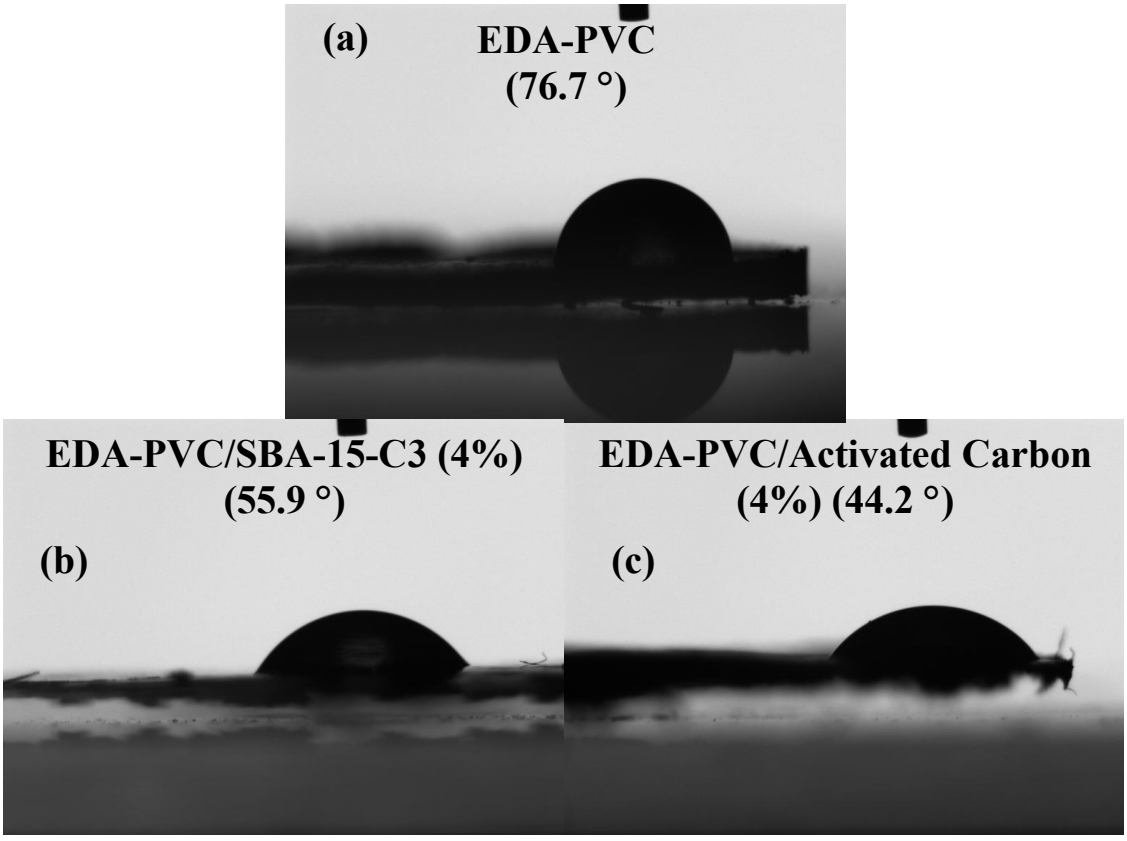

Figure 4.5 Contact angle experiments of unsuppported EDA-PVC, EDA-PVC/activated carbon (4%) composite material and EDA-PVC/SBA-15-C3 composite material.

4.4.3 Gravimetric CO_2 Adsorption of Hydrophobic Composite Materials

Cyclic gravimetric CO_2 adsorption experiments were carried out on EDA-PVC/CMK-3 (4%) composite material and the results shown in Figure 4.6. This material was observed to exhibit a CO_2 adsorption capacity of 0.56 $mmolg^{-1}$, 0.51 $mmolg^{-1}$ and 0.54 $mmolg^{-1}$ during the first, second and third adsorption cycles respectively. This represents an average CO_2 adsorption capacity of 0.54 $mmolg^{-1}$ for this EDA-PVC/CMK-3 (4%) composite material. The adsorption capacity would be expected to lower between cycles as some adsorption sites would not be completely vacated on the desorption timescale of 30 minutes. However, the variation in CO_2 capacity between these cycles can be considered to be within experimental error for these experiments. Regardless, the CO_2 adsorption capacity does not appear to lower substantially between cycles for the EDA-PVC/CMK-3 (4 %) composite material, indicating it is highly regenerable at the low temperature of 75 °C.

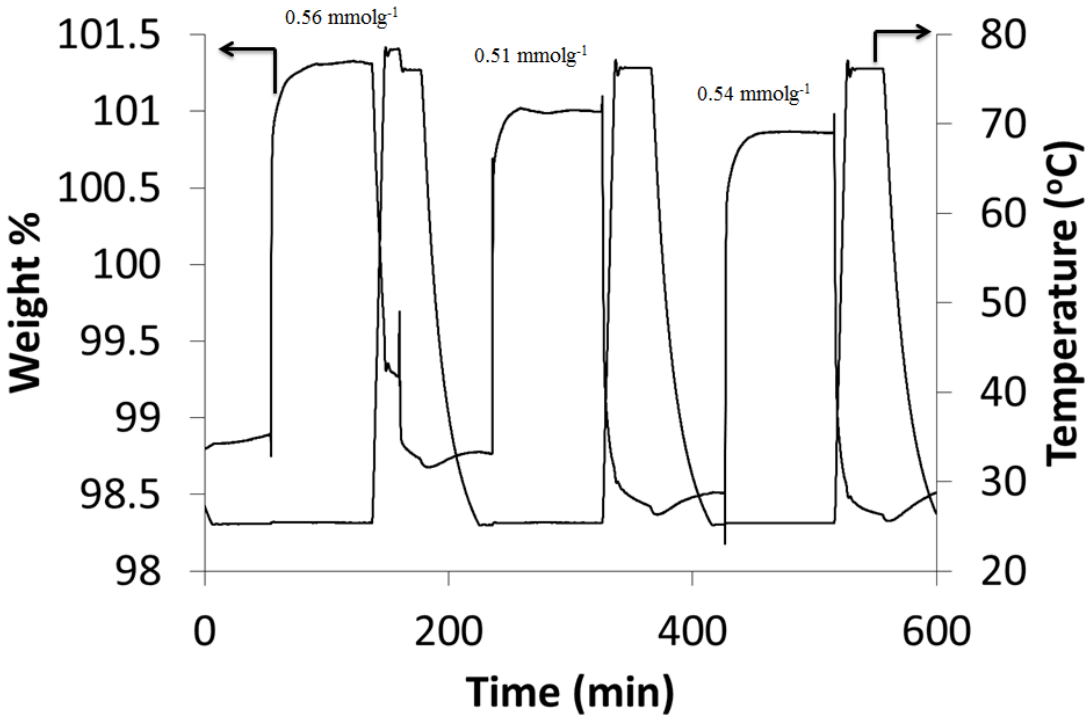

Figure 4.6 Gravimetric CO_2 adsorption of EDA-PVC/CMK-3 (4 %) using 50:50 v/v CO_2:N_2. Three adsorption cycles are shown with an initial adsorption capacity of 0.56 $mmolg^{-1}$.

Gravimetric CO_2 adsorption was carried out on EDA-PVC/activated carbon (4 %) composite material using 50:50 v/v CO_2:N_2 and the results depicted in Figure 4.7.

One adsorption cycle was performed and an adsorption capacity of 0.74 $mmolg^{-1}$ measured for the activated carbon composite material. Such a high CO_2 adsorption capacity is not an unexpected result for this material, as the suitability of microporous supports for deposition of EDA-PVC has already been demonstrated in Chapter 3, when using SBA-15 and MCF-3 mesoporous silica supports.

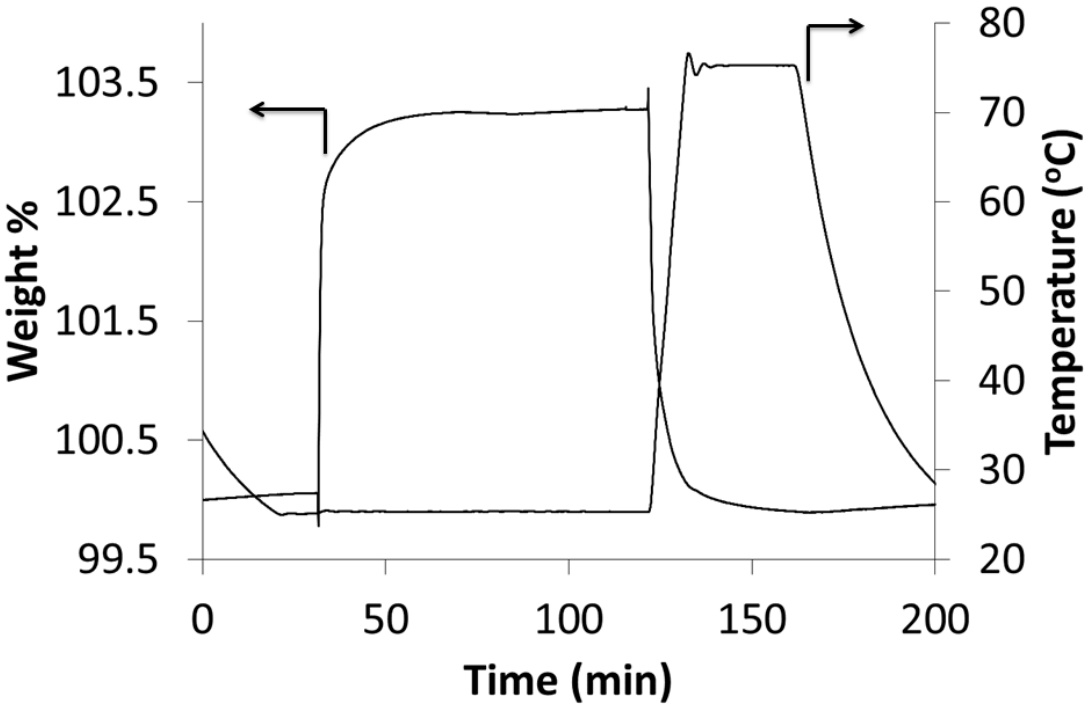

Figure 4.7 Gravimetric CO_2 adsorption of EDA-PVC/activated carbon (4 %) using 50:50 v/v CO_2:N_2. One adsorption cycle is shown with an adsorption capacity of 0.74 $mmolg^{-1}$.

The EDA-PVC/carbon nanofibre (4%) composite material exhibited no apparent CO_2 adsorption when analysed using a gravimetric method. The low surface area of the support material, of 54 m^2g^{-1} (measured by supplier), can account for this apparent lack of CO_2 adsorption. In order to see large CO_2 adsorption capacities, both a suitable pore structure and a high surface area for adsorption are required. This data suggests that large mesoporous materials, such as carbon nanofibres, may not be suitable for deposition of EDA-PVC, or indeed any solid state adsorbent that requires deposition to increase the availability of CO_2 adsorbing groups.

CO_2 adsorption analysis of EDA-PVC/SBA-15-C3 (4 %) composite material indicated an adsorption capacity of 0.14 $mmolg^{-1}$. This value is lower than that observed for the EDA-PVC/SBA-15 (4 %) composite material measured in Chapter 3 of 0.48 $mmolg^{-1}$. This suggests that functionalisation of the silica has led to a decrease in the CO_2 adsorption capacity. When comparing EDA-PVC/SBA-15 (4%) from Chapter 3 and EDA-PVC/SBA-15-C3 (4%) composite materials synthesised in this chapter, the CO_2 adsorption capacity is higher for the less hydrophobic composite material from Chapter 3. The EDA-PVC/SBA-15 (4%) composite material exhibited a contact angle 35.6 ° and had a CO_2 adsorption capacity of 0.48 $mmolg^{-1}$. Whereas, the EDA-PVC/SBA-15-C3 (4%) composite material exhibited a contact angle of 55.9 ° and a CO_2 adsorption capacity of 0.14 $mmolg^{-1}$. An increase in surface hydrophobicity has been achieved for the EDA-PVC/SBA-15-C3 composite material through grafting of alkyl chains to the surface but a decrease in CO_2 adsorption capacity also observed. This is likely due to blockage of the SBA-15 cylindrical pores upon silanisation rather than attributed to any change in the surface hydrophobicity. By grafting the alkyl chains to the surface of the SBA-15 a reduction in pore size is also observed. This may make deposition of EDA-PVC into the pore network more difficult, resulting in more pore blockage and a lowering of the CO_2 adsorption capacity.

Comparison of EDA-PVC/activated carbon (4%) and EDA-PVC/CMK-3 (4%) composite materials suggested the activated carbon composite to be the most suitable for CO_2 adsorption. Both materials have a high surface area, suggesting the results are likely attributed to the differences in pore structure of the support materials. Both materials exhibit an interconnected pore structure, with activated carbon having an interconnected microporous structure and CMK-3 an interconnected mesoporous structure. From the results presented in Chapters 2 and 3, it is evident that mesoporous pore networks are suitable for deposition of aminated polymer to boost selective CO_2 adsorption. Unsurprisingly, the interconnected mesopores of CMK-3 have proven suitable for deposition of EDA-PVC with a high CO_2 adsorption capacity of 0.56 $mmolg^{-1}$ measured. However, the high adsorption capacity of 0.74 $mmolg^{-1}$ obtained for the EDA-PVC/activated carbon composite material however, suggests that a microporous pore structure is more suitable for deposition of EDA-PVC for the hydrophobic adsorption of CO_2.

CO_2 adsorption capacity measurements were also performed on EDA-PVC/CMK-3 (2%) composite material and the results shown in Figure 4.8. Upon reducing the EDA-PVC content of the composite material to 2%, an increase in CO_2 adsorption capacity of 0.68 $mmolg^{-1}$ is observed, compared to 0.56 $mmolg^{-1}$ for the composite material containing 4% EDA-PVC. This is likely due to less pore blockage of the CMK-3 support material upon deposition of a lower amount of EDA-PVC polymer. This allows for a more even distribution of EDA-PVC throughout the pore structure, leading to a higher availability of surface NH_2 groups, thus an increase in CO_2 adsorption capacity. CO_2 adsorption measurements were also performed on EDA-PVC/activated carbon (2%) composite material, Figure 4.9. Contrasting the results from EDA-PVC/CMK-3 (2%), a decrease in CO_2 adsorption capacity was observed with EDA-PVC/activated carbon (2%), with a CO_2 adsorption capacity of 0.68 $mmolg^{-1}$ measured for the composite material. Deposition of only 2% EDA-PVC limits the number of available amine sites for adsorption of CO_2 leading to a decrease in CO_2 adsorption capacity.

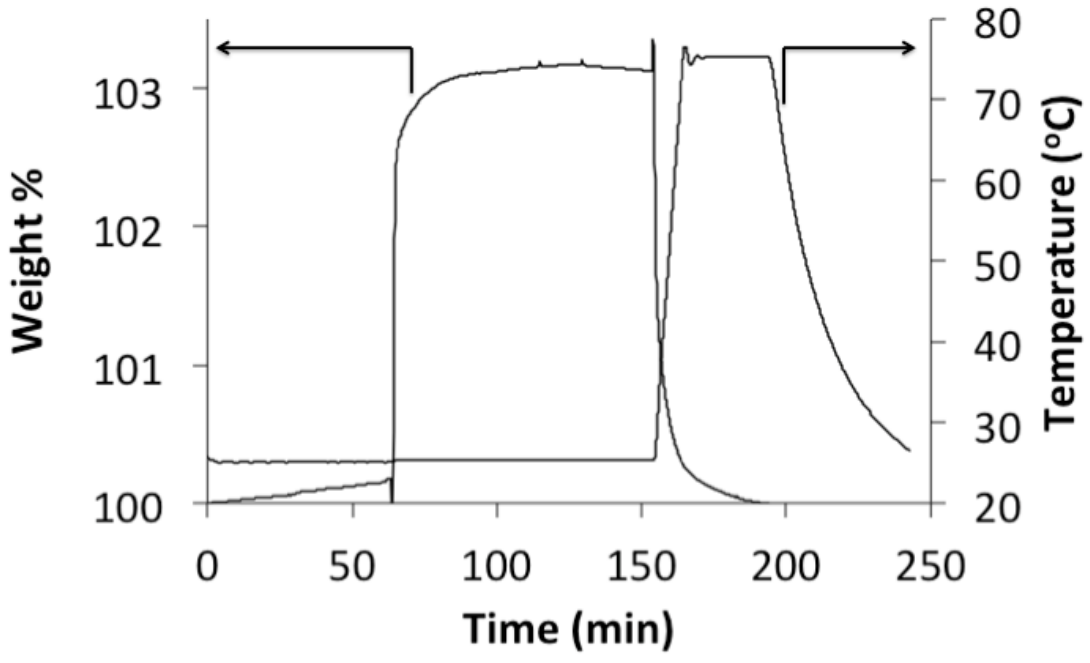

Figure 4.8 Gravimetric CO_2 adsorption of EDA-PVC/CMK-3 (2 %) using 50:50 v/v CO_2:N_2. One adsorption cycle is shown with an adsorption capacity of 0.68 $mmolg^{-1}$.

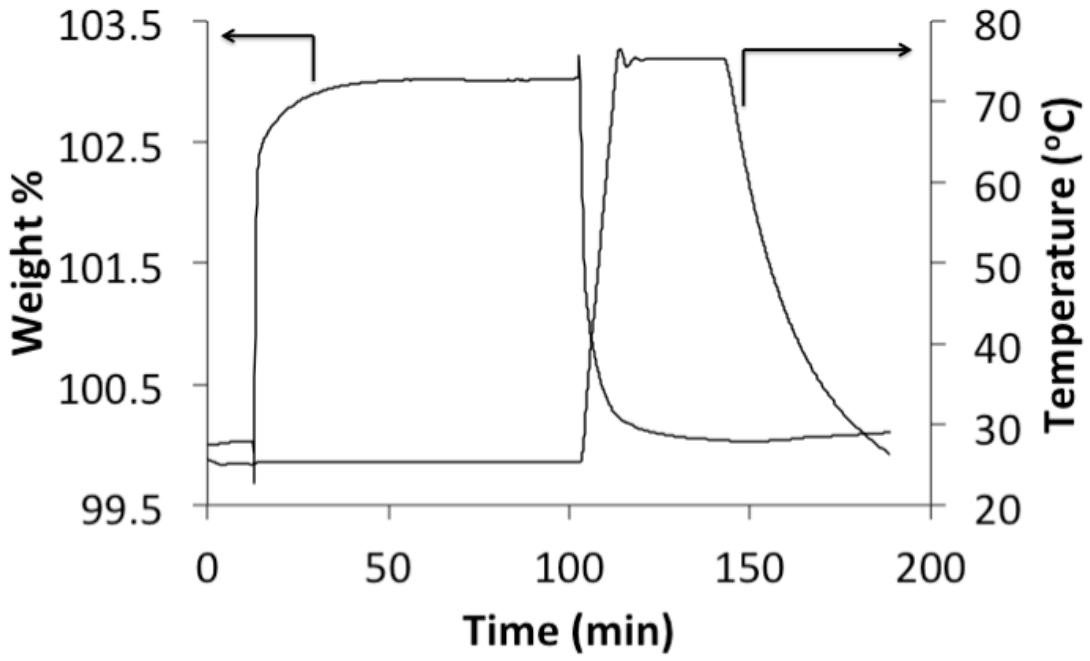

Figure 4.9 Gravimetric CO_2 adsorption of EDA-PVC/activated carbon (2 %) using 50:50 v/v CO_2:N_2. One adsorption cycle is shown with an adsorption capacity of 0.68 $mmolg^{-1}$.

4.5 Conclusion

A series of hydrophobic composite materials were synthesised using both hydrophobic supports and hydrophobic EDA-PVC polymer for deposition. An improvement in hydrophobicity was observed after functionalization, when comparing the EDA-PVC/SBA-15 (4%) composite material from chapter 3 with the EDA-PVC/SBA-15-C3 (4%) composite material. However, this improvement in hydrophobicity of the composite material did not lead to an increase in the CO_2 adsorption capacity but a decrease. This was attributed to a reduction in the pore diameter, as a result of functionalization of the SBA-15 surface with n-propyl chains, making impregnation of the pores with EDA-PVC more difficult. The EDA-PVC/carbon nanofibre composite material did not show any CO_2 adsorption during gravimetric CO_2 adsorption experiments. This was determined to be due to the low surface area and the ultralarge mesoporous structure being unsuitable for deposition of EDA-PVC. Both activated carbon and CMK-3 hydrophobic supports were determined to be suitable supports for EDA-PVC deposition, for selective CO_2 adsorption. CO_2 adsorption capacities of 0.56 $mmolg^{-1}$ and 0.68 $mmolg^{-1}$ were recorded for loadings of 4% and 2% of EDA-PVC.

Loading of only 2% EDA-PVC results in less pore blockage when compared to a 4% loading of EDA-PVC, allowing for greater availability of surface amine groups. The microporous pore structure of activated carbon was determined to be the best hydrophobic support for deposition of EDA-PVC in this study. Loadings of 4% and 2% EDA-PVC provided CO_2 adsorption capacities of 0.74 $mmolg^{-1}$ and 0.68 $mmolg^{-1}$ respectively. A lowering of the CO_2 adsorption capacity upon deposition of 2% EDA-PVC compared to the increase in capacity observed for EDA-PVC/CMK-3 (2%), suggests a complex relationship between pore structure and EDA-PVC deposition ratios.

This research could be further improved by examining the surface basicity of the composite materials. Using a titration method, the availability of surface amines can be determined, providing useful information about the selectivity of the adsorbent materials towards acidic groups such as CO_2. Different mesoporous carbon materials could also be studied, such as CMK-1 using a MCM-48 template or CMK-8 using a KIT-6 template, to investigate the effect of pore structure on hydrophobicity and CO_2 adsorption capacity.

4.6 References

[4.1] A. S. Ello, L. K. C. de Souza, A. Trokourey, M. Jaroniec, *Coconut shell-based microporous carbons for CO2 capture,* Microporous Mesoporous Mater., **180**, 280-283 (2013)

[4.2] N. N. A. H. Meis, A. M. Frey, J. H. Bitter, K. P. de Jong, *Carbon Nanofiber-Supported K2CO3 as an Efficient Low-Temperature Regenerable CO2 Sorbent for Post-Combustion Capture,* Ind. Eng. Chem. Res., **52**, 12812-12818 (2013)

[4.3] M. Sevilla, A. B. Fuertes, *CO_2 adsorption by activated templated carbons,* J. Colloid Interface Sci., **366**, 147-154 (2012)

[4.4] S-H. Hsu, C. Lu, F. Su, W. Zeng, W. Chen, *Thermodynamics and regeneration studies of CO_2 adsorption on multiwalled carbon nanotubes,* Chem. Eng. Sci., **65**, 1354-1361 (2010)

[4.5] C. Lu, H. Bai, B. Wu, F. Su, J. Fen-Hwang, *Comparative study of CO_2 capture by carbon nanotubes, activated carbons, and zeolites,* Energy Fuels, **22**, 3050-3056 (2008)

[4.6] L. S. Ying, M. A. B. Salleh, H. B. M. Yusoff, S. B. A. Rashid, J. B. Abd Razak, *Continuous production of carbon nanotubes – A review*, J. Ind. Eng. Chem., **17**, 367-376 (2011)

[4.7] F. Stoeckli, T. A. Centeno, *On the determination of surface areas in activated carbons*, Carbon, **43**, 1184-1190 (2005)

[4.8] Z. Zhang, M. Xu, H. Wang, Z. Li, *Enhancement of CO_2 adsorption on high surface area activated carbon modified by N-2, H-2 and ammonia,* Chem. Eng. J., **160,** 571-577 (2010)

[4.9] G. Mezohegyi, F. P. van der Zee, J. Font, A. Fortuny, A. Fabregat, *Towards advanced aqueous dye removal processes: A short review on the versatile role of activated carbon*, J. Environ. Management, **102**, 148-164 (2012)

[4.10] K. Moller, T. Bein, *Inclusion Chemistry in Periodic Mesoporous Hosts*, Chem. Mater., **10**, 2950-2963 (1998)

[4.11] S. Jun, S. H. Joo, R. Ryoo, M. Kruk, M. Jaroniec, Z. Liu, T. Ohsuna, O. Terasaki, *Synthesis of new, nanoporous carbon with hexagonally ordered mesostructure,* J. Am. Chem. Soc., **122**, 10712-10713 (2000)

[4.12] P. Michorczyk, P. Kuśtrowski, P. Niebrzydowska, A. Wach, *Catalytic performance of sucrose-derived CMK-3 in oxidative dehydrogenation of propane to propene*, Appl. Catal., A-General, **445**, 321-328 (2012)

[4.13] E. C. de Oliveira, C. T. V. M. T. Pires, H. O. Pastore, *Why are carbon molecular sieves interesting?*, J. Braz. Chem. Soc., **17**, 16-29 (2006)

CHAPTER 5: CONCLUSIONS AND FUTURE WORK

5.1 Conclusion

The overall aim of this thesis was to develop adsorbent materials from sustainable sources for the purpose of CO_2 adsorption from the flue gas stream. This approach has utilised the waste polymers chitosan and polyvinylchloride (PVC) for CO_2 adsorption, with modification of the PVC polymer required before use in the application of carbon capture.

Parameters required for the ideal CO_2 adsorbent were explored in Chapter 1, along with the current state-of-the-art methods employed for carbon capture, storage and utilisation. The literature suggested that surface area and pore volume/structure of the adsorbent material play a key role when considering a material for CO_2 adsorption. Selectivity for CO_2 molecules is also an important consideration to avoid adsorption of unwanted species from the flue gas. This can be achieved by either tailoring the pore structure to be selective to CO_2 by size exclusion, or by introducing CO_2 selectivity through basic surfaces with amine groups.

A waste polymer, chitosan was successfully used for CO_2 adsorption through deposition on mesoporous silica supports. Chitosan is suitable for CO_2 adsorption without chemical modification as it naturally contains amine functionality without chemical modification. However, chitosan has a low surface area, limiting the CO_2 adsorption capacity to 0.02 $mmolg^{-1}$ without any modification of the chitosan material. A variety of mesoporous silica supports and deposition ratios were investigated, to determine the ideal chitosan/silica support ratio. Deposition of 19 wt% chitosan into the interconnected mesoporous structure of MCF-3 was determined to be the best support and deposition ratio, with a volumetric CO_2 adsorption of 0.98 $mmolg^{-1}$ and a gravimetric CO_2 adsorption of 0.34 $mmolg^{-1}$. Furthermore, CO_2 adsorption experiments utilising chitosan/fumed silica (19%) composite material indicated an adsorption capacity of 0.47 $mmolg^{-1}_{chitosan}$ when considering only the chitosan content of the composite material. Since the fumed silica support indicated no uptake of CO_2 during experiments conducted on the support alone, this is a fair comparison to make. The

chitosan/MCF-3 (19%) composite was also shown to be highly regenerable at a low temperature 75°C, with a retention of 85% of the capacity after 4 regeneration cycles. However, chemical modification of chitosan can be difficult due to limitations in available solvents for dissolution, with dilute acetic acid solutions commonly used to achieve full dissolution of chitosan. Therefore, modification of chitosan is most likely to be achieved through heterogeneous reactions. Unfortunately, heterogeneous reactions proceed at a lower reaction rate when compared to homogeneous reactions, resulting in long reactions times necessary to achieve functionalisation of chitosan. Furthermore, any modifications in a heterogeneous reaction would be limited to surface available groups only. The low surface area of chitosan means only a low percentage of potential modification sites can be reached.

Polyvinylchloride (PVC) was investigated for CO_2 adsorption after chemical modification to introduce amine functionality into the polymer backbone. The primary amine used for modification of PVC was ethylenediamine (EDA), although other amines such as diethylenetriamine (DETA), monoethanolamine (MEA) and diethanolamine (DEA) were also investigated. As with chitosan experiments, a variety of mesoporous silica supports were investigated, to identify the most suitable support for EDA-PVC/mesoporous silica composite materials. Among the composite materials studied EDA-PVC/SBA-15 (4%) was determined to be the best adsorbent, with a high surface area, pore volume and CO_2 adsorption capacity recorded of 0.48 $mmolg^{-1}$. Of the other amines studied in addition to EDA for functionalisation of PVC, none were able to make EDA-PVC in terms of CO_2 adsorption capacity. The use of hydrophobic EDA-PVC polymer also introduced a greater hydrophobicity to the composite material when compared to the SBA-15 support alone. Hydrophobicity of adsorbent materials for CO_2 adsorption is an important and welcoming property, as deactivation of adsorbent materials by water, an inevitable component of the flue gas stream, is a commonly observed phenomenon. The enhanced hydrophobicity of the produced EDA-PVC/mesoporous silica composite materials presents a distinct advantage, by reducing the interaction of water at the adsorption sites on the adsorbent surface.

To further enhance the hydrophobicity of the composite materials, a series of EDA-PVC/hydrophobic support materials were investigated for CO_2 adsorption.

Introduction of a hydrophobic support as well as hydrophobic EDA-PVC polymer will reduce further the role of water in the CO_2 adsorption process. The SBA-15 support material used in Chapter 3 was functionalised by grafting n-propyl chains to the surface in an attempt to increase hydrophobicity of the support material. An increase in hydrophobicity was observed when using EDA-PVC/SBA-15-C3 (4%) composite material, although a decrease in CO_2 adsorption capacity was also observed. This was attributed to the narrowing of pores through grafting of alkyl chains, making even deposition of EDA-PVC more difficult and causing pore blockage. The ultralarge mesoporous structure of carbon nanofibres was determined to be unsuitable for deposition of EDA-PVC, with no apparent adsorption observed during CO_2 adsorption experiments. Both activated carbon and CMK-3 hydrophobic materials were determined to be well suited to deposition of EDA-PVC, with high CO_2 adsorption capacities recorded for both composite materials. The microporous structure of activated carbon provided the greatest CO_2 adsorption capacities for composite materials utilising 4% EDA-PVC (0.74 $mmolg^{-1}$) and 2% EDA-PVC (0.68 $mmolg^{-1}$). The interconnected mesoporous structure of CMK-3 also exhibited high CO_2 adsorption capacities of 0.56 $mmolg^{-1}$ and 0.68 $mmolg^{-1}$, for 4% and 2% EDA-PVC loadings respectively. The increase in CO_2 adsorption capacity observed upon loading less EDA-PVC polymer material can be attributed to less pore blockage, as less polymer material allows for a more even loading across the support surface. Tests on the regenerability of EDA-PVC/CMK-3 (4%) composite materials at 75°C indicated no significant loss of adsorption capacity after 3 adsorption cycles.

5.2 Future Work

In industrial CO_2 adsorption processes adsorbents in the form of membrane can be considered superior to powdered solid-state CO_2 adsorbents as they are easier to handle, making the technical design procedure easier [5.1]. For example, membrane materials can bisect the flue gas stream directly without the need of a packed bed. During experimental work in Chapter 3 using diethanolamine (DEA), membrane materials were produced from DEA-PVC/SBA-15 and DEA-PVC/MCF-3 at higher DEA-PVC loadings, see Table 5.1. A loading of 19% DEA-PVC was sufficient to produce a membrane when using both SBA-15 and MCF-3 supports, although the DEA-PVC/SBA-15 (19%) membrane material was observed to be more brittle, Figure 5.1(a). However, the DEA-PVC/MCF-3 (19%) membrane material was observed to be flexible and durable, even after a double soxhlet extraction with ethanol. Deposition of DEA-PVC onto SBA-15 and MCF-3 silica supports at higher loadings allows for more durable membranes to be produced, Figure 5.1(b). A more robust membrane with greater durability is advantageous when implementing in an industrial setting.

Silica Support	Membrane Produced at DEA-PVC Loading of			
	19%	24%	29%	32%
SBA-15	✓	✓	✓	✓
MCF-3	✓	✓	✓	✓

Table 1. Results of membrane production experiments investigating different DEA-PVC loadings on SBA-15 and MCF-3 mesoporous supports. (✓) indicates membrane formation, (x) indicates no membrane formation.

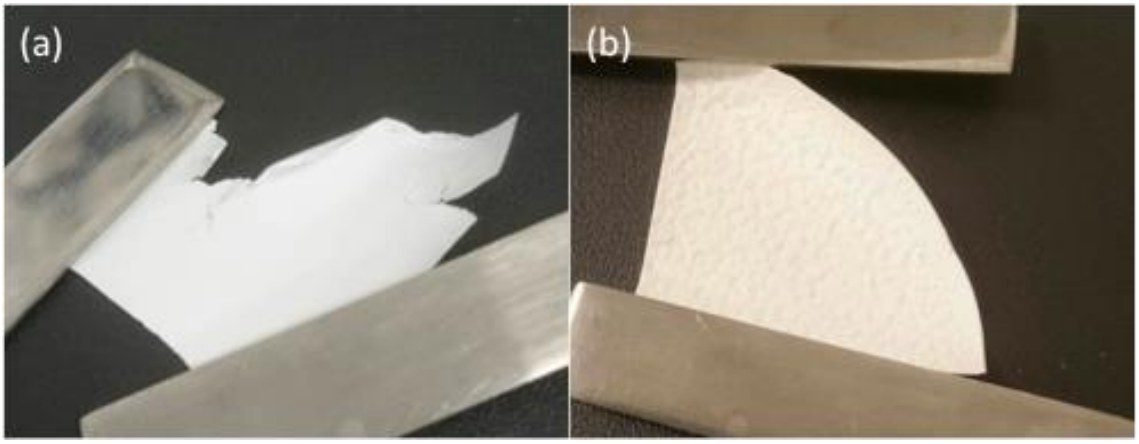

Figure 5.1. Membranes produced by deposition of DEA-PVC on SBA-15 and MCF-3 mesoporous silica supports. (a) brittle membrane produced from DEA-PVC/SBA-15 (19%), (b) durable membrane produced from DEA-PVC/MCF-3 (29%)

These membrane materials did not suffer from any losses in CO_2 adsorption capacity when compared to the DEA-PVC/silica powdered composite materials produced in Chapter 3, with both membranes recording a CO_2 adsorption capacity of 0.23 $mmolg^{-1}$ (Figures 5.2 and 5.3). Indeed, DEA-PVC/SBA-15 (4%) powdered composite material recorded a CO_2 adsorption capacity of 0.21 $mmolg^{-1}$, indicating marginal improvement of CO_2 adsorption capacity through membrane formation.

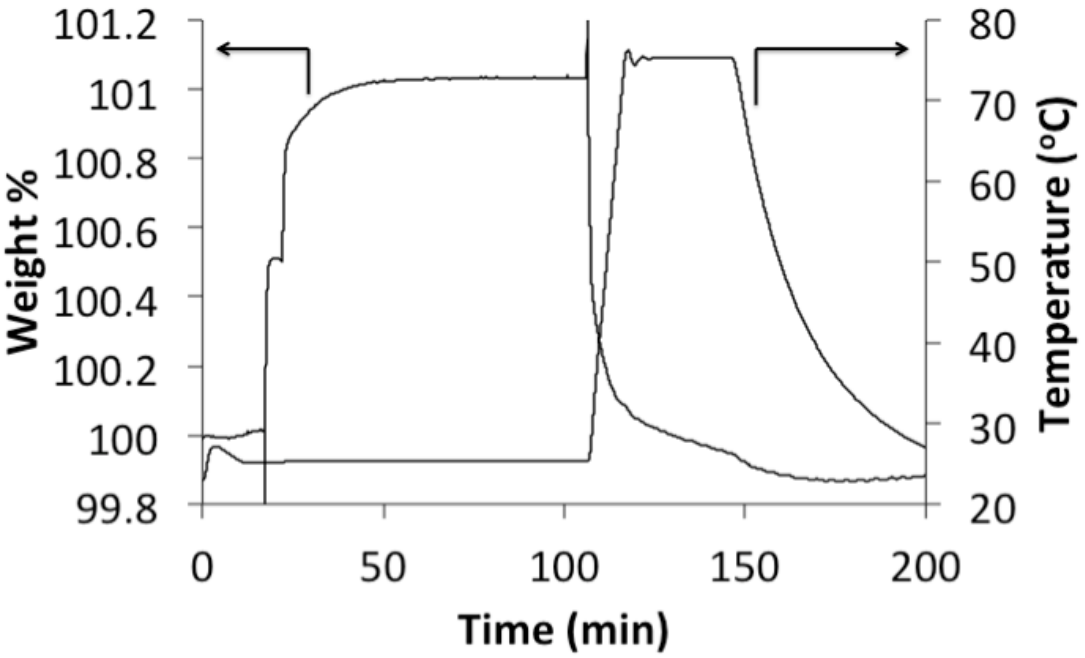

Figure 5.2. Gravimetric CO_2 adsorption experiments carried out on DEA-PVC/SBA-15 (19%) membrane material. A CO_2 adsorption capacity of 0.23 $mmolg^{-1}$ was recorded.

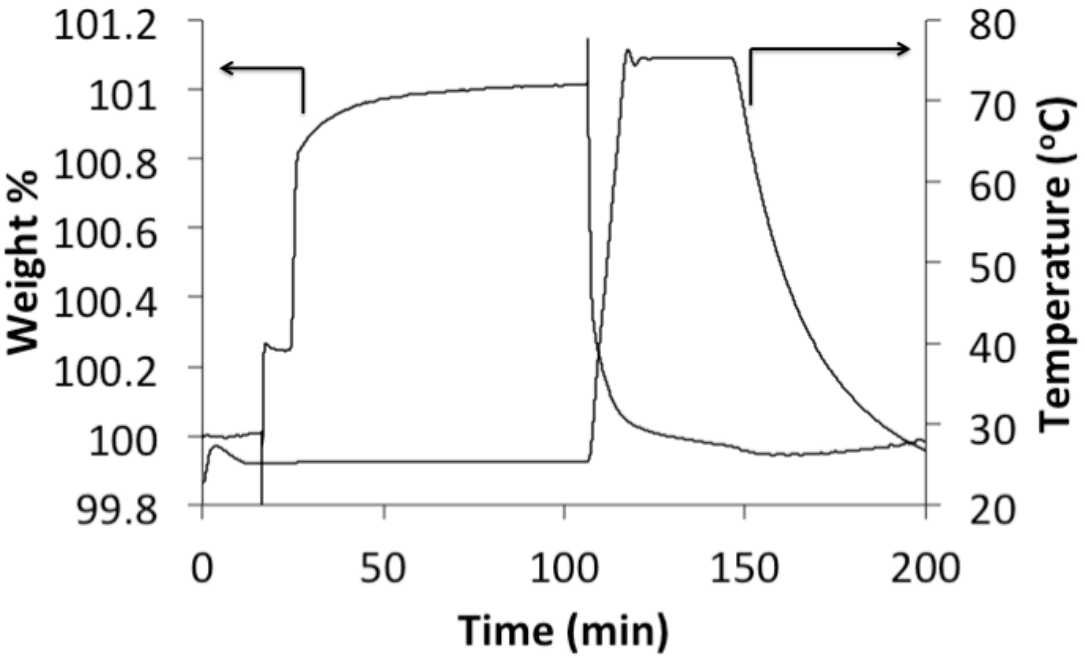

Figure 5.3. Gravimetric CO_2 adsorption experiments carried out on DEA-PVC/MCF-3 (19%) membrane material. A CO_2 adsorption capacity of 0.23 $mmolg^{-1}$ was recorded.

Membrane formation was limited to DEA-PVC/mesoporous silica composite materials, with no membranes observed from other amine modified PVC composite materials. This suggests a specific interaction between the modified polymer and the silica support. This is likely due to hydrogen bonding between the hydroxyl groups of DEA-PVC and the hydroxyl groups present throughout the mesoporous silica support. The fact that monoethanolamine (MEA) modified PVC material do not form membrane materials suggests there is some limit on the number of hydroxyl groups required for membrane formation. However, without further investigations using a variety of supports and amine modified PVC materials, no solid conclusions can yet be determined from this work.

5.3 References

[5.1] N. Jusoh, Y. F. Yeong, K. K. Lau, A. M. Shariff, *Enhanced gas separation performance using mixed matrix membranes containing zeolite T and 6FDA-durene polyimide*, J. Membr. Sci., **525,** 175-186 (2017)

[5.2] A. A. Ramirez-Santos, C. Castel, E. Favre, *Utilization of blast furnace flue gas: Opportunities and challenges for polymeric membrane gas separation processes*, J. Membr. Sci., **526**, 191-204 (2017)